A Thermistor Based Sensor for Flow Measurement in Water

by

John P Moore BSc

A Thesis presented to

Dublin City University

For the Degree of Master of Science

August 2003

Supervisor Dr Brian Lawless

School of Physical Sciences

Dublin City University

Ireland

I hereby certify that this material, which I now submit for assessment on the programme of study leading to the award of Master of Science is entirely my own work and has not been taken from the work of others save and to the extent that such work has been cited and acknowledged within the text of my work

Signed John Moore ID No 96330902

Date 19 9 2003

A Thermistor Based Sensor for Flow Measurement in Water

Acknowledgements

There are a number of people who have made invaluable contributions at various stages during the course of this work and to whom I am extremely grateful

My supervisor, Dr Brian Lawless, for his much valued assistance and advice throughout the course of the project and also for painstakingly proof reading previous drafts of the thesis

Mr Des Lavelle, the workshop technician at DCU, for his help in the construction of the various facilities that were developed

Mr Pat Wogan, for being an untiring source of information in answering my endless electronics questions

Finally, I wish to thank my family, especially my parents for their undying support and encouragement, which has brought me thus far today

John P Moore

August 2003

Contents

Abstract 1

Chapter 1 Introduction 2

Chapter 2 . Theory of Thermal Anemometry 7

2 1 Introduction 7

2 2 Basics 7

2 3 Sensor Materials 8

2 4 Determination of Response to Velocity 9
2 4 1 Theoretical Models 9

2 5 Modes of Operation 12
2 5 1 Consequences of Bubble Formation 12
2 5 2 Constant Current 13
2 5 3 Constant Voltage 14
2 5 4 Constant Temperature 15
2 5 4 1 Operating Resistance of Sensor 17
2 5 4 2 Calculating Sensor Voltage from Circuit Output 17
2 5 4 3 Alternative Methods of Constant Temperature Control 18

2 6 Fluid Temperature Effects 18
2 6 1 Manual Compensation 19
2 6 2 Automatic Compensation 19
2 6 3 Mathematical Compensation 20
2 6 4 Velocity Sensitivity and Frequency Response of Temperature Sensor 21
2 6 5 Single Sensor Systems 21

2 7 Sensor Types 21
2 7 1 Hot Wire 21
2 7 2 Hot Film 22
2 7 3 Thermistor Based Sensors 23
2 7 3 1 Velocity Response of Thermistor based Anemometers 23
2 7 3 2 Material Choice 24
2 7 3 3 Resistance-Temperature Characteristics 25
2 7 4 Thermistor Anemometer Coating 26
2 7 4 1 Calibration of Coated Sensors 29

Chapter 3 Design and Implementation 30

3 1 Control Circuit 31
3 1 1 Sensor Output 32
3 1 2 Oscillation and Circuit Stability 33
3 1 3 Saturation of Circuit Output 33
3 1 3 1 Determination of Sensor Voltage 35
3 1 4 Selection of Resistor Values 35
3 1 5 Setting Operating Temperature 36
3 1 6 Control Circuit With Offset Voltage Injection 37
3 1 6 1 Open Loop Gain 38
3 1 6 1 1 Maximising Open Loop Gain 39

3 1 6 1 2 Gain Composition 40
3 1 6 2 Circuit Output 40
3 1 7 *Power Supply Considerations* 40

3 2 Temperature Compensation **41**
3 2 1 Circuit 41
3 2 2 Series Resistor Selection 42
3 2 3 Temperature Measurement 43
3 2 3 1 Resistance-Temperature Characteristics 43
3 2 4 Uncertainty in Temperature Measurements 45
3 2 5 Temperature Compensation Circuit with Amplifier 48
3 2 5 1 Setting the Reference Voltage 49
3 2 6 Non-Linearity of Thermistor Response Characteristics 50

3 3 Data Acquisition and PC Interfacing **50**
3 3 1 Pico ADC22 51
3 3 2 Signal Conditioning 52
3 3 2 1 Determining the Necessary Offset Voltage and Scaling Factor 53
3 3 3 ADC Software 53
3 3 4 ADC Calibration 55
3 3 5 Sampling Frequency 55

3 4 Final Circuit and Data Processing Equations **55**
3 4 1 Velocity Sensor 57
3 4 2 Temperature Sensor 57
3 4 3 Using the Measurement System 58

3 5 Calibration Facilities and Procedure **58**
3 5 1 Gravity Tank 59
3 5 2 Tow Tank 61
3 5 2 1 Velocity Measurement 62
3 5 2 2 Trolley Oscillation 65
3 5 2 3 Chopper Location 67
3 5 2 4 Sensor and Cable Mounting 67
3 5 2 5 Sample Rate 68
3 5 2 6 Data Synchronisation 68

3 6 Sensor Design **69**
3 6 1 Glass Bead 69
3 6 1 1 Performance 70
3 6 2 Sensor Range 70
3 6 2 1 Glass Bead Thermistor Sensor Range 73
3 6 3 Sensor Choice 75
3 6 4 Surface Mount Chip Thermistors 76
3 6 4 1 Coating Materials 76
3 6 4 2 Coating Techniques 77
3 6 4 3 Influence of Thermistor Geometry on Required Coating Thickness 78
3 6 4 4 Stability and Annealing 78
3 6 5 Bubble Formation 79

Chapter 4 Results and Analysis **80**

4 1 Frequency Response and Offset Voltage Injection **81**
4 1 1 Square Wave Testing 82
4 1 1 1 Optimum Damping 84
4 1 1 2 Comparison of Frequency Response of Basic and Offset Injection Circuits 85
4 1 2 Tuning Offset Voltage 86
4 1 2 1 Influence of Offset Voltage on Operating Temperature of Sensor 86
4 1 3 Effect of Open Loop Gain on Sensor Dynamics 87

4 2 Noise 88
4 2 1 Setting the Corner Frequency of the Sensor System 89
4 2 2 RF Noise and Circuit Shielding 90

4 3 Calibration and Curve Fitting 90
4 3 1 Expressing Sensor Output in Terms of Power Dissipation 91
4 3 2 Calibration Data 92
4 3 2 1 Synchronised and Interpolated Data 93
4 3 2 2 Smoothing of Velocity Data 96
4 3 3 Velocity Response of the Sensor 99
4 3 3 1 Improved General Response Equations 103
4 3 3 1 1 Logarithmic Polynomial 104
4 3 3 1 2 Alternate Logarithmic Functions 106
4 3 4 Temperature Response 107

4 4 Measuring Water Velocity with Calibrated Thermistor Anemometer Probe 111
4 4 1 Calculating the Roots of the Calibration Equation 112
4 4 1 1 Downfall of Root finding Method 113
4 4 2 Alternative Calibration Equations 114
4 4 3 Successive Approximation Technique 114

4 5 Sensor Range 115

4 6 Influence of Coating Thickness on Sensor Characteristics 117
4 6 1 Frequency Response 119

4 7 Effects of Coating Failure on Sensor Performance 119
4 7 1 Detecting Coating Failure 120

4 8 Stability and Contamination Induced Drift 121

4 9 Directional Sensitivity 121

4 10 Calibration by Inference 122

4 11 Multi Sensor Arrays 122

Chapter 5 · Conclusions 123

References I

Appendix A Derivation of Equation (2 21) and Data in Table 2 2 VII

Appendix B Guide to Using the Sensor IX

Appendix C Code Listings XI

Appendix D Notation XXIX

Abstract

There is limited experimental data describing the mixing processes and coherent velocity structures near the surface of the ocean These play an important part in the interactions between the atmosphere and the ocean and thus affect the climate of the earth A robust, low cost thermistor based sensor suitable for use in the detection and quantification of velocity structures has been designed and developed The flow sensor, a thermal anemometer, consists of a self-heated thermistor that is maintained at constant temperature using a feedback control circuit The thermistor is exposed to the moving fluid and the heat transfer from it is a function of the velocity of the fluid The sensor has been interfaced with a PC to facilitate data acquisition A tow tank calibration and testing facility also interfaced to a PC was developed The sensor is compensated for changes in ambient fluid temperature, which is a major problem for all thermal anemometers that operate in water The calibration relation that is normally used for thermistor anemometers has been improved upon and gives better results than any found in the literature In order to provide electrical isolation from the water the sensor was protected with an insulating coating The effect of coating thickness and the type of coating used on sensor performance was investigated It was found that a polymer coating resulted in a sensor that did not show any appreciable drift due to sensor contamination over a number of months This is a significant improvement over glass coated hot film sensors, which are widely used for velocity measurements in water and previously developed thermistor based sensors The effect of various control circuit parameters on the frequency response of the sensor was determined and these parameters were tuned to give maximum frequency response A procedure for easily replacing broken/damaged sensors in the field was also developed

Chapter 1 : Introduction

Previous work carried out by Lawless (1976) using an inverted echo sounder found evidence of the transport of packets of surface water to considerable depths during storm conditions at sea The existence of downward transport has also been investigated by Toba and Kawamura (1996) using a laboratory wave tank and by Osborn et al (1993) using ultrasonic sensors mounted on a diving submarine It is believed that the packets of downward moving water are coherent velocity structures generated by wind driven breaking waves, however there is a lack of conclusive experimental evidence so the aim of this work is to develop a velocity sensor that could be used as part of a multi sensor array that would provide a means of investigating this and other coherent velocity structures that occur at sea The investigation of such structures is important from the point of view of the development of more accurate climate models etc (Thorpe 1995)

Such a sensor would be required to have a high spatial and time resolution, be relatively cheap as loss of an entire sensor array is a distinct possibility in such measurement circumstances and they must also cause minimal disturbance to the flow in their vicinity

There are quite a number of velocity sensors available for water, however very few of them are suitable for such an application Possibly the simplest type of velocity sensor for use in water is the propeller based sensor (e g Weller and Davis 1980, Johnson 1987 and Lane 1999) While these would be easy to use, they have quite poor spatial and time resolution and are quite expensive The next possibility is an ultrasonic based sensor, which have been used quite extensively for measurements in water, for example Williams (1993), Lane (1999) and Thorpe (1985), however these also have quite poor spatial resolution and the transmitter and receiver would interfere considerably with velocity structures in their vicinity

Another possibility is Laser Doppler Anemometry (LDA) (Adrian 1983, Kim et al 1992 and Veloso-Gomes et al 2001), which works by detecting the Doppler shift in laser light that is reflected from "seeding" particles that are dispersed in the fluid The Doppler shift is directly related to the velocity of the particle and if it can be assumed that the particle is moving with the fluid then the velocity of the fluid in the vicinity of the particle can be measured LDA is a powerful technique that would be very useful, however LDA systems are very expensive and it would not be feasible to have an array of them or to risk their loss in rough seas

Another measurement technology that has seen much development in the past number of years, primarily due to the emergence of relatively low cost high performance computers, is Particle Image Velocitmetry (PIV) (Raffel 1998, Adrian 1983) The operating principle of a PIV system is that a topographical 3-D image of the velocity structures in a given body of fluid is constructed using light reflected from seeding particles in the fluid This technique allows for detailed investigation of a particular velocity structure and would possibly give good results in the application being considered, however PIV systems and data processing packages are very expensive and are therefore immediately excluded from consideration Another problem is that relatively uniform seeding is required and while air bubbles can be used as the seeding particles in LDA they are not suitable for PIV, due to lack of uniformity Therefore the volume of water of interest would have to be seeded with appropriate particles before measurements could be obtained and this would not be viable given the scale on which any such seeding would have to be undertaken

Sensors based on the principle of thermal anemometry are widely used in the measurement of fluid flow, primarily in air (e g Bruun 1995, Perry 1982) and to a lesser extent in water (e g Rasmussen 1962, LeBarbera and Vogel 1976) and fulfill many of the requirements of the application at hand They work on the principle that the heat transfer from a heated body that is exposed to a moving fluid is related to the velocity of the fluid Thermal anemometers are much smaller and less expensive than any of the other measurement techniques that have been considered This small size implies that they will have good spatial resolution and will cause minimal interference to the structure being investigated Also, their low cost makes them the ideal choice for use in a multi-sensor array that is to be operated in a hostile environment

There are three main types of thermal anemometers, namely, hot wire, hot film and thermistor anemometers with only hot film and thermistor anemometers being suitable for measurements in water Hot film sensors have been used extensively in controlled laboratory environments (e g Wu and Bose 1993, Samways 1994, Bruun 1995, d) however they are not very well suited to measurements in open water as a result of their susceptibility to contamination-induced drift Thermistor anemometers have been used in open, completely uncontrolled environments, (e g MacIntyre 1986, Le Barbera and Vogel 1976, Riedl and Machen 1972) and it has been found that they are much less susceptible to contamination and drift than their hot film counterparts and yielded good results

As a result it was decided to concentrate on thermistor anemometers. It was found that while hot wire and hot film anemometers are commercially available, that thermistor anemometers are not, so it was necessary to design, develop and construct a complete thermistor anemometer system. In broad terms, this would require the development of the sensor, control electronics, data acquisition system including interface electronics and a calibration facility that would allow the calibration of the sensor over a suitable range of velocities. A number of investigators have developed thermistor-based thermal anemometers, beginning with Rasmussen (1962) who seems to have been the first to explore the possibility of using thermistors as the sensor element in thermal anemometers. Grahn (1962) developed a thermistor-based sensor for monitoring blood flow in anaesthetised dogs. Riedl and Machen (1972), Le Barbera and Vogel (1976) and MacIntyre (1986) have developed thermistor-based sensors for use in the marine environment. A considerable number of thermistor-based sensors have also been developed for use in air, including those of Okamoto (1994), Catellani (1982/83) and Fujita (1995). The sensor that has been developed during the course of this work shows improved performance over all of the thermistor-based sensors to which reference could be found in the literature, with the most significant improvements being the increase in long-term stability (see section 4.8) and the introduction of a considerably more accurate calibration equation (see section 4.3).

The work begins with an investigation of the basic operating principles of thermal anemometers. The fact that the sensor is to operate in water places a number of restrictions on its operating parameters and these are discussed in terms of the measures that must be taken to accommodate them. A theoretical analysis of the effects of coating thickness on the velocity response characteristics of a coated, self-heated thermistor was carried out. The analysis indicated that the coating thickness impacts considerably on the velocity response of a thermistor anemometer. This became a major consideration at the sensor design stage and has been proven to be correct by experimental results that were obtained with sensors with different coating thicknesses. Details of these results are discussed in Chapter 4.

With the conclusion of the discussion of general background and theoretical considerations in Chapter 2, Chapter 3 then deals with the actual design and implementation of the various components of the sensor system. It begins with the control circuit, an area in which a number of improvements have been made over the standard design. A modified circuit has allowed both the operating range and the

efficient use of power supplies to be maximised A technique for setting up the circuit has been developed that eliminates the problems associated with using commercially available thermistors with standard tolerances, which is a significant obstacle to the development of a low cost multi-sensor array An advanced control circuit that gives the user control over the response dynamics of the system has also been implemented and has proven to be of great benefit The operation of sensors at sea would require the use of batteries and to this end, comprehensive voltage regulation circuitry has been included, in order to avoid problems with supply voltage drift

The problem of sensitivity to changes in ambient water temperature has been overcome by using a second sensor in temperature sensing mode to measure the ambient temperature of the water in the vicinity of the velocity sensor This sensor is used in conjunction with an instrumentation amplifier in order to increase its measurement accuracy

Calibration of the sensor has been facilitated by the development of gravity tank and tow tank calibration facilities As a result of the superior performance of the tow tank at low velocities, it has been used for much of the calibration work that has been carried out A velocity measurement system has been incorporated into the tank that allows the velocity of the sensor relative to the water to be measured with a maximum error of just 0 18%

A data acquisition system that utilises a multi-channel Analog to Digital Converter (ADC) has been implemented and can support up to eleven sensor units each consisting of a velocity sensor and an ambient temperature sensor A data acquisition system has also been developed for the calibration facilities and a method of synchronising the sensor and calibration data acquisition systems has been implemented This allows the sensor to be calibrated together with the data acquisition system that, which prevents the possibility of errors occurring as a result of mismatched ADC's etc Programs have been written that allow all of the necessary data processing to be performed in a number of simple steps

We then move on to the development of the sensor element itself Analysis revealed that there were considerable benefits to be gained from using sensors with different coating thicknesses and materials than are commercially available and this led to the decision to construct and coat sensors in the lab The construction and coating techniques used are described, including an appraisal of the various coating

techniques that were used The resulting sensor was found to have much improved performance over those that have been developed previously by other investigators

In Chapter 4 the analysis techniques for hot wire and hot film anemometers, which are well documented in the literature (e g Bruun (1995, m), Perry (1982, e), Freymuth 1977), are applied to the thermistor anemometer that has been developed Such an analysis of thermistor anemometers has not been found in the literature

Also covered is the development of the general equation that describes the response of the sensor and the curve fitting techniques that are used to determine the exact response of a particular sensor from this general equation A general equation has been found that describes the response of the sensor much more accurately than any of the general equations that have been reported by other investigators, for example MacIntyre (1986), Rasmussen (1962), Yang (1988) Okamoto (1994) and Grahn (1962) The use of this equation, a third order polynomial, is complicated by the fact that it must be inverted in order to be able to us it to convert raw sensor data into velocity data The inversion process results in three possible solutions that are all equally valid and in certain circumstances it is not possible to determine which one is correct This problem has been overcome by the use of a standard iterative technique, which has turned out to be many times more efficient than the inversion approach would have been

In Chapters 3 and 4 a technique for calculating the measurement range of the sensor has been developed It allows the determination of the velocity at which the maximum permissible uncertainty in measurements obtained with the sensor will occur In principle this technique could be applied to any sensor that has a non-linear response and therefore represents a significant contribution to the field of sensor design

Finally, it should be mentioned that while, strictly speaking, the term "anemometer", implies measurements in air, it is widely used in the literature to describe measurement systems that operate in water, so for the sake of consistency the term "anemometer" has also been used in this report

The use of symbols has been as consistent as possible throughout the report and the notation used is listed in Appendix D

****

Chapter 2 : Theory of Thermal Anemometry

2 1 Introduction

The fundamental concept behind Thermal Anemometry is that the heat transfer from a heated object, exposed to a moving fluid, is a function of the velocity of the fluid The possibility of using this phenomenon to measure the velocity of fluids has been known since the 19th century (King (1914), however it was not until well into the 20th century and the advent of modern electronics that Thermal Anemometry became fully developed The first commercial Thermal Anemometry systems became available in the 1940's and since then huge advances in the understanding and technology of Thermal Anemometry have been made, most notably the development of Constant Temperature systems in the 1960's Today, Thermal Anemometry is used in many experimental and commercial applications, including, supersonic airflow studies (Smits 1990, Kegerise 1996), turbulence investigation (Bruun 1995), volume and mass flowmeters (Catellani 1982/83), velocity structure identification in air and water and blood flow measurement (Grahn 1962) to name but a few

2 2 Basics

All thermal anemometer systems consist of a sensing element that is heated with an electrical current and a control circuit that supplies the heating current and facilitates the monitoring of the parameters necessary to determine the fluid velocity The convective heat transfer from a heated body is given by Newton's law of cooling (Holman 1992, a)

$$H = hS\left(T_s - T_a\right) \tag{2 1}$$

where H is the heat dissipation rate (power), h is a quantity referred to as the convective heat transfer co-efficient, S is the surface area of the sensor, T_s is the surface temperature of the body and T_a is the fluid temperature

The heat transfer co-efficient h is a function of the velocity of the fluid, U , and the physical properties of the sensor and the fluid If the dependence of h on the velocity of the fluid can be determined then the above expression could be used to determine the velocity of the fluid This is the theoretical basis of thermal anemometry In order to implement an effective velocity measurement system the quantities, H , S , T_s and T_a must be determined together with the velocity dependence of h In practice,

measurement of the quantities, H, S, T_s and T_a proves to be straightforward but the velocity dependence of h can be very complex and in some cases may be impossible to determine

For steady state conditions the power dissipated by the sensor, H, is equal to the power generated in it due to electrical heating and therefore can be expressed as

$$H = \frac{V_s^2}{R_s} \tag{2.2}$$

where V_s is the voltage drop across the sensor and R_s is its resistance While the power being dissipated by the sensor, H, would have been difficult to measure directly, we now have an expression that describes it in terms of the quantities, V_s and R_s, which can be easily measured V_s can be determined using any standard voltage measurement technique and R_s can be determined by the use of bridge circuitry

Combining (2.1) and (2.2) and including the sensor surface area S in h we get

$$\frac{V_s^2}{R_s} = h(U)(T_s - T_a) \tag{2.3}$$

where $h(U)$ is the notation that is used to show that h is a function of the velocity, U, of the fluid

In the majority of thermal anemometry systems the sensor consists of a material that has a large temperature coefficient of resistance so that its operating temperature can be determined by measuring its resistance, which, as we have seen, must be measured anyway As well as providing an elegant method of measuring the temperature of the sensor, the use of materials with a temperature coefficient of resistance is the basis for some advanced control principles, which will be discussed later The only quantity in (2.3) that can vary during a set of measurements and which therefore must be measured that is yet to be accounted for is the ambient water temperature, T_a This can be measured using a number of methods, for example, thermocouples, thermistors and resistance elements (see Sherif and Pletcher 1986)

2.3 Sensor Materials

The materials used for thermal anemometer sensors can be divided into two groups - metals and semi-conductors While there are a large number of metals that exhibit a significant temperature coefficient of resistance, the most commonly used are platinum, platinum alloys and tungsten (Bruun 1995, a) The semi-conductors, which

are broadly referred to as thermistors are generally metal oxides Material choice is discussed in greater detail in section 2 7

2 4 Determination of Response to Velocity

The ideal way of determining the response of the anemometer to fluid velocity, and thus the quantity $h(U)$ discussed in the last section, would be to have a theoretical model that fully describes the system However, heat transfer from a heated body due to forced convection effects is complex and very difficult to describe theoretically for all but the simplest of situations A complete theoretical model would require the measurement of a large number of the physical parameters of the sensor At best this would be a very time consuming process and would need to be repeated for every sensor but in most cases it would not be possible to accurately measure all of the required parameters For this reason the standard approach is to use a relatively simple theoretical model to determine the general form of the sensor response equation and then use a calibration procedure and curve fitting technique to determine the exact form of the response equation The advantages of this technique are that all of the parameters of the sensor that are required are obtained by taking one set of measurements and that errors in the theoretical model will be corrected for in the curve fitting process

This method works well and is widely used with thermal anemometers that employ sensors for which good theoretical models exist, such as hot wire and hot film sensors (e g Perry 1982, Bruun 1995), however there are thermal anemometers, such as those using a thermistor-based sensor operated in water, whose general response cannot be determined from a theoretical model In these cases, the form of the general equation that is curve fitted to the calibration data has to be determined by an empirical analysis of the data A selection of such empirically derived general equations that describe the velocity response of various thermistor-based anemometers can be found in section 2 7 3 1

2 4 1 Theoretical Models

The first significant theoretical and experimental work on Thermal Anemometry was completed by King (1914) in which he theoretically derived the heat transfer from heated wires exposed to a moving fluid based on the assumptions of two dimensional equipotential flow around a circular cylinder and uniform heat flux across the entire

heated element - fluid interface The equation obtained by King, expressed in terms of the dimensionless quantities Nu, Pr and Re is

$$Nu = \frac{1}{\pi}\left(1+\sqrt{2\pi PrRe}\right) \tag{2 4}$$

where $Nu = \frac{hd}{k}$ Nusselt Number

$\Pr = \frac{c_p \mu}{k}$ Prandtl Number

$\mathrm{Re} = \frac{\rho U d}{\mu}$ Reynolds Number

and U is the velocity of the fluid, h is the heat transfer co-efficient, d is the diameter of the cylindrical element, k is the thermal conductivity of the fluid, ρ is the density of the fluid, μ is the molecular viscosity of the fluid and c_p is the specific heat of the fluid at a constant pressure

The assumptions made by King in his derivation of (2 4) are invalid (Lueck 1980), however researchers have since found that the general form of (2 4) is correct and that the heat transfer from heated cylinders exposed to a moving fluid can be described by

$$Nu = A + BRe^{0\,5} \tag{2 5}$$

where A and B are arbitrary constants that depend on the properties of the cylindrical element and fluid in question Despite the fact that A and B are not related to the work of King (1914) equation (2 5) is commonly referred to as "Kings Law" Kramers (1946) who carried out experiments on heated wires placed in air, water and oil found that heat transfer from them could be described by the empirical equation

$$Nu = 0\,42Pr^{0\,2} + 0\,57Pr^{0\,33}Re^{0\,5} \tag{2 6}$$

This can be written as

$$Nu = A + BRe^{0\,5} \tag{2 7}$$

where

$$A = 0\,42\,\mathrm{Pr}^{0\,2}$$

$$B = 0\,57\,\mathrm{Pr}^{0\,33}$$

which is the same form as (2 5)

Expressing the Nusselt number (Nu) and the Reynolds number (Re) in terms of their constituent quantities leads to

$$\frac{hd}{k} = A + B\frac{\rho d}{\mu}U^{05} \tag{2 8}$$

If it is assumed that the quantities d, k, ρ and μ will remain constant for a given measurement situation they can be included in the constants A and B to obtain the following expression for the velocity dependant heat transfer coefficient $h(U)$

$$h(U) = A + BU^{05} \tag{2 9}$$

However this assumption is not correct as all of these quantities have some dependence on temperature, but this dependence can be taken into account at the calibration stage

Substituting (2 9) into (2 3) gives

$$\frac{V_s^2}{R} = (A + BU^{05})(T_s - T_a) \tag{2 10}$$

If the sensor is operated in constant temperature mode the resistance of the sensor will remain virtually constant so it too can be included in the calibration constants A and B resulting in

$$V_s^2 = (A + BU^{05})(T_s - T_a) \tag{2 11}$$

which is also commonly referred to as Kings Law There seems to be some ambiguity in the literature in that both (2 5) and (2 11) are referred to as Kings Law, however it has been decided to refer to (2 11) as Kings Law in this report since this expression actually describes the response of the sensor, whereas (2 5) is just a heat transfer relationship In some texts such as Perry (1982, a), the $T_s - T_a$ term is expressed in terms of the resistances of the sensor and the other resistors in the Wheatstone Bridge Equation (2 11) does not take conductive losses to the wire supports into account and it has been found that these losses have a considerable effect on the response of a typical hot wire element (Bruun 1995, b)

Swaminathan (1986), Bruun (1995, b) and others have found that this can be accomplished by replacing the square root relationship of (2 11) by an arbitrary exponent n, which can be determined during the curve fitting process to obtain

$$V_s^2 = (A + BU^n)(T_s - T_a) \tag{2 12}$$

We now have a general equation that describes the response of a cylindrical sensor to velocity, however many systems employ sensors that have spherical geometry

A number of researchers have obtained relationships for the heat transfer from spheres in various fluids Kramers (1946) found that the heat transfer form spheres in water and oil could be described by

$$Nu = 2\,0 + 1\,3Pr^{0\,15} + 0\,66Pr^{0\,31}Re^{0\,5} \qquad (2\,13)$$

for $1 < Re < 2000$

This expression is of the same form as the relation for cylinders (2 5), which means that the same expression, (2 12), can be used to describe the response of both spheres and cylinders

In combining the work of a number of researchers, Whitaker (1972) obtained the relation

$$Nu = 2 + \left(0\,4Re^{0\,5} + 0\,06Re^{2/3}\right)Pr^{0\,4}\left(\mu_\infty/\mu_0\right)^{0\,25} \qquad (2\,14)$$

for liquids and gases for $3\,5 < Re < 8\times10^4$, where μ_∞ is the viscosity of the fluid at ambient temperature and μ_0 is the viscosity of the fluid at the surface of the sphere

The format of Whitakers expression is significantly different to that of Kramers and leads to an anemometer response equation of the form

$$V_s^2 = \left(A + BU^m + CU^n\right)\left(T_s - T_a\right) \qquad (2\,15)$$

A calibration equation of this form has been used by a number of individuals, including Bruun (1995, c), Swaminathan (1986) who have found that it gives a more accurate description than (2 12) in certain circumstances, such as with hot-film sensors in low Reynolds number flows (Bruun 1995, c)

2 5 Modes of Operation

In thermal anemometers the sensor can be operated under a number of different modes, the most widely used being *Constant Current*, *Constant Temperature* and *Constant Voltage* In the following sections a brief description of each of these modes is given and it will be seen that *Constant Temperature* mode is the best choice for sensors operating in water as a result of the fact that bubble formation, which is discussed below, can be completely avoided on sensors under constant temperature control

2 5 1 Consequences of Bubble Formation

It has been found by Rasmussen (1967) and Bruun (1995, d) that if the temperature difference between the sensor and the surrounding water is greater than about 20°C,

then bubbles will form on the sensor The presence of these bubbles has a dramatic effect on the stability of the output of the sensor and effectively renders it ineffective To obtain stable operation, with no drift due to bubble formation, the temperature difference between the sensor and the water must be kept below 20°C This is trivial to implement under *Constant Temperature* control, however it is not possible under *Constant Voltage* or *Constant Current* control due to the fact that the temperature of the sensor varies as a function of velocity under these modes and that for low velocities the temperature difference between the sensor and the water, $T_s - T_a$, will rise above 20°C

The 20°C limit results in thermal anemometers that are operated in water being less sensitive to velocity and more susceptible to ambient temperature changes (see section 2 6) than their counterparts in air Bubble formation is also affected by the coating on the sensor as is discussed further in section 3 6 5

2 5 2 Constant Current

When a sensor is operated in *Constant Current* mode the current in the sensor is maintained at a constant value Figure 2 1 below shows a typical classical constant current circuit

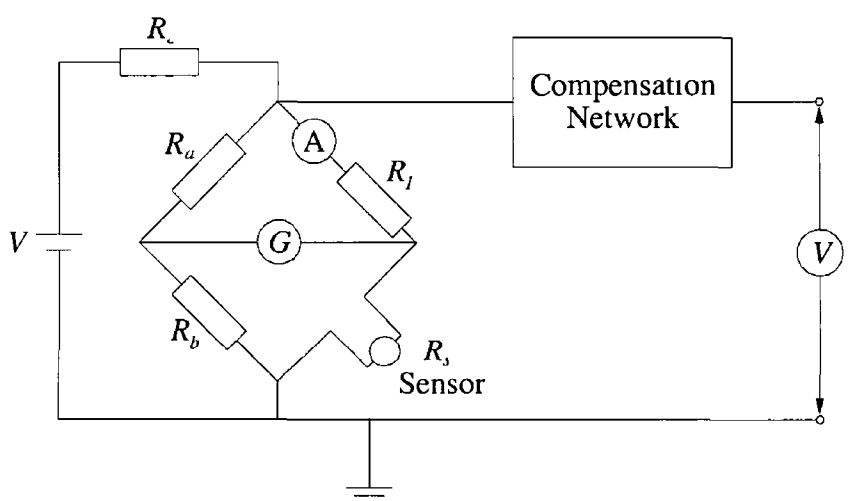

Figure 2 1 Basic Constant Current control circuit as given by Perry (1982, b)

The current in the sensor, R_s, is kept constant by ensuring that $R_c \gg R_l + R_s$ The circuit also incorporates a wheatstone bridge, a galvanometer (nowadays replaced by an instrumentation amplifier) and an ammeter, which are necessary for calibration and a compensation network, the purpose of which is to improve the frequency response

of the sensor The details of the calibration techniques and the compensation circuit are not discussed here but can be found in Perry (1982, c) and Bruun (1995, e)

An intrinsic problem with constant current operation is that changes in the velocity of the fluid result in changes in the operating temperature of the sensing element The associated thermal inertia results in the sensor having a poor response to high frequency velocity fluctuations Another significant problem with *Constant Current* systems is that they are very laborious to calibrate and use (Bruun 1995, e) These problems and the availability of the superior *Constant Temperature* mode have resulted in constant current mode rarely being used in modern thermal anemometry systems

Although they are no longer used, basic *Constant Current* systems are easy to construct and can provide valuable insight into the fundamentals of thermal anemometry Figure 2 2 shows the circuit diagram of a very simple constant current circuit that was used at the beginning of this investigation to gain an understanding of the fundamental principles involved

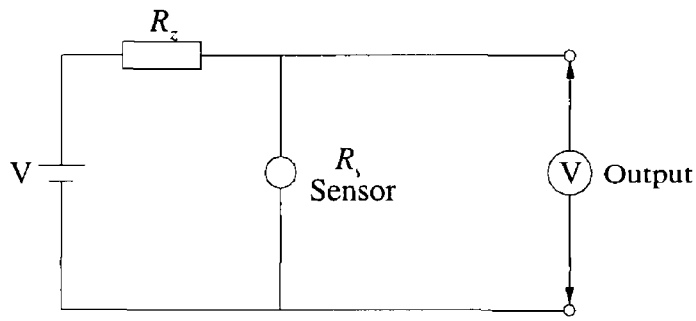

Figure 2 2 Very basic constant current circuit that was used in the early stages to gain an understanding of the principle of thermal anemometry

The current in the sensor is kept nearly constant by ensuring that $R_z >> R_s$ The voltage that appears across the output terminals is a function of the fluid velocity and temperature No attempt was made to calibrate the sensor in this configuration due to the problems mentioned previously

2 5 3 Constant Voltage

For constant voltage operation the voltage across the sensor is maintained constant by a feedback circuit such as that shown in Figure 2 3, which has been taken from Sarma (1998a)

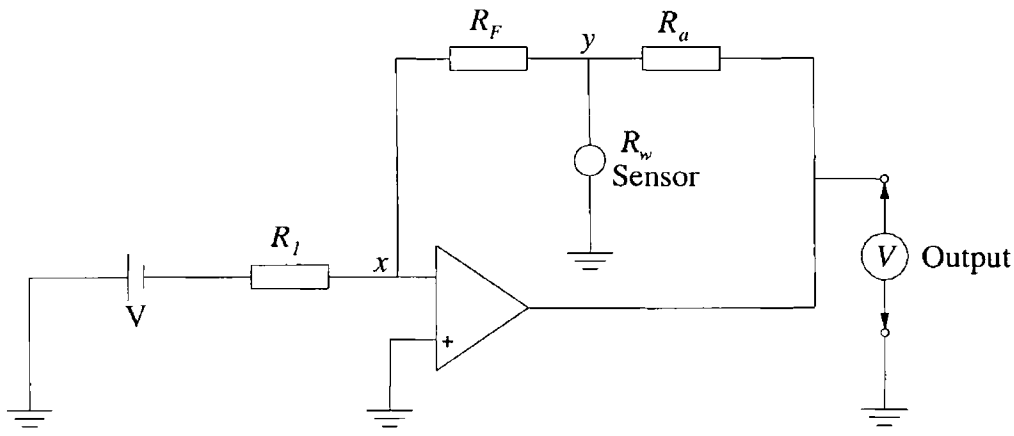

Figure 2 3 Constant voltage control circuit of Sarma (1998a)

The voltage at point x in the circuit will be kept at 0V by the action of the op-amp, which means that the voltage at point y will always remain constant, regardless of the resistance of the sensor, R_w, therefore as R_w varies the output voltage of the op-amp will vary such that the voltage at y remains constant The current in the resistor and thus its power dissipation can be determined by measuring the output voltage of the op-amp

Researchers (Sarma 1998a, Compte-Bellot 1999) have found that systems under constant voltage control exhibit a larger signal-to-noise ratio than other common control modes and that the time constant of these systems is much smaller than their constant current counterparts This has resulted in considerable work being carried on the development of constant voltage control most notably by Sarma and Compte-Bellot They have implemented a software compensation technique to further reduce the sensors time constant and improve its frequency response (Sarma 1998b) Its superior signal to noise ratio and frequency response characteristics mean that a Constant Voltage system would have many advantages over its Constant Current and Constant Temperature counterparts, however as a result of the bubble formation problem, which is discussed in section 2 5 1, it is not the most suitable control method for thermal anemometers operated in water Further information on Constant Voltage anemometers can be found in Sarma (1999), Sarma (2002), Truzzi (2002) and Kegerise (2000)

2 5 4 Constant Temperature

While early anemometers were operated in constant current mode, researchers were aware of the advantages of constant temperature operation from an early stage

(Ossofsky 1948) The emergence of highly stable low drift Integrated Circuit amplifiers in the 1960's has led to the use of constant temperature mode for all but a small number of applications

A simple constant temperature circuit is shown in Figure 2 4

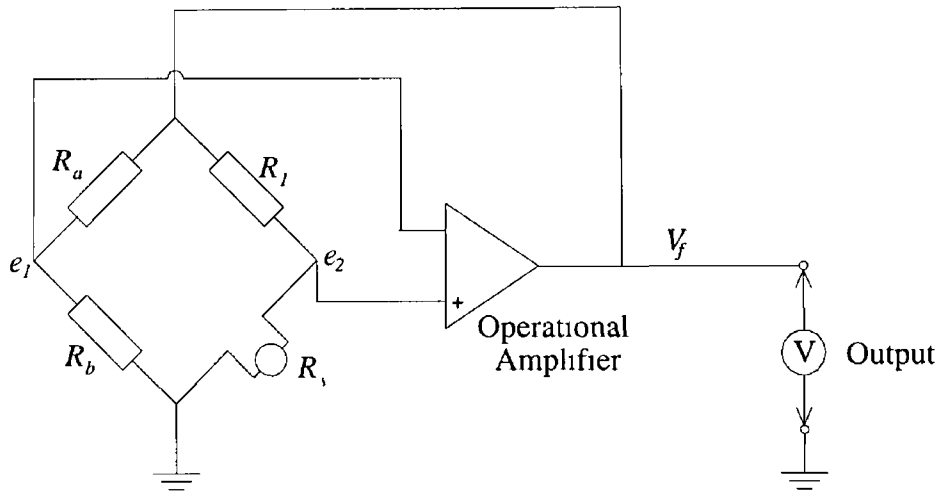

Figure 2 4 Basic Constant Temperature control circuit e_1 and e_2 are the voltages at the corners of the bridge and V_f is the feedback voltage, which is also the output voltage of the circuit

The voltage supplies of the operational amplifier have been omitted for clarity

The operational amplifier, which is connected as a feedback differential amplifier acts to keep the bridge in balance An intrinsic requirement of this Constant Temperature control circuit is that the sensor exhibits a temperature coefficient of resistance If this were not the case then the state of balance of the bridge would not be dependant on the temperature of the sensor A change in the temperature of the sensor will cause a change in the bridge voltage e_2 When such a change occurs, the bridge will no longer be in balance and the error voltage, $e_1 - e_2$, will be amplified and fed back to the top of the bridge where it causes a change in the current flowing in the sensor, which, if the circuit is configured correctly, acts to change the temperature of the sensor in such a direction that it returns to its set point, where the bridge is in balance The circuit configuration in Figure 2 4 is for a sensor that has a negative temperature coefficient of resistance For a sensor with a positive temperature coefficient, R_1 and R_s, or the inputs of the op-amp would need to be interchanged The temperature of the sensor will not remain fully constant, as some change is required in order for the circuit to operate, however if the gain of the amplifier is large then these temperature changes will be very small and constant temperature operation can be assumed

The main advantage of constant temperature operation over other modes is that since there are no appreciable changes in operating temperature there are no thermal inertia problems This results in constant temperature systems having good frequency response characteristics Other key advantages include the fact that bubble formation on sensors using this method of control can be avoided and that the constant temperature operation of the sensor simplifies the calculations involved in determining velocity from sensor output

2 5 4 1 Operating Resistance of Sensor

The operating resistance and thus the operating temperature of the sensor is determined by the values of the resistors in the bridge If the gain of the operational amplifier is sufficiently large it can be assumed that the bridge is in balance and that

$$e_1 = e_2 \tag{2 16}$$

This leads to

$$\frac{R_a}{R_b} = \frac{R_1}{R_s} \tag{2 17}$$

which can be rearranged to get the following expression for the operating resistance R_s of the sensor

$$R_s = \frac{R_1 R_b}{R_a} \tag{2 18}$$

Once the resistance temperature characteristics of the sensor are known the temperature of the sensor can be set by choosing values of R_1, R_a and R_b according to equation (2 18) In practice, the choice of values for R_a and R_b is affected by the desire to maximise efficiency by keeping current in the passive side of the bridge as small as possible This results in values of R_a and R_b that are between five and twenty times larger than R_1 and R_s being used in most practical circumstances

2.5 4 2 Calculating Sensor Voltage from Circuit Output

According to equation (2 3), in order to be able to calculate the velocity of the fluid to which the sensor is exposed, the voltage drop across the sensor, V_s, its resistance, R_s, and its temperature, T_s, must be calculated Since the sensor is being operated in constant temperature mode its temperature and resistance remain constant and are known In principle, the voltage drop across the sensor could be measured simply by

connecting a voltmeter in parallel with it, however as will be discussed further in section 3 1, it was found doing this made the control system unstable This problem can be overcome by measuring the feedback voltage of the circuit, V_f, as indicated in Figure 2 4 Since the sensor resistance, R_s, and the bridge resistor, R_1, remain constant, the sensor voltage V_s can be determined from V_f using the standard potential divider relation to get

$$V_s = V_f \frac{R_s}{R_1 + R_s} \tag{2 19}$$

2 5.4.3 Alternative Methods of Constant Temperature Control

The control circuit described above is essentially a proportional control system – the output of the controller is proportional to the error signal This method of constant temperature control has been widely used since its development in the 1960's and has proven to give very satisfactory performance Recently however, researchers have started to look at the possible advantages of using other, more sophisticated methods of controlling the sensor temperature Steurer (1998) has developed an adaptive control system for use with miniature Germanium thermistor sensors The use of adaptive control has maximised the sensor response to large changes in flow and also its sensitivity to small changes in relatively constant flow This represents the two extremes of flow measurement and in most systems a choice must generally be made between them, therefore the development of a control technique whereby both criterion can be maximised represents a significant advance It was decided that the basic Constant Temperature control technique was sufficient for this work and that the added complexity of adaptive control could not be justified

2 6 Fluid Temperature Effects

The basic response of thermal anemometers is given by (2 3), which is

$$\frac{V_s^2}{R_s} = h(U)(T_s - T_a)$$

Since the sensor is being operated in Constant Temperature mode this expression can be simplified further by including R_s in $h(U)$ to get

$$V_s^2 = h(U)(T_s - T_a) \tag{2 20}$$

From this expression it can be seen that changes in the anemometer output V_s due to changes in ambient temperature of the water, T_a, will be indistinguishable from changes due to velocity fluctuations Therefore, accurate measurement of T_a is necessary in order to obtain reliable velocity data

If the output of the sensor, SO, is taken as the quantity V_s^2 in (2 20), which as will be seen in section 4 3 1 is a perfectly valid course of action then the change in the sensor output, ΔSO, that results from a change in ambient temperature of ΔT_a is be given by

$$\Delta SO = SO\frac{\Delta T_a}{(T_s - T_a)} \tag{2 21}$$

which has been derived in Appendix A The quantity ΔSO is representative of the sensitivity of the sensor to the change ΔT_a in ambient temperature Since ΔSO is inversely proportional to $(T_s - T_a)$ it follows that the sensitivity of a thermal anemometer to changes in ambient temperature will be minimised by operating the sensor at the maximum possible temperature As we have mentioned in section 2 5 1, the temperature difference between the sensor and the surrounding water must be less than 20°C or bubbles will start to form on the sensor A typical operating temperature for a thermal anemometer operated in air is 400°C so therefore it follows from (2 21) that the sensitivity of thermal anemometers operated in water to changes in ambient temperature is much greater than that of those operated in air This is further exacerbated by the fact that the temperature dependence of the fluids properties is much greater for water than for air (Sherif and Pletcher 1986) The effects of changes in ambient temperature and techniques for compensating for it have been investigated by Bruun (1995, f), Sherif and Pletcher (1986) and Katz (1987, 1988) among others

The various compensation techniques can be described under three broad headings

2 6 1 Manual Compensation

This method was used in early systems and involves manually adjusting the operating temperature of the sensor to cancel out the effects of changes in the fluids temperature This method is not very useful and is never used nowadays

2.6.2 Automatic Compensation

Compensation for changes in the temperature of the fluid is achieved by incorporating a temperature sensitive component into the circuit in such a manner as to cancel the

effects of changes in fluid temperature Figure 2 5 shows a constant temperature control circuit that has an incorporated fluid temperature sensor

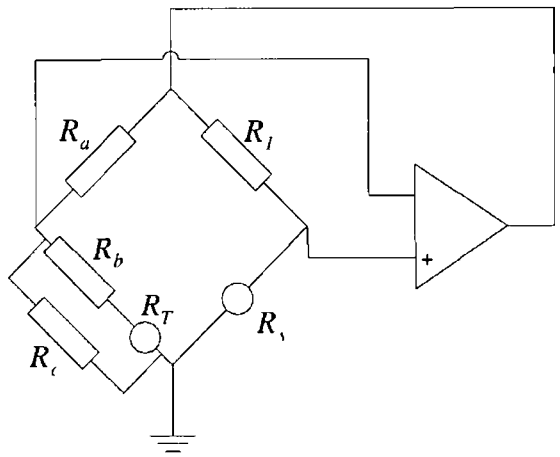

Figure 2 5 Constant Temperature circuit incorporating a fluid temperature sensor R_T, which has been taken from Bruun (1995, g) This is the standard circuit used in the implementation of automatic compensation The values of R_b and R_c are chosen such that the combination of R_b, R_c and R_T will have the same response to ambient temperature changes as R_s

The fluid temperature sensor is placed in the opposite side of the bridge to the velocity sensor Any changes in fluid temperature that occur will affect both sensors and the quantity $T_s - T_a$ will be kept constant If this method can be implemented without error then it is the simplest and easiest method to employ if fluid temperature data is not required There are a number of problems however Both sensors must have matched time and resistance response to changes in fluid temperature It can prove quite difficult to obtain/manufacture sensors with closely matched characteristics and such sensors can be considerably more expensive than those with standard tolerances The main advantage of using this method is that compensation occurs in real-time, which is useful in some applications

2 6 3 Mathematical Compensation

With this method the fluid temperature is measured using a separate temperature measurement sensor, such as a thermocouple, resistance thermometer etc, and the velocity sensor output and fluid temperature is recorded simultaneously The velocity data can then be adjusted to take account of fluid temperature variations at the data processing stage or else if a suitable calibration equation exists, the velocity of the fluid can be calculated directly from the velocity sensor output and ambient fluid temperature data The main advantage of this mathematical compensation is that the temperature and velocity sensors are not required to have the same temperature

response characteristics It can be slightly more time-consuming than automatic compensation since the response of the velocity sensor to temperature variations must be known and this usually requires separate calibration

2 6 4 Velocity Sensitivity and Frequency Response of Temperature Sensor

In both automatic and mathematical compensation it is important that the fluid temperature sensor is not sensitive to velocity This can be achieved by keeping the electrical power in the sensor as low as possible thus ensuring that heating of the sensor is minimised In certain circumstances the response time of the anemometer sensor to changes in ambient fluid temperature may not be the same as that of the fluid temperature sensor This must be taken into account when designing thermal anemometer systems that are required to contend with rapid ambient temperature variations

2 6 5 Single Sensor Systems

While most systems employ two independent sensors, it is possible to use the same sensor to measure both fluid velocity and temperature A number of different methods of accomplishing this have been implemented including those of Katz (1987,1988) and Sarma (2002) The basic principle is that the sensor is switched between two modes, a low current mode, in which it will be largely insensitive to changes in velocity, to determine the fluid temperature and a higher current Constant Current, Constant Temperature or Constant Voltage mode, in which the velocity of the fluid can be determined This system is only viable for fluids with slowly varying velocity and temperature, where low frequency measurements will suffice

2 7 Sensor Types

There are many different types of sensor used for thermal anemometry The most common being hot wire, hot film and thermistor sensors

2 7.1 Hot Wire

Hot wire sensors consist of a very thin wire (<5μm), usually made of Platinum or Tungsten mounted between two supporting prongs Hot wire sensors, which have good frequency response due to their small size, are primarily used for velocity measurements in air Their response characteristics can be described by expressions leading from those of King (1914) and Kramers (1946) due to their cylindrical geometry and as such are very well known Information on some of the many

different applications of hot wire sensors can be found in Bruun (1995), Perry (1982) and Fingerson and Freymuth (1983)

While being ideal for measurements in air, they are not suitable for use in conductive liquids such as water as they are difficult to coat with an insulating material (Bruun 1995, h)

2 7 2 Hot Film

Hot film sensors consist of a thin conductive film, usually Nickel or Platinum deposited on an insulating substrate, such as quartz A variety of substrate shapes are used depending on the specific application Common shapes include wedges, cylinders and cones (Bruun 1995, i) The substrates used are large enough to allow the film to be coated with a thin film of insulating material such as quartz, thus making them suitable for measurements in water and other conducting liquids The frequency response characteristics of hot film sensors are different from that of hot wire sensors and must be taken into account for certain applications

Quartz coated hot film probes used in water have been found to be susceptible to drift caused by the build up of contaminants and algae on the surface of the sensor Bruun (1995, j) found that in order to achieve sensor stability all measurements had to be carried out in a closed circuit environment that contained water that was very well filtered He also found that the temperature of the tank had to be kept at or below 16°C in order to inhibit the growth of algae Wu and Bose (1993) found that the drift in unfiltered water could be reduced to ~1% in a 7 hour period by aging the sensor in the water for a number of days before the measurement While aging results in stability for a number of hours there will still be drift over longer periods of time The sensors may be required to operate for several weeks at a time between calibrations, which means that unless some method of stabilising the output of the sensor for a much longer period than is currently possible, that hot film sensors are unsuitable for the current application

Commercial hot films are quite expensive and would be difficult to manufacture onsite making it difficult and expensive to prototype and test new sensor designs Another problem that has been documented by Bruun (1995, k) is cracking of the quartz coating Many of these problems can be overcome by using thermistor sensors

2 7 3 Thermistor Based Sensors

Thermistor sensors have been found to be more robust and less prone to drift due to sensor contamination than hot film sensors (Mac Intyre 1986), making them the ideal choice for thermal anemometers that are to be used in a marine environment Also, the large temperature coefficient of resistance of thermistors is an advantage when operating in water due to the relatively small temperature difference between the sensor and the water

Thermistor based sensors usually consist of a coated thermistor, mounted in one of the two configurations shown in Figure 2 6

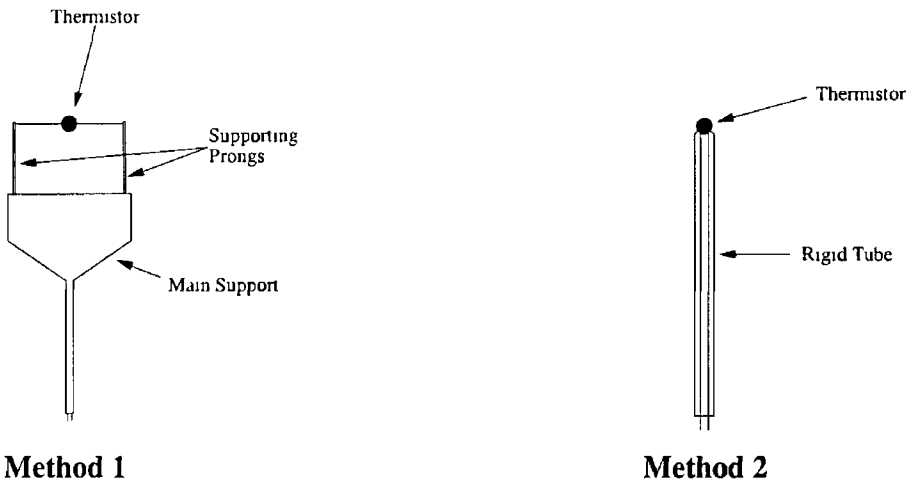

Figure 2 6 Diagrams of the two most common types of thermistor probe assemblies

The low cost and ready availability of a wide range of thermistors and the fact that thermistor probe assemblies can be manufactured without the use of specialist equipment make them suitable for exploratory work that will involve the prototyping and testing of new sensor designs

2 7 3 1 Velocity Response of Thermistor based Anemometers

Numerous investigators have been successful in developing thermistor-based anemometers for measurements in water including, Rasmussen (1962), Riedl (1972), Le Barbera (1976), MacIntyre (1986), Fanney (1987) and Yang (1988), and in air, Catellani (1982/83), Okamoto (1994), Fujita (1995) and Steurer (1998) Thermistor anemometers have also been used in blood flow measurements, examples being Grahn (1968) and Katz (1987) The majority of these have found that the response of thermistor-based sensors cannot be described using theoretical models such as those discussed in section 2 4 1, and the remainder seem to have assumed without question that the velocity response was given by (2 11) Various empirical equations describing

the velocity response of thermistor sensors have been presented by investigators over the years and some of these are listed in Table 2 1

Investigator	Response Equation
Rasmussen (1962)	$h(U) = A + B\left(1 - e^{CU}\right)$
Le Barbera and Vogel (1976), Mac Intyre (1986)	$V_s = A + B \ln U$
Okamoto (1994)	$h(U) = \frac{A}{\ln U - B}$
Grahn (1962), Katz (1987)	$h(U) = A + B \ln U$
Riedl and Machen (1972), Yang (1988)	$V_s^2 = A + BU^{0.5}$

Table 2 1 Some of the relations that have been used to describe the velocity response of thermistor anemometers

Each of these expressions has been fitted to the response of sensors designed during this investigation and an analysis of the quality of the fit obtained can be found in section 4 3 3 Riedl and Machen (1972) and Yang (1988) have used Kings Law however as will be seen later it provides a poor description of the response of the sensor developed during this work It is of interest to note that neither Riedl and Machen (1972) or Yang (1988) have given an analysis of the quality of the fit of Kings Law to their data

No reference could be found to a theoretical explanation of why the velocity response of thermistor-based anemometers does not follow that which is predicted by the standard theoretical models

2 7 3 2 Material Choice

There are two types of thermistor materials, Negative Temperature Coefficient (NTC) and Positive Temperature Coefficient (PTC) The resistance of NTC thermistors drops with increasing temperature while that of PTC thermistors increases Both NTC and PTC thermistors have been used in thermistor-based anemometers, however NTC thermistors are more readily available with a much more comprehensive range than their PTC counterparts and were chosen for use in this investigation for this reason NTC thermistors are generally manufactured from amalgamations of metal oxides and

an overview of the manufacturing process is given by Thermometrics (http //www thermometrics com/assets/images/ntcnotes pdf)

2 7 3 3 Resistance-Temperature Characteristics

In order to utilise thermistors as sensors in thermal anemometers, it is necessary to have a thorough understanding of their resistance temperature-characteristics The resistance-temperature characteristics of NTC thermistors can be described by the well-known relation

$$R_2 = R_1 \exp\left(\frac{\beta}{T_2} - \frac{\beta}{T_1}\right) \tag{2 22}$$

where R_1 is the resistance of the sensor at temperature T_1 R_2 is the resistance of the sensor at temperature T_2 and β is the slope of a graph of $\ln R$ vs $1/T$ for the material

In this relationship the slope of $\ln R$ vs $1/T$ is assumed to be linear over the temperature range in question Steinhart and Hart (1968) improved on the accuracy of (2 22) by taking into account the non-linearity of $\ln R$ vs $1/T$ by expressing $1/T$ as a polynomial in $\ln R$ to obtain

$$\frac{1}{T} = A + B(\ln R) + C(\ln R)^2 + D(\ln R)^3 \tag{2 23}$$

where A, B, C and D are calibration constants of the sensor in question and can be determined by curve fitting the above expression to $\ln R$ vs $1/T$ data Note that A, B, C and D will have different values for each sensor whereas β in (2 22) is a general property of the material that the sensor is made from Steinhart and Hart (1968) found that eliminating the $C(\ln R)^2$ term has very little effect on the accuracy of the expression This leaves

$$\frac{1}{T} = A + B(\ln R) + D(\ln R)^3 \tag{2 24}$$

If a sensor is to be used in a constant temperature system, then only its resistance at the operating temperature is required and this can be obtained using a single measurement, eliminating the need to determine the constants A, B and D However if the sensor is to be operated at a number of temperatures during its lifetime, it can be advantageous to evaluate these constants and use equation (2 24)

2 7.4 Thermistor Anemometer Coating

As with any thermal anemometer that is to be operated in water, thermistor-based sensors need to be coated with an electrically insulating material If the sensor and its connecting leads are not insulated electrolysis and corrosion will take place, destroying the sensor Another problem that has been discovered during this work is that if any conduction path exists between the sensor and the water in which it is operating then its performance will be adversely affected This phenomenon will be discussed in more depth later

It was believed that the coating which is present on virtually all thermistors, be they operating in air or water was a likely cause for the deviation of the velocity response of thermistor anemometers from that which is predicted by the standard heat transfer models This has been confirmed by expanding on the work of Lueck (1980), who developed a theoretical model that describes the heat transfer from a coated thermistor, which takes the presence and thickness of the coating into account While Lueck developed the model in order to analyse the sensitivity of velocity sensors to ambient temperature changes and vice versa, it is quite straightforward to expand upon his work and show that the altered velocity response characteristics of thermistors is due in a large part to their coating

Lueck (1980) found that the heat transfer rate, Q, from the bead could be described by

$$Q = \frac{2\pi(r+\Delta)k_2(T_s - T_a)Nu}{\left(1+\frac{k_2}{k_1}\frac{\Delta}{2r}Nu\right)} \qquad (2\ 25)$$

where r is the radius of the bead, Δ is the thickness of the coating, Nu is the Nusselt number of the bead (which is a function of fluid velocity), k_1 is the coefficient thermal conductivity of the coating, k_2 is the coefficient of thermal conductivity of the fluid and T_s and T_a are the temperatures of the core of the bead and the fluid respectively The heat transfer rate or power dissipation of the sensor is labelled as Q and not H as used previously in order to remain consistent with the terminology of Lueck The Nusselt number, Nu, is defined as

$$Nu = \frac{hd}{k} \tag{2 26}$$

and substituting this into (2 25) leads to

$$Q = \frac{hS(T_s - T_a)}{1 + \frac{\Delta}{k_1} h} \tag{2 27}$$

The heat transfer coefficient, h, is a function of velocity, U, and by including the surface area of the sensor in this function, as before, we get

$$Q = \frac{h(U)(T_s - T_a)}{1 + \frac{\Delta}{k_1 S} h(U)} \tag{2 28}$$

Comparing this expression and the basic definition of heat transfer due to forced convective flow as defined in (2 1) it can be seen that the effects of applying a sensor coating can be accounted for by introducing the extra term

$$\frac{\Delta}{k_1 S} h(U) \tag{2 29}$$

into the denominator The heat transfer coefficient $h(U)$ can be taken to be that of a sphere which was found in (2 9) to be

$$h(U) = A + BU^{0.5}$$

Substituting this into (2 28) and expanding the surface area term, S, gives

$$Q = \frac{\left(A + BU^{0.5}\right)(T_s - T_a)}{1 + \frac{\Delta}{4\pi k_1 (r + \Delta)^2}\left(A + BU^{0.5}\right)} \tag{2 30}$$

If the sensor output is considered in terms of its dissipated power, Q, then we now have an expression that relates the sensor output to the fluid velocity, U, the coating thickness, Δ, the size of the sensor, in terms of its radius, r and the thermal conductivity, k_1, of the coating As the coating thickness, Δ, tends to zero, the denominator of (2 30) will tend to one and the velocity response of the sensor will be given by Kings Law

The effects of coating thickness would be best demonstrated by graphs of the sensor output for a range of velocities for a number of coating thicknesses, however in order to achieve this using (2 30), the quantities A and B for a particular sensor must be evaluated This has been accomplished by assuming that the sensor is a 3mm diameter

metal sphere and using the results of Kramers (1946). While the response curves obtained can be expected to be considerably different from those that would be obtained using a thermistor sensor, they will still give a valid indication of the effects of coating thickness on the velocity response of thermal anemometers in general. The values of A and B that were obtained are given in Table 2.2 and details of the calculations can be found in Appendix A.

Coefficient	Value
A	0.023
B	0.414

Table 2.2 A and B values for a metal sphere that are required in order to be able to graph (2.30) for a number coating thicknesses.

Equation (2.30) was used with the values of A and B given in Table 2.2, an ambient water temperature, T_a, of 20°C, a sensor core temperature, T_s, of 40°C and the thermal conductivity, k_1, of glass at 20°C, to obtain dissipated power data for the velocity range 0 to 2ms^{-1} for a number of coating thicknesses. Graphs of this data are shown in Figure 2.7.

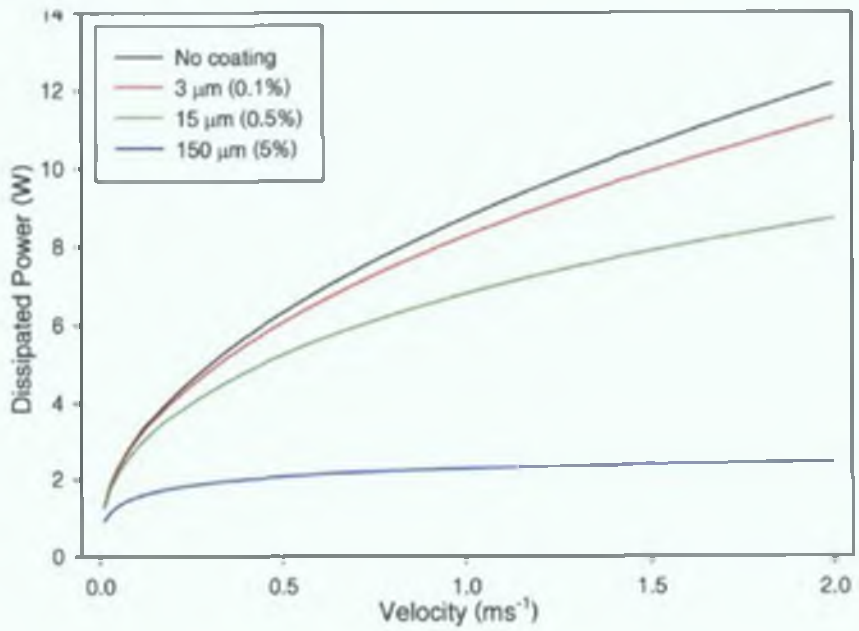

Figure 2.7 Theoretical prediction of the power dissipated by a coated spherical sensor operating at constant temperature for a range of coating thicknesses. The % in parentheses is the coating thickness relative to the diameter of the sensor

Figure 2.7 shows that the velocity response of a coated thermal anemometer is dramatically altered by the addition of a coating thickness of just 5% of the diameter of the sensor, which is typical of the coating thickness that is to be found on the

majority of thermistor anemometer sensors The graphs also provide insight into why the response of glass coated hot film anemometers operated in water can still be described by theoretical models even though they are coated The thickness of the coating used on hot film sensors is of the order of a few microns (Bruun 1995, 1) and it can be seen that the general form of the velocity response of the sensor described in Figure 2 7 has not changed appreciably by the addition of a 3μm coating

2 7 4 1 Calibration of Coated Sensors

While this model gives a good indication of the influence of the coating on the performance of a coated anemometer, there are a number of problems associated with it that would make it difficult to use in the calibration of a sensor

It has been assumed that the thermal conductivities k_1 and k_2 remain constant, however they will vary as a function of temperature (Holman 1992, b) and thus the velocity of the fluid This additional velocity dependence in the denominator of (2 25) would need to be taken into account, however it would be extremely difficult if not impossible to do so because of the complexity of the temperature distribution in the coating This leads to the next problem The derivation of (2 25) by Lueck (1980) was based on the assumption that the heat flux through, and temperature distribution in, the coating are uniform, which is not the case The third major problem is that heat loss through the connecting leads has not been taken into account and it would be difficult to do so

All of the background and theory that is necessary to be able to design a thermal anemometer has been discussed and we will now move on to the design and implementation of a Constant Temperature Thermistor Anemometer for measurements of velocities in water

****

Chapter 3 : Design and Implementation

This chapter details the design and implementation of the entire constant temperature thermistor-based anemometer and all of the necessary calibration facilities We begin with the constant temperature control circuit and describe the two distinct control circuits that have been developed, one with and one without offset voltage injection An alternative circuit configuration has also been introduced which allows for an extended measurement range while still utilising the existing power supply This circuit also reduces the voltage drop across the coating, that is, between the sensor and that water, thus reducing the possibility of coating failure A procedure has been developed for setting the operating temperature of the sensor that overcomes the problems caused by the wide production spread in the resistance of commercially available thermistors, a significant problem that must be dealt with if thermistor based sensors are to be used in multi-sensor arrays

The development of a thermistor-based ambient water temperature sensor is then discussed This is necessary if the sensor is to be used in a non-isothermal environment As part of the design process for this sensor it was necessary to devise a technique for evaluating the temperature measurement uncertainty that resulted from the finite resolution of the ADC used to acquire the sensor data This leads on to the ADC and data acquisition facilities that were put in place A circuit diagram of the final velocity and temperature sensor system is presented in conjunction with a block diagram analysis that combines the equations describing the individual parts of the circuit to obtain expressions that are necessary to process the raw ADC data that is obtained

The gravity and tow tank calibration facilities that were developed are discussed with the emphasis being placed on the tow tank facility, which was found to be the most suitable from an early stage Initially, a sensor that is typical of those used in previous investigations was developed and it was found that it had a number of shortcomings that justified the development of sensors with reduced coating thicknesses and alternate coating materials The sensor design phase saw the development of a very useful technique for determining the maximum range of the sensor as a function of the allowed fractional uncertainty in the measurement The various coating techniques and materials that were used are reviewed and the chapter concludes with a basic analysis of the performance of the resulting sensor before the analysis proper commences in Chapter 4

3.1 Control Circuit

There are many Constant Temperature control circuits in use, the majority of which have similar operating principles to that of Perry (1982, d), which is shown in Figure 3 1

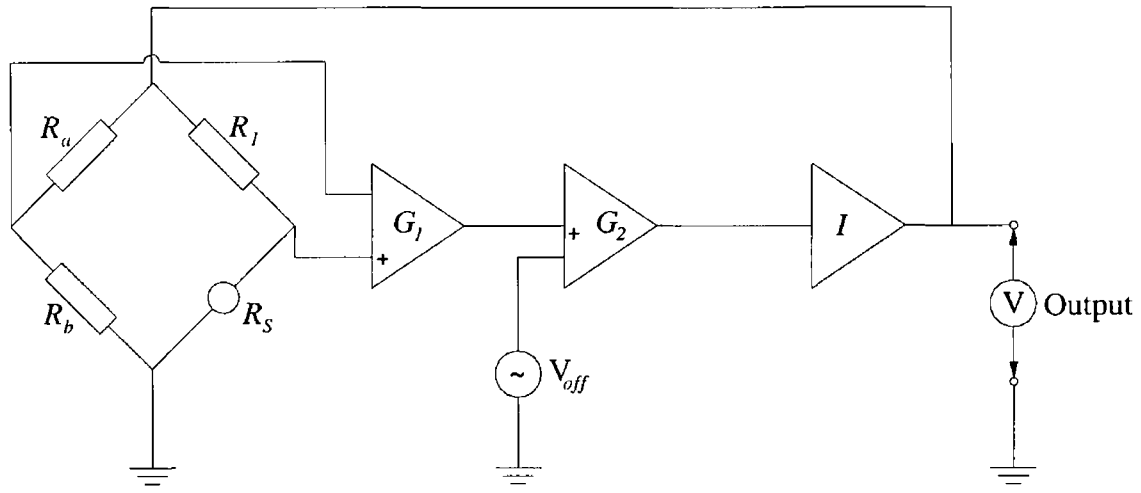

Figure 3 1 Constant Temperature Control Circuit

The circuit consists of a Wheatstone Bridge, in which the sensor, R_s, is placed, two stages of voltage gain, G_1 and G_2 and a current gain stage, I, which provides the necessary current to drive the bridge The circuit is based on the basic circuit shown in Figure 2 4, however there is one major difference in that a voltage, V_{off}, termed the offset voltage, is injected into the feedback loop via the second amplifier According to Perry (1982, e) this offset voltage has a significant influence on the stability and dynamic response characteristics of the system As will be seen in Chapter 4 this has been verified during the course of this work

Initial attempts to reproduce the circuit in Figure 3 1 resulted in circuits that were unstable and prone to oscillation, which in hindsight can be attributed to a lack of understanding of the effect the offset voltage, V_{off}, has on the stability of the circuit Extensive testing of modified circuit designs led to the circuit shown in Figure 3 2, which gave stable performance

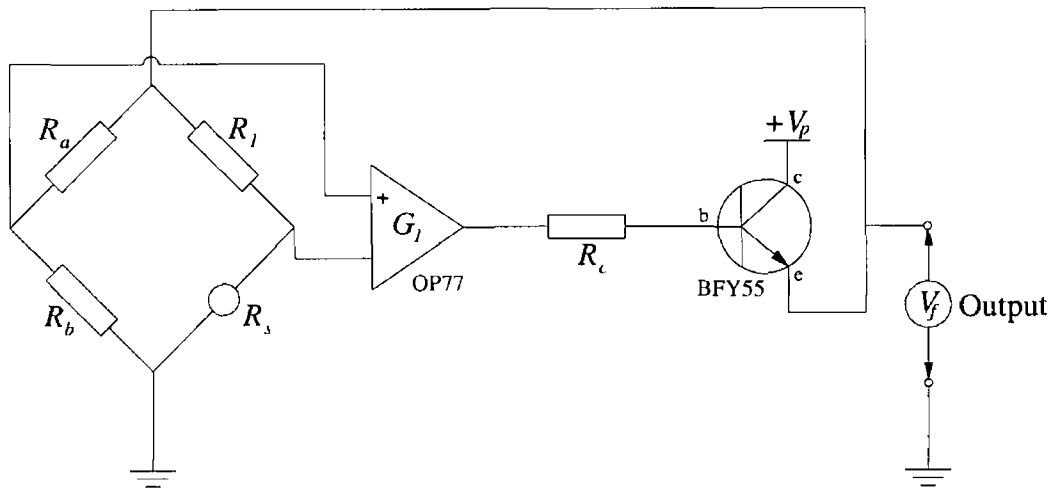

Figure 3 2 Modified Constant Temperature Control Circuit The use of a transistor eliminates the need for an offset to initiate the circuit on start-up

The circuit, which does not incorporate any facility for the injection of an offset voltage, consists of a single stage of gain, G_1, and a transistor that provides the necessary current gain It was found that the choice of components was critical and that only certain types of op-amps and transistors would give stable operation It was also found that the components that gave the best performance depended on the type of sensor being used The components given in Figure 3 2 are the ones that gave the best performance with the glass bead sensors (see section 3 6 1), while those given in Figure 3 4 are for the chip thermistor sensors (see section 3 6 4)

Perry (1982, f) has said that the offset voltage, as well as controlling the response dynamics of the system, is also required to initiate the system at start-up, however the circuit in Figure 3 2 functions as required without the presence of an offset voltage It is believed that this is due to the intrinsic leakage current through the transistor being large enough to cause a voltage difference between opposite arms of the bridge that is of sufficient magnitude to initiate the circuit

3 1 1 Sensor Output

The voltage drop across the sensor is the quantity that is related to the velocity of the fluid, however it was found that any attempt to directly measure the voltage drop across the sensor, or indeed to measure the voltage of any point in the circuit that is directly connected to the inputs of the amplifier, immediately resulted in the circuit becoming unstable and going into oscillation As discussed in section 2 5 4 2, this problem can be overcome by measuring the feedback voltage of the circuit and

calculating the voltage drop across the sensor, V_s, from the measured feedback voltage, V_f, using (2 19), which is

$$V_s = V_f \frac{R_s}{R_1 + R_s}$$

3 1 2 Oscillation and Circuit Stability

A problem that has been encountered throughout the circuit design phase of this work is oscillation and instability of the sensor system A typical example of the output of a circuit that is undergoing oscillation is shown in Figure 3 3 Once oscillation starts to occur the circuit can no longer be considered to be in Constant Temperature mode, which means that the data from it cannot be interpreted from a Constant Temperature stand-point In principle it should be possible to obtain meaningful data from an oscillating system by calibrating it in its oscillating state, however attempts were made to implement this technique and it was found that the oscillation that occurred was not stable and could change dramatically in an unpredictable fashion

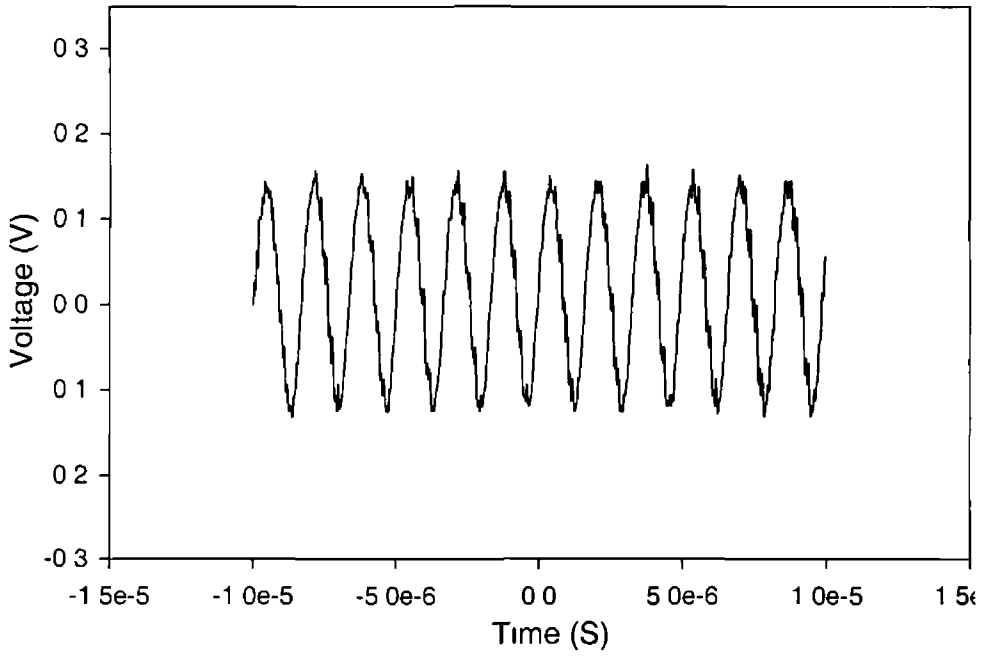

Figure 3 3 Typical output voltage of a control circuit undergoing oscillation The circuit here was oscillating at 600kHz

3 1 3 Saturation of Circuit Output

The output of the amplifier in the circuit shown in Figure 3 2 was found to saturate for large velocities, which indicated that the supply voltages of the circuit needed to be

increased It was found that increasing the supply voltages, V_p and V_n, of the circuit to the maximum rated values of the op-amp, which are +15V and –15V respectively, was not sufficient and that stable operation could not be achieved using op-amps that were rated for use with larger supply voltages The problem of saturation was overcome by the modifying the circuit to that which is shown in Figure 3 4

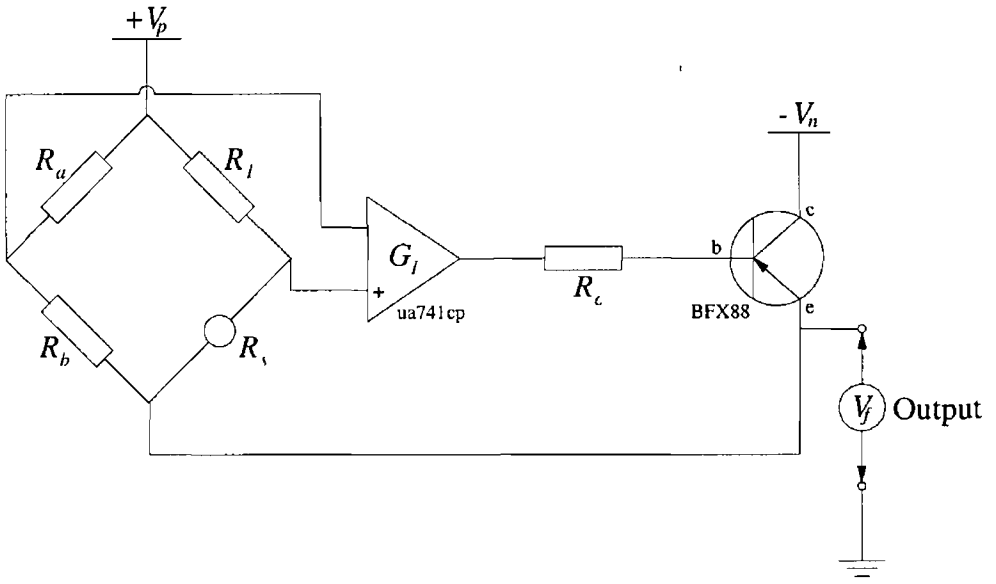

Figure 3 4 Circuit that overcomes the problem of saturation at high power dissipation The component types given are those that resulted in the best performance with a chip thermistor sensor

The top of the bridge is connected to the positive supply rail and the bottom of the bridge is driven by the feedback circuitry The connections at the inputs of the operational amplifier had to be reversed because its output must now be a negative voltage This configuration effectively doubled the maximum voltage that could be applied across the bridge and had no detrimental effects on the stability of the circuit As well as solving the saturation problem there are a number of additional advantages associated with the use of this control circuit The supply voltages of the sensor will be symmetrical about ground, which means that the voltage drop across the insulating coating of the sensor will be lower than would have been the case with the earlier circuit with the result being that failure of the coating is less likely to occur Also, the electrical current demands of the circuit will be approximately evenly distributed between both power supplies, which means that more efficient battery usage and thus longer measurement times can be obtained with battery powered sensor systems being used for field measurements than would be the case with the standard Constant Temperature circuit configuration

3 1 3 1 Determination of Sensor Voltage

As a result of the change in configuration, the relationship between the sensor voltage, V_s, and the feedback voltage, V_f, of the circuit in Figure 3 4 can no longer be described by equation (2 19) and is instead given by

$$V_s = (V_p - V_f)\frac{R_s}{R_1 + R_s} \tag{3 1}$$

3 1 4 Selection of Resistor Values

It was found in section 2 that during operation the resistance of the bridge resistors are related by

$$\frac{R_s}{R_1} = \frac{R_a}{R_b} \tag{3 2}$$

In theory, once the required set point resistance of the sensor is known, arbitrary values of R_1, R_a and R_b can be chosen so that they satisfy (3 2), however in practice there are limitations on the range of values of R_1, R_a and R_b that can be used

As mentioned in section 2 5 4 1, the efficiency of the circuit is maximised by keeping R_a and R_b as large as possible The performance of the control circuit was tested with a wide range of values of R_a and R_b and it was found that the control circuit did not function correctly if $R_a + R_b$ exceeded 80kΩ This is most likely due to the voltage drop across the input impedance of the op-amp becoming large enough to affect the operating characteristics of the circuit Typical values of R_a and R_b are 10kΩ and 20kΩ respectively

It is desirable to keep R_1 as small as possible in order to minimise the required voltage drop across the bridge and also to minimise the power dissipated in R_1 As a result values of R_1 of the order of 50 to 100Ω were used in early circuits however it was found that using such small values sometimes caused the destruction of the sensor, due to excessive heating, in the event of a circuit malfunction that resulted in the maximum possible voltage being applied across the bridge This occurred regularly during the circuit design and testing phase and which resulted in the loss of a significant number of sensors Under conditions where the maximum voltage is being applied across the bridge, the resistor R_1 will act as a current limiting resistor and therefore the current in the sensor and thus the maximum temperature it reaches is

determined by the value of R_1 This means that destruction of the sensor can be prevented by choosing a value of R_1 such that the temperature reached by the sensor in the event of a circuit malfunction will be lower than that at which failure occurs It was found that keeping R_1 above 200Ω achieved this for the two main sensor types, namely glass bead and chip thermistors, that were used during this work

3 1 5 Setting Operating Temperature

A relatively simple method for setting the operating temperature of the sensor that takes all of the constraints mentioned previously into account has been developed

The minimum operating resistance R_s of the sensors being used was found to be ~ 450Ω, therefore setting the ratio given in (3 2) equal to 0 5 to get

$$\frac{R_1}{R_s} = \frac{R_a}{R_b} = 0\,5 \tag{3 3}$$

will ensure that R_1 always remains greater than 200Ω The resistors R_a and R_b are chosen such that $R_a + R_b \leq 80k\Omega$ and are not altered from the values at any stage during set-up or operation Typical values of R_a and R_b that were used during this work are 10kΩ and 20kΩ respectively The required operating resistance R_s of the sensor is determined from its resistance-temperature equation (see section 2 7 3 3) if known, or if not, then the sensor is immersed in water at the required operating temperature and its resistance is measured The value of R_1 that is necessary to achieve this operating resistance is calculated using

$$R_1 = \frac{R_s}{2} \tag{3 4}$$

which follows directly from (3 3)

This method of determining and setting the required sensor operating resistance overcomes one of the main problems associated with the use of thermistor-based sensors, that being that the resistance of thermistors in a particular batch can vary considerably from thermistor to thermistor, with the standard tolerance for commercially available thermistors being 20% For a constant temperature anemometer it is the temperature and not the resistance of the sensor that is critical and this method allows the operating temperature of a sensor, or more importantly of

a number of sensors, to be accurately set to the required value, regardless of the resistance of the sensor

3 1 6 Control Circuit With Offset Voltage Injection

The control circuit shown in Figure 3 4 was used in conjunction with the resistance constraints detailed in the last section during the sensor development phase and functioned satisfactorily with a large number of different thermistor sensors On commencement of testing in the tow tank calibration facility (see section 3 5 2) it was discovered that this circuit had poor frequency response characteristics that prevented accurate calibration of the sensor using this technique (see section 4 1) As mentioned previously, Perry (1982, e) and many more state that the stability and dynamic response of a Constant Temperature system are influenced dramatically by the injection of an "offset voltage" into the feedback loop of the control circuit and they go on to say that the frequency response characteristics of a system can be maximised by "tuning" this offset voltage to the correct value As a result of the newfound desire to improve the frequency response of the system in order to be able to calibrate the sensor using the tow tank, new attempts were made to build a circuit that incorporated offset injection and the circuit shown in Figure 3 5 was developed

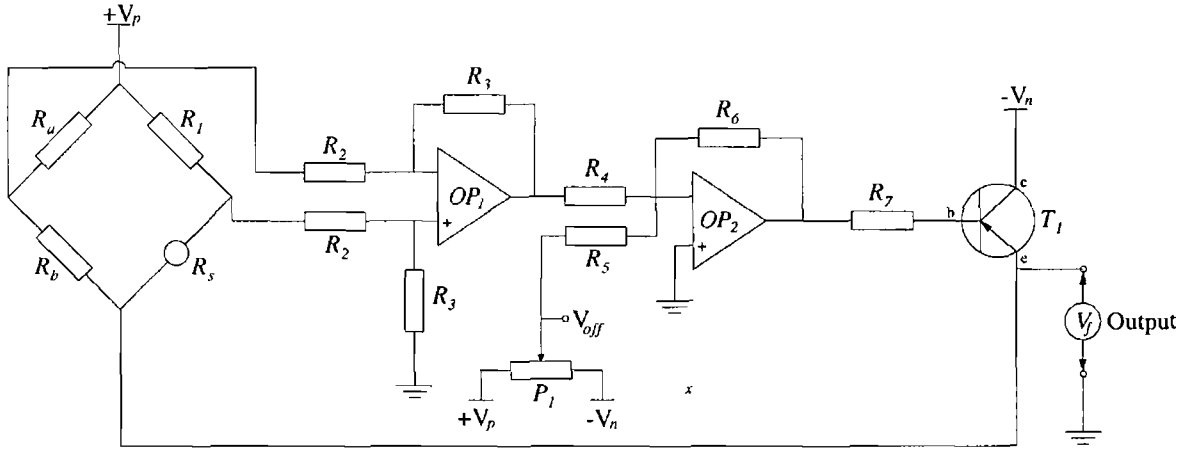

Figure 3 5 Constant Temperature control circuit with offset voltage injection The offset voltage V_{off} is set using a potentiometer (P_1)

The circuit consists of two amplifiers and a current boosting stage with offset injection taking place at the second stage of amplification The saturation limiting design introduced in Figure 3 4 has been used The offset voltage, V_{off}, can be varied by adjusting potentiometer P_1 and a terminal has been included in the circuit to

facilitate its measurement The circuit is very similar to that of Perry (1982, d), which is shown in Figure 3 1, and the method by which constant temperature operation is achieved, is identical to that of the general circuit discussed in section 2 5 4

The stability and frequency response of a system employing the circuit shown in Figure 3 5 has been analysed and details of that analysis are given in section 4 1 It was found that stable operation could only be realised for a certain range of offset voltages and that the frequency response of the system when the offset voltage was tuned for optimum response was a factor of eighty times greater than for the old circuit with the same sensor in identical operating conditions Details of the procedure involved in tuning the offset voltage are also discussed in section 4 1

The stability of this circuit does not rely on the use of selected components, as was the case with earlier circuits, which has substantially increased the usability of the sensor system

3 1 6 1 Open Loop Gain

It has been found that the open loop gain of the control circuit also affects the response dynamics of the system and according to Perry (1982, g) this is to be expected An analysis has been left until section 4 1 3 as some concepts that are not introduced until then are needed in order to interpret the results We will now move on to calculating the open loop gain of the circuit

The first amplifier, consisting of OP_1, R_2, R_2', R_3 and R_3' is a standard difference amplifier, the output of which is described by

$$V_{OP1} = G_1(e_1 - e_2) \tag{3 5}$$

where the quantity $e_1 - e_2$ is the error voltage between the arms of the bridge and

$$G_1 = \frac{R_3}{R_2} = \frac{R_3'}{R_2'} \tag{3 6}$$

The resistors R_2 and R_2, R_3 and R_3 must be very closely matched or the amplifier will have poor common mode rejection and circuit noise will propagate around the closed loop leading to oscillation It was found that metal film resistors with 1% tolerance and a temperature coefficient of resistance of 50ppm gave good performance

The second amplifier, which consists of OP_2, R_4, R_5 and R_6 is an inverting adder The output of the difference amplifier, V_{OP1}, and the offset voltage V_{off} are added

together and the resultant voltage is then amplified and inverted The output, V_{OP2}, is given by

$$V_{OP2} = -\left(V_{off} \frac{R_6}{R_4} + V_{OP1} \frac{R_6}{R_5} \right) \quad (3\ 7)$$

If the resistances R_4 and R_5 are equal then both signals will be amplified by the same amount and (3 7) can be rewritten as

$$V_{OP2} = -G_2 \left(V_{off} + V_{op1} \right) \quad (3\ 8)$$

where

$$G_2 = \frac{R_6}{R_5} = \frac{R_6}{R_4} \quad (3\ 9)$$

The open loop gain, G_{OL}, of the circuit can be found by multiplying G_1 and G_2 This gives

$$G_{OL} = G_1 G_2 = \frac{R_4 R_6}{R_3 R_5} \quad (3\ 10)$$

3.1 6 1.1 Maximising Open Loop Gain

As will be seen in section 4 1 3 it is desirable to have the open loop gain as large as possible The performance of the circuit has been tested for a range of open loop gains and it has been found that it will not function correctly for open loop gains in excess of approximately 50,000 It is believed that this is due mainly to the input impedance of the difference amplifier becoming excessively low for gains above this value A number of techniques of increasing the input impedance of the differential amplifier with the aim of increasing open loop gain were attempted however they were all found to adversely affect the performance and stability of the circuit An AD620 instrumentation amplifier with very high input impedance was tested but its use caused the transient response time of the system to increase by a factor of five Attempts were also made to place voltage follower based buffers between the bridge and the differential amplifier, which would dramatically increase input impedance, however this resulted in occasional system instability and a dramatic increase in noise levels

3 1 6 1 2 Gain Composition

The open loop gain, G_{OL}, is given by the expression

$$G_{OL} = G_1 G_2 \tag{3 11}$$

so therefore a number of different combinations of G_1 and G_2 will result in the same open loop gain For large gains the range of values of G_1 and G_2 that can be used is limited by the maximum and minimum resistance values that can be used with OP_1 and OP_2 such that G_1 and G_2 must be nearly equal For lower gains, a large number of different combinations can be used and it was found that the combination that was used had no discernible effect on the systems performance, i e for an open loop gain of 1000 it did not matter if it was made up by (20×50) or (50×20)

3 1 6.2 Circuit Output

As with all of the control circuits discussed previously it is not possible to measure the sensor voltage V_s directly without inducing oscillation in the circuit so, as before, the feedback voltage V_f is taken as the output of the circuit The anti-saturation configuration introduced in section 3 1 3 is used in this circuit and therefore the sensor voltage V_s is given by (3 1), which is

$$V_s = \left(V_p - V_f\right)\frac{R_s}{R_1 + R_s}$$

3 1 7 Power Supply Considerations

Up to now details of the power supplies have been omitted from the circuit diagrams for the sake of clarity All of the amplifiers in the circuits that have been discussed to date were externally powered from the positive and negative rails, which were at V_p and V_n respectively

A specific requirement of the final system is that it be capable of obtaining measurements in the field This immediately implies the use of batteries, which will have a load dependant and charge related drift Any drift of the supply voltages would be detrimental to the quality of the data obtained with the sensor so therefore voltage regulators are necessary A voltage regulation circuit based on the 78 and 79 series of voltage regulators was implemented It was found that rigorous decoupling of the regulators, according to the manufacturers specifications was necessary or else a low

level oscillation at several hundreds of kilohertz would appear on the outputs This is especially the case for the 79 series negative voltage regulators The voltage regulator circuit, including the required decoupling capacitors is shown in Figure 3 6

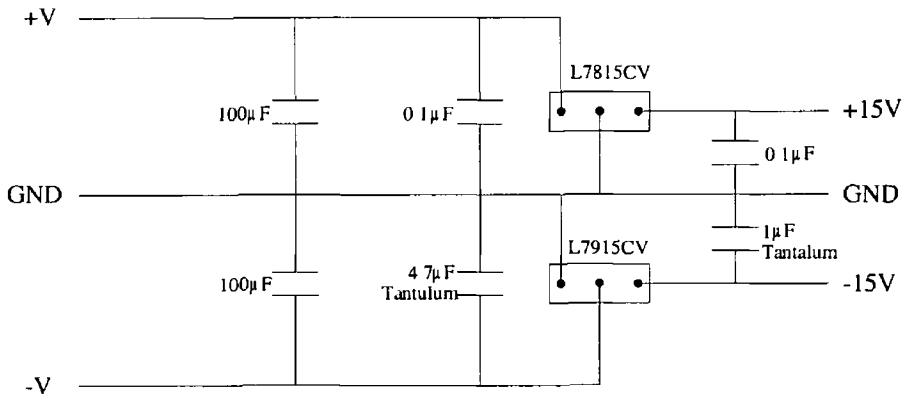

Figure 3 6 Diagram of the voltage regulator circuit The input voltages can be anything up to +24 and –24 volts The exact capacitors shown are necessary for optimum, oscillation free performance of the voltage regulator IC's

When this circuit was implemented in the lab using laboratory power supplies it was found to be necessary to place large 100µF capacitors between the positive and negative inputs and ground to eliminate noise that was present on the output of the supplies These have also been included in Figure 3 6, however it should be noted that they are not required when batteries are powering the circuit

3 2 Temperature Compensation

The difficulty in matching the resistance temperature characteristics of two thermistors as is required for automatic compensation resulted in the decision to implement a mathematical compensation technique as described in section 2 6 3 A second thermistor sensor, operated at low current, was mounted next to the velocity sensor where it would also experience any variations in ambient temperature of the fluid experienced by the velocity sensor The temperature sensor data and velocity sensor data is recorded simultaneously using separate channels of the Analog to Digital converter (see section 3 3)

3.2.1 Circuit

The temperature sensing thermistor is connected in series with a resistor so that the voltage drop across the sensor will be a function of the resistance and thus the temperature of the thermistor This resistor also acts to limit the current in the

thermistor that would cause self-heating that would result in the temperature sensor being sensitive to velocity as well as temperature This "velocity contamination" of the temperature data would be highly undesirable and as a result the series resistance should be kept as large as possible

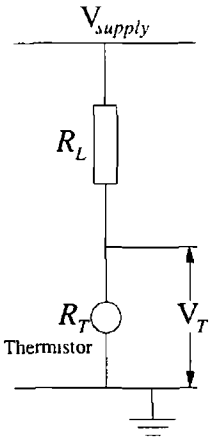

Figure 3 7 Circuit diagram for ambient fluid temperature sensor The resistor R_L limits the current flowing in the sensor and prevents self-heating, which would lead to velocity contamination of the temperature data The resistance of the thermistor sensor is determined by measuring the voltage drop across it, V_T

The calculations and component selection procedures that are described in the following section require the knowledge of the temperature sensors characteristics The characteristics of Sensor 2, which has been used as the temperature sensor for the majority of temperature compensated work that has been carried out, are used The necessary characteristics of this sensor are listed in Table 3 1

Property	Value
Resistance (Ω)	1700
Material Constant, β (K)	3000
Temperature Coefficient of Resistance, α (K^{-1})	0 036

Table 3 1 Properties of Sensor 2 at 15°C

3 2 2 Series Resistor Selection

Comparing the difference between the power dissipated by the temperature sensor when it is in temperature sensing mode and velocity sensing mode should give a good indication of its susceptibility to velocity contamination in the temperature sensing

mode The power dissipated by the temperature sensor in the configuration shown in Figure 3 7 is given by

$$P = R_T I^2 = R_T \left(\frac{V_{supply}}{R_T + R_L} \right)^2 \quad (3\ 12)$$

Using a supply voltage of 5V and a series resistance, R_L, of 10kΩ results in a power dissipation of 0 31mW in Sensor 2 When it is operated in velocity sensing mode this sensor has a power dissipation of the order of 300mW (see Figure 4 17), which means that the power dissipated by Sensor 2 in temperature sensing mode with a supply voltage, V_{supply}, of 5V and a series resistance, R_L, of 10kΩ is a factor of 1000 less than the dissipated power that is required for the sensor to operate in velocity sensing mode, therefore there will be negligible contamination of the temperature data if the sensor is used in conjunction with the stated values of V_{supply} and R_L

3 2 3 Temperature Measurement

Temperature measurement using a thermistor is achieved by measuring the resistance of the thermistor and using its known resistance temperature characteristics to determine the corresponding temperature

The voltage drop across the thermistor is given by

$$V_T = V_{supply} \frac{R_T}{R_L + R_T} \quad (3\ 13)$$

Solving this expression for the resistance of the sensor R_T yields

$$R_T = \frac{V_T R_L}{V_{supply} - V_T} \quad (3\ 14)$$

We now have an expression that allows the resistance of the sensor to be calculated from the voltage drop, V_T, across it, however in order to be able to determine the temperature of the water form this value, the resistance temperature characteristics of the temperature sensing thermistor must be known

3 2 3 1 Resistance-Temperature Characteristics

As a result of the large tolerances in the characteristics specified by the manufacturers of the thermistors being used, it is necessary to determine the characteristics of each thermistor individually if it is to be used for temperature measurement purposes This

can be accomplished by measuring the resistance of the thermistor for a range of temperatures and then fitting an appropriate general equation to the resulting data In section 2 7 3 3 we discussed the fact that there are two possible equations that can be used to describe the resistance temperature characteristics of a thermistor and that of those, the Steinhart Hart (1968) equation is the most accurate Since it is desirable to have the maximum possible accuracy, this is the equation that is being used The resistance of Sensor 2 has been determined experimentally for a range of temperatures A graph the inverse of the temperature, $1/T$, as a function of the resistance of the sensor is shown in Figure 3 8

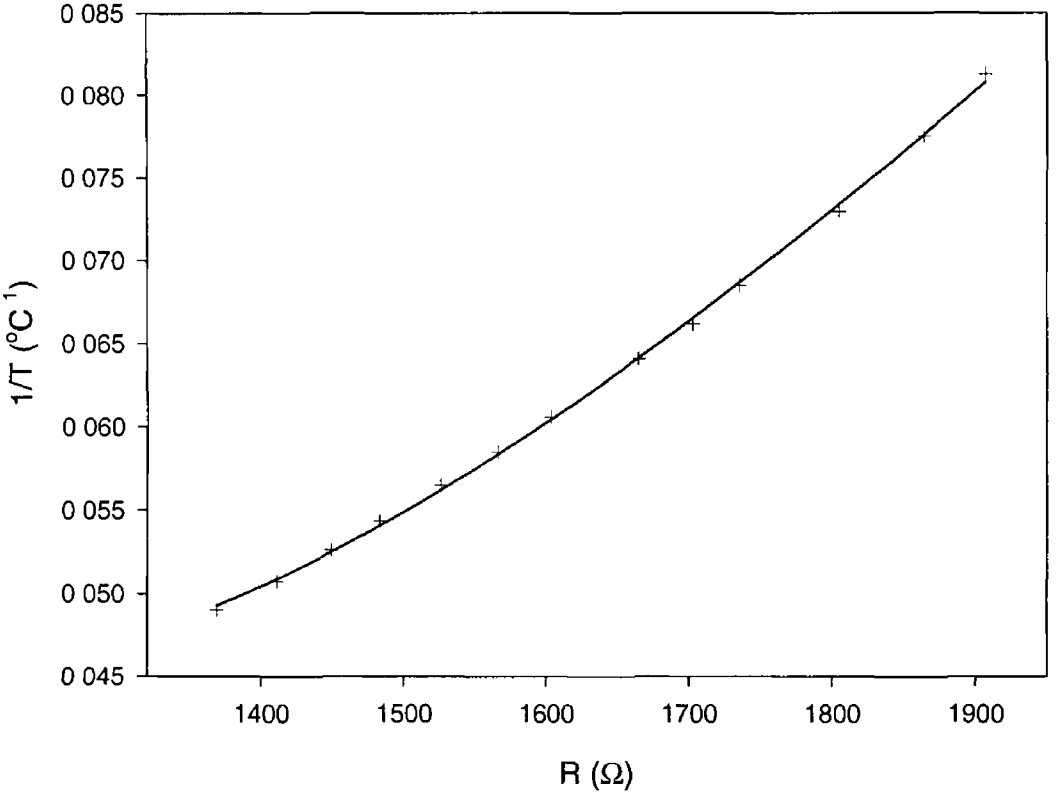

Figure 3 8 Graph of the resistance-temperature characteristics of Sensor B $(+)$ and the Steinhart Hart (1968) function that describes it $(-)$

The best fit of the three-term Steinhart Hart equation

$$\frac{1}{T} = A + B(\ln R) + D(\ln R)^3 \qquad (3\ 15)$$

has been determined and is also shown in Figure 3 8 The values of A, B and D that were obtained are listed in Table 3 2

A	4 472461
B	-0 943083
D	0 006339037

Table 3 2 Coefficients of the three-term Steinhart Hart equation that describes the resistance-temperature characteristics of Sensor 2

Combining the Steinhart Hart equation of the sensor and (3 14) and solving for the ambient water temperature, T_a, results in

$$T_a = \frac{1}{4\,472461 - 0\,943083\left(\ln\left(\frac{V_T R_L}{V_{supply} - V_T}\right)\right) + 0\,006339037\left(\ln\left(\frac{V_T R_L}{V_{supply} - V_T}\right)\right)^3} \quad (3\ 16)$$

which relates the ambient temperature of the water to the measured voltage drop across the sensor

3 2 4 Uncertainty in Temperature Measurements

The output of the temperature sensor circuit is sampled using an Analog to Digital converter and as a consequence of its finite resolution there will be an uncertainty in the temperature measurements obtained In order to be able to evaluate the performance and usefulness of the sensor it is necessary to evaluate this temperature measurement uncertainty If the derivative of (3 16) with respect to sensor voltage, V_T, remains constant for a change in V_T that corresponds to the measurement resolution, δV, of the ADC then the temperature measurement uncertainty, δT, can be given by

$$\delta T = \frac{dT_a}{dV_T}\delta V \quad (3\ 17)$$

where dT_a/dV_T is the derivative of (3 16) with respect to V_T

The quantity dT_a/dV_T does in fact remain virtually constant over the required interval as can be seen in Figure 3 9, which is a graph of (3 16) for a temperature sensor voltage range of 2 37mV, which is the measurement resolution, δV, of the ADC

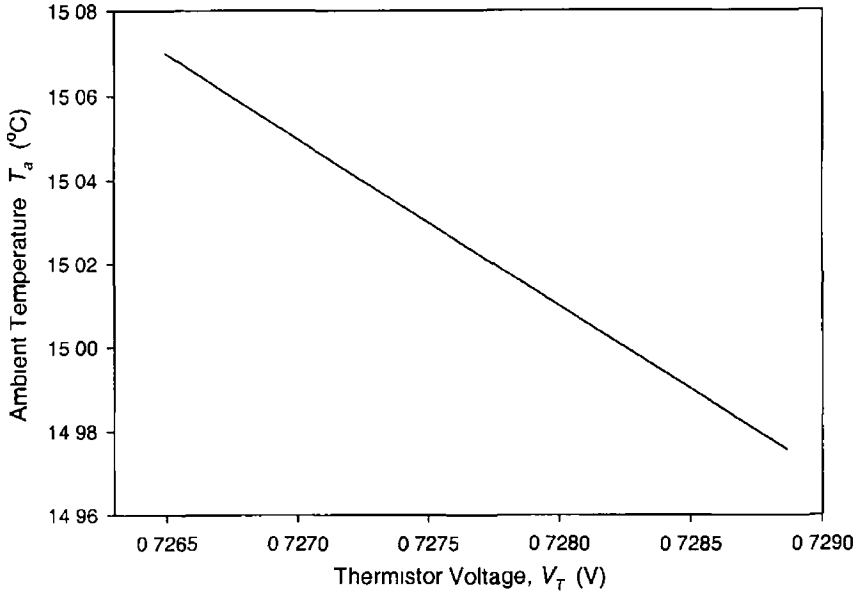

Figure 3 9 Graph of the ambient temperature of the water, as given by (3 16), for a range of values of temperature sensor voltage, V_T that corresponds to the measurement resolution of the ADC being used

In principle it would be possible to evaluate the quantity dT_a/dV_T graphically from Figure 3 9, however it is desirable to obtain an analytical expression that describes it It is quite difficult to obtain an analytical expression for the derivative, dT_a/dV_T , of (3 16), however there is an alternative Using the chain rule, the derivative dT_a/dV_T can be expressed as

$$\frac{dT_a}{dV_T} = \frac{dT_a}{dR_T}\frac{dR_T}{dV_T} \tag{3 18}$$

so that equation (3 17) becomes

$$\delta T = \frac{dT}{dR_T}\frac{dR_T}{dV_T}\delta V_{ADC} \tag{3 19}$$

This can be rewritten as

$$\delta T = \frac{\left(\frac{dR_T}{dV_T}\right)}{\left(\frac{dR_T}{dT_a}\right)}\delta V_{ADC} \tag{3 20}$$

where the quantity

$$\left.\frac{dR_T}{dT_a}\right|_{T_0} \tag{3 21}$$

is the rate of change of the resistance of the thermistor with respect to its temperature at the temperature T_0, which is given by

$$\left.\frac{dR_T}{dT_a}\right|_{T_0} = \alpha R_{T_0} \tag{3 22}$$

where α is the temperature coefficient of resistance of the thermistor at the temperature T_0 The value of α can be calculated from the resistance-temperature data that has been supplied by the manufacturers, which is based on the model that assumes that the relationship between $\ln R$ and $1/T$ is linear This will result in the calculated value of the measurement uncertainty, δT, being less accurate than would have been the case if (3 16) was differentiated directly, however this is not a problem as δT is simply an indicative quantity and as such the reduction in accuracy that results from switching models is of little consequence

The temperature coefficient of resistance of a thermistor is defined by the well-known equation

$$\alpha = -\frac{\beta}{T^2} \tag{3 23}$$

where β is the material constant of the thermistor, which is the slope of a linear fit to a graph of $\ln R$ and $1/T$ data for the sensor and T is its temperature measured in Kelvin Equation (3 23) was used to calculate the values of α quoted in Table 3 1 and Table 3 3 Substituting (3 23) into (3 22) gives

$$\frac{dR_T}{dT_a} = -\frac{\beta}{(T_a + 273)^2} R_T \tag{3 24}$$

This has dealt with the quantity dR_T/dT_a in equation (3 20) and we will now move on to the remaining quantity, dR_T/dV_T, which can be determined by getting d/dV_T of equation (3 14), which gives

$$\frac{dR_T}{dV_T} = \frac{V_{supply} R_L}{(V_{supply} - V_T)^2} \tag{3 25}$$

Finally, substituting (3 24) and (3 25) into (3 20) and dropping the negative sign in (3 24) gives

$$\delta T = \frac{V_{supply} R_L (T_a + 273)^2}{\beta R_T (V_{supply} - V_T)^2} \delta V \tag{3 26}$$

which gives us an analytical expression that can be used to calculate the ambient temperature measurement uncertainty, δT, for a given set of circuit and temperature sensor parameters Note that it is necessary to measure the voltage drop across the temperature sensor for a given temperature in order to be able to evaluate (3 26) This is somewhat cumbersome and it would be desirable to express the voltage drop across the sensor in terms of ambient temperature, T_a, however this would require the inversion of (3 16), which is a cubic polynomial and as we will see in section 4 4 1, this is a very complicated task and is certainly not a viable option in this case

Using the thermistor parameters at 15°C quoted in Table 3 1 and the Analog to Digital converter resolution δV given in Table 3 6 results in a measurement uncertainty δT of 0 11°C Observations have revealed that a change of temperature of less than 0 05°C causes a significant change in the output of the velocity sensor Therefore a temperature resolution of 0 11°C is not sufficient to provide accurate compensation for fluctuations in ambient water temperature Amplifying the output voltage V_T of the sensor by a certain factor will result in a decrease in dR_T/dV_T and thus the temperature measurement uncertainty, δT, by approximately the same factor It was decided to amplify the output voltage of the sensor by a factor of 100, which resulted in the temperature measurement uncertainty decreasing to 0 0011°C, which was found to be more than adequate (see section 4 3 4)

3 2 5 Temperature Compensation Circuit with Amplifier

The temperature sensor circuit incorporating an amplifier is shown in Figure 3 10

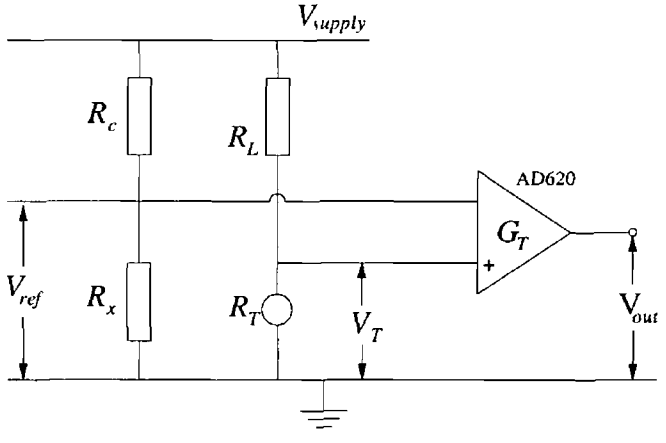

Figure 3 10 Ambient fluid temperature sensor that employs an amplifier to improve resolution

The circuit consists of an instrumentation amplifier with low noise and high CMRR to minimise output noise and measurement error. If the output of the amplifier is to stay within its operating range then the second input of the amplifier must be connected to a reference source that is close to V_T. A potential divider constructed from components with small temperature coefficients (<50ppm) has been found to give good performance. This results in a standard bridge circuit.

The amplifier used is an Analog Devices AD620 instrumentation amplifier. The gain G_T of this amplifier is set by the value of a gain resistor, R_G, connected between pins 1 and 8 of the chip. The manufacturers have provided the following formula for calculating the required value of R_G.

$$R_G = \frac{49.4k\Omega}{G-1} \tag{3.27}$$

For a gain of 100, (3.27) gives a value of R_G of 489Ω. A resistor with this exact value could not be sourced and a 495Ω resistor was used instead. This increased the gain to 100.8.

The output of the amplifier is given by:

$$V_{out} = G_T(V_{ref} - V_T) \tag{3.28}$$

Replacing V_T with (3.13) and solving the resulting expression for R_T yields:

$$R_T = \frac{R_L\left(V_{out} - G_T V_{ref}\right)}{G_T\left(V_{ref} - V_{supply}\right) - V_{out}} \tag{3.29}$$

which allows calculation of the resistance of the thermistor from the output voltage, V_{out}, of the circuit.

3.2.5.1 Setting the Reference Voltage

The reference voltage, V_{ref}, determines the temperatures at which the output of the amplifier goes into saturation and thus defines the operating range of the temperature sensor. In order to minimise the possibility of the need to adjust the reference voltage arising, it should be set such that the output of the amplifier is equal to zero at the centre of the required operating range. There are a number of possible methods of setting the offset voltage at the required value, but since the resistance temperature characteristics of the temperature sensor are known the simplest of these is to use the same resistance as the temperature sensor series resistance, R_L, for R_c and to set R_x

equal to the resistance of the temperature sensor at the required temperature This has been implemented with Sensor 2 for a temperature of 15°C and it was found that the operating range of the temperature sensor was 11 to 20°C, which meant that V_{ref} did not have to be adjusted at all during the calibration process (see section 4 3 4)

3 2 6 Non-Linearity of Thermistor Response Characteristics

Previously, the ambient temperature measurement uncertainty, δT, was evaluated at 15°C, which is approximately at the centre of the required operating range of the sensors being developed during this work, however inspection of (3 26), which is the analytical expression that δT is given by, reveals that it is temperature dependant and that the measurement uncertainty will be greater for higher temperatures This is a direct consequence of the non-linearity of the resistance-temperature characteristics of thermistors If the increase in δT over the operating range of the sensor is significant, then some action may have to be taken to correct for or negate the effects of the non-linearity of the temperature sensors response The measurement uncertainty will decrease for temperatures below 15°C so the measurement uncertainty of interest is that at the upper limit of the operating range, which in this case is 20°C The properties of Sensor 2 were evaluated at 20°C and are given in Table 3 3

Property	Value
Resistance (Ω)	1390
Material Constant, β (K)	3000
Temperature Coefficient of Resistance, α (K ^{1})	0 035

Table 3 3 Properties of Sensor 2 at 20°C

Using these values with (3 26) the measurement uncertainty, δT, at 20°C was found to be 0 0013°C This constitutes a 0 0002°C increase over the uncertainty at 15°C, which is negligible and therefore the non-linearity of the response of the temperature sensor causes no problems and no linearisation etc is necessary

3 3 Data Acquisition and PC Interfacing

The raw velocity and temperature data needs to be digitised and stored on a computer to facilitate processing and analysis This was achieved using an Analog to Digital

Converter (ADC) that connects directly to a PC via its printer port Analog to Digital Converters are specified in terms of their input voltage range, resolution, number of channels and sampling rate

The number of discrete values N that the input voltage range is divided into by an n-bit ADC is given by

$$N = 2^n \tag{3 30}$$

so it follows that the voltage resolution, δV , will be given by

$$\delta V = \frac{V_R}{2^n} \tag{3 31}$$

where V_R is the input voltage range of the ADC This formula shows that for every additional bit in the output of the ADC there will be a factor of two improvement in its resolution The rounding off or quantisation error associated with the discretisation carried out by an ADC manifests itself as steps in the output The measurement uncertainty discussed in the previous section is a direct consequence of this quantisation error

The sampling rate of an ADC determines the maximum frequency that it can resolve The Shannon Sampling Theorem states that in order to be fully reconstructed without any loss, a signal of frequency f must be sampled at a rate S such that

$$S \geq 2f \tag{3 32}$$

For example, an ADC with a sampling rate of 100,000s^{-1} will facilitate the measurement of fluctuations up to 50kHz

3 3 1 Pico ADC22

A Pico ADC22 twenty-two channel ADC was chosen for use with this work Its specifications are listed in Table 3 4

Input Voltage Range (V)	0 – 2 5
No of Bits in Output, n	10
No of Input Channels	22
Voltage Resolution, δV (mV)	2 441
Max Sampling Rate (s^{-1})	10000

Table 3 4 Specifications of Pico ADC22 Analog to Digital converter that was used for data acquisition

The ADC22 can be used with up to eleven velocity sensors with temperature compensation and connects directly to the printer port of any x86 compatible

computer making it simple to use The manufacturer provided a software driver that reads in the data from the ADC and controls its operation Modifications of this driver were necessary and details of these and of the software aspects of the ADC in general can be found in section 3 3 3

3 3 2 Signal Conditioning

The input voltage range of the ADC22 is 0 to 2 5 volts, however the output of the sensors can be anywhere in the range –15 to +15 volts, so therefore the output voltage of the sensors may not lie in the input range of the ADC This problem can be overcome by adding an offset voltage to the output of the sensor and scaling the resulting voltage so that the output range of the sensor matches the input range of the ADC, if necessary The circuit shown in Figure 3 11 has been designed to implement this signal conditioning process It is placed between the output of each sensor that is being used and the relevant inputs of the ADC

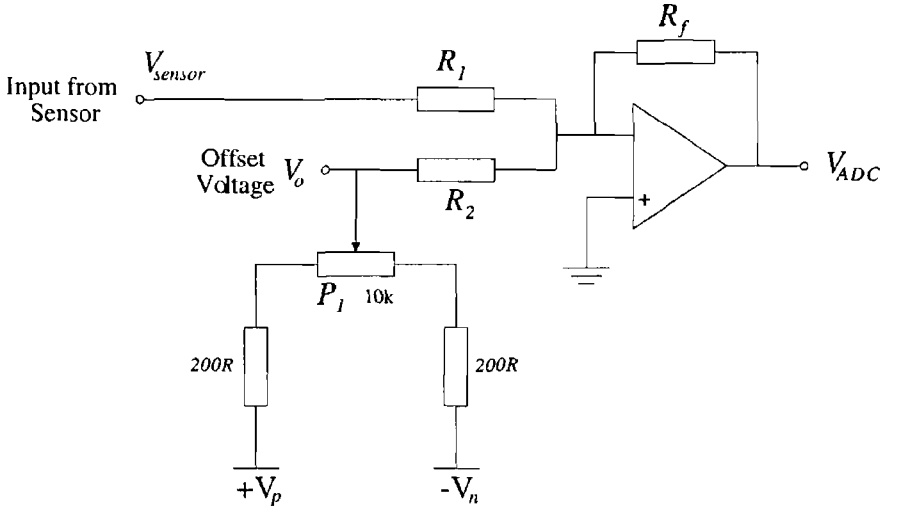

Figure 3 11 Circuit for offsetting and scaling sensor output voltage so to facilitate the use of an ADC The offset is set by adjusting potentiometer P_1 A terminal has been placed in the circuit that allows the offset voltage to be measured with ease

The circuit, which utilises an inverting adder, adds a variable offset voltage, V_o, that is set by adjusting potentiometer P_1, to the sensor output voltage, V_{sensor}, and the resulting voltage can be scaled if so required by adjusting the value of R_f relative to R_1 and R_2 The output of an inverting adder is given by (3 7) and when applied to this circuit results in

$$V_{ADC} = -\left(\frac{R_f}{R_1} V_{sensor} + \frac{R_f}{R_2} V_o \right) \tag{3 33}$$

In order to achieve addition of V_{sensor} and V_o the resistors R_1 and R_2 must be equal so that (3 33) becomes

$$V_{ADC} = -G_{SC} \left(V_{sensor} + V_o \right) \tag{3 34}$$

where the scaling gain G_{SC} is defined as

$$G_{SC} = \frac{R_f}{R_1} = \frac{R_f}{R_2} \tag{3 35}$$

These equations show that the circuit adds the sensor and offset voltage and then amplifies the result by a factor of G_{SC} It is important to note that the signal conditioning offset voltage, V_o, referred to here and the offset voltage, V_{off}, that is injected into the feedback loop of certain control circuits are in no way related

3 3 2 1 Determining the Necessary Offset Voltage and Scaling Factor

We now have a circuit that allows offset addition and scaling and a method of determining the necessary offset voltage and scaling factor must be determined It has been found that the simplest way to set the offset voltage is to force the sensor output to the minimum value in its output range, e g by placing a velocity sensor in still water, and to adjust the offset voltage until the voltage reaching the ADC is very nearly zero This is the required offset voltage and it should be recorded, as it will be needed to process the data that is obtained It was found that it was never necessary to scale the input of the ADC during the course of this work, however the facility to do so is in place if the need ever arose For the sake of completeness, the signal conditioning gain is included in all of the data processing formula although it is always equal to one

3 3.3 ADC Software

Software was provided with the ADC22 that controlled its operation and retrieved the converted data It was necessary to modify the software to overcome a number of shortcomings/limitations, those being

1 The data was written to the screen and not a file so it was not possible to save it for future use

2 There was no facility to adjust the sampling rate or specify how many samples to take before stopping

3 It was not possible to specify the number of channels being used

The modified program now writes the ADC data to a file and prompts the user to specify the filename, number of active channels and duration of the sampling period at start-up A facility was also introduced that allows the user to easily change the sampling rate

As will be seen in section 4 3 2 1, in order to facilitate the use of certain calibration methodologies, it is necessary that the exact time that each data point is recorded by the ADC be known To this end, a function has been added to the program that determines the exact time that each sample is measured at, in terms of the elapsed time since the program started This time data or time-stamp is then written to the output file along with the data point

The modified program, which is written in C, can be found in Appendix C 1 The code contains comments that explain the details of all of the modifications

Typical velocity and temperature ADC data is given in Table 3 5 The format of the table indicates the output format of the file

Identifier	Time Stamp (s)	Digitised Velocity	Digitised Temperature
1	0 000162	675	76
2	0 041095	674	75
3	0 081647	676	75
4	0 122211	678	76
5	0 162759	679	75
6	0 203310	680	75

Table 3 5 Typical output file generated by ADC interface software The time stamp is the exact time that the data was recorded at in terms of elapsed time since the program started This data was obtained at a sampling rate of approximately 25Hz

The data from the ADC is stored as a number z, in the range [0-1023] This data can be converted to voltage by multiplying the number by the resolution, δV , of the ADC as defined in (3 31) The input voltage V_{ADC} corresponding to a given output z is then

$$V_{ADC} = z\delta V \tag{3 36}$$

3 3.4 ADC Calibration

Tests found that the input range of the ADC was slightly different than the value quoted by the manufacturer This causes a change in the calculated resolution, δV , of the ADC and thus affected the conversion of ADC data to voltage These altered values are given in Table 3 6 All of the channels were tested and were found to have the same characteristics

Input Voltage Range (V)	0 – 2 43
Voltage Resolution, δV (mV)	2 374

Table 3 6 Measured range and voltage resolution of the Pico ADC22 These values were used in all calculations instead of those quoted by the manufacturer

3 3 5 Sampling Frequency

The manufacturers of the ADC22 specify a maximum sampling rate of 10,000s ^{1} when used in conjunction with a 33MHz PC It was found that the ADC22 could be used with faster PC's at sampling rates of up to 20,000s ^{1} without any degradation in performance This allows the investigation of velocity fluctuations up to 10kHz, which is more than adequate for the task at hand

3 4 Final Circuit and Data Processing Equations

Each section of the circuit and the equations that describe them have been developed in a piecewise fashion and it is the purpose of this section to bring them all together and to arrive at the complete circuit diagrams and response equations of the final velocity and temperature sensor control and interface circuits The complete circuit diagram containing both circuits is shown in Figure 3 12 and the individual velocity and temperature sensor circuits are analysed in terms of block diagrams in sections 3 4 1 and 3 4 2 respectively

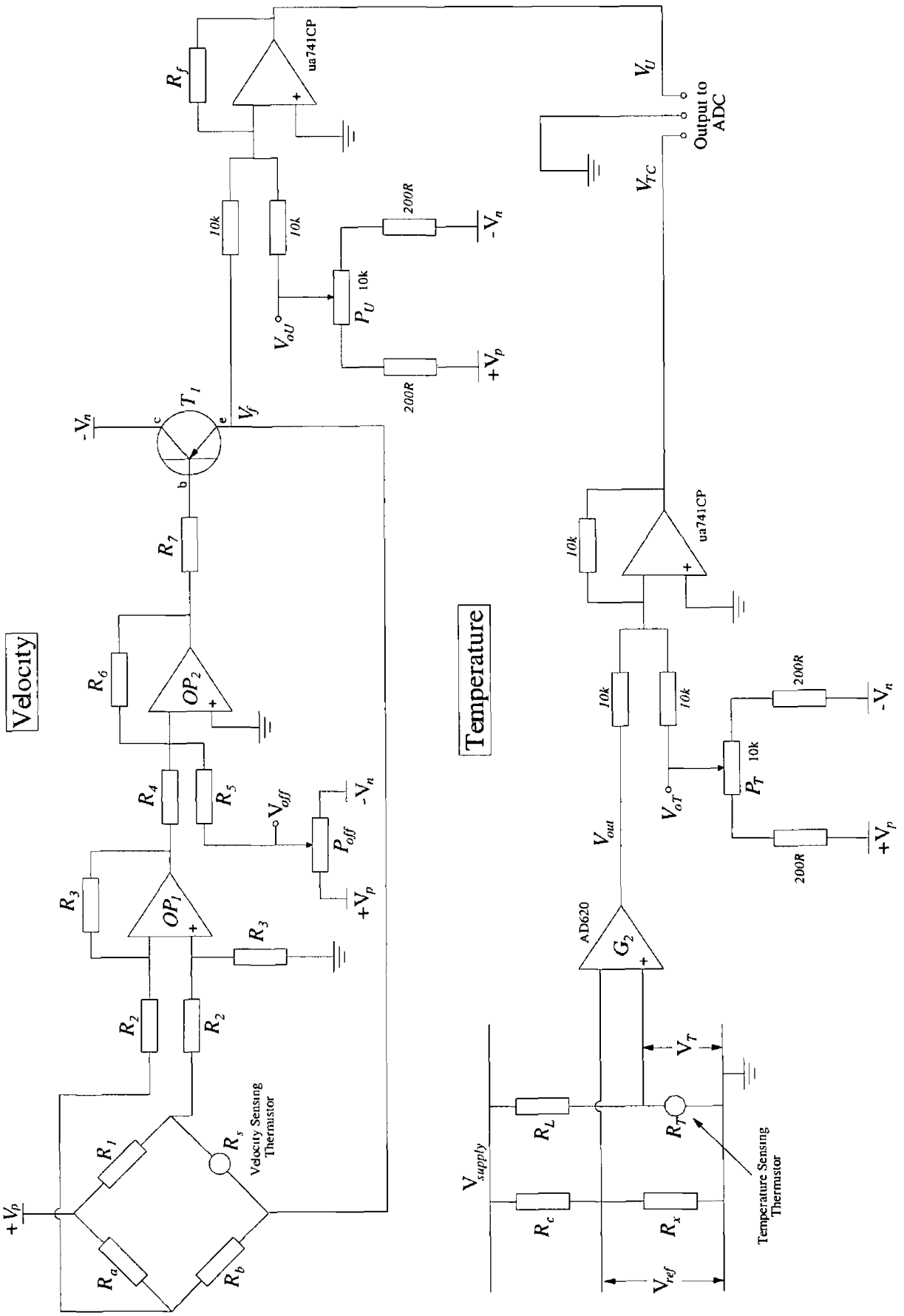

Figure 3 12 Final Velocity and Temperature sensor circuit including Signal Conditioning circuitry

3 4 1 Velocity Sensor

A block diagram of the major components of the velocity circuit is shown in Figure 3 13 The equations describing the response of each individual section have also been included in the diagram

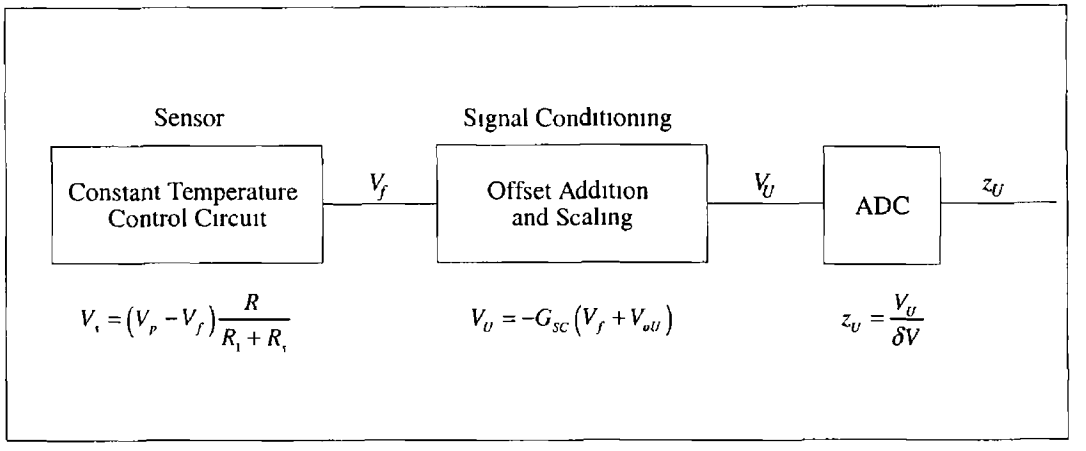

Figure 3 13 Block diagram of the major components of the velocity sensor circuit and the equations that describe their response

The quantity V_{oU} is the velocity sensor signal conditioning offset voltage and V_U is the velocity sensor voltage, as measured by the ADC

Combining the response of each of sections of the circuit as given in Figure 3 13 and solving for the sensor voltage, V_s, results in

$$V_s = \left(V_p + V_{oU} + \frac{z_U \delta V}{G_{SC}} \right) \frac{R_s}{R_1 + R_s} \tag{3 37}$$

which is the expression that is necessary to convert the velocity sensor ADC data to sensor voltage The values of V_{oU}, G_{SC} and V_p are measured directly from the circuit and the values of R_1 and R_s will be known as a result of setting the operating temperature

3 4 2 Temperature Sensor

A block diagram of the major components of the temperature sensor circuit is shown in Figure 3 14

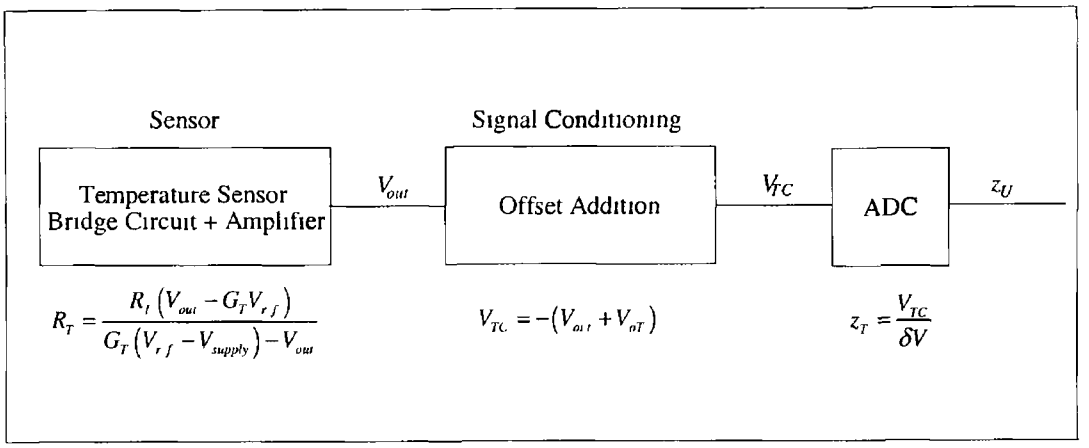

Figure 3 14 Block diagram of the main sections in the temperature sensor sections and the response equations that describe each one

As with the velocity sensor, combining the expressions for each of the sections, as given in Figure 3 14 and this time solving for the sensor resistance, R_T, results in

$$R_T = \frac{R_L\left(-V_{oT} - z_T\delta V - G_T V_{ref}\right)}{G_T\left(V_{ref} - V_{supply}\right) + V_{oT} + z_T\delta V} \tag{3 38}$$

This expression can be used with the Steinhart Hart equation of the thermistor temperature sensor being used to convert raw ADC temperature data into ambient water temperature A function has been written to implement this and can be found in the programs listed in Appendices C 3 and C 4

3 4 3 Using the Measurement System

While this would be a good location for a guide to using the system, a knowledge of some aspects of its operation that are not discussed until chapter 4 is necessary so the guide is instead given in Appendix B

3 5 Calibration Facilities and Procedure

As we have discussed in section 2 7 3 1 theoretical models do not adequately describe the response of thermistor based anemometers to fluid velocity so therefore the exact response of the sensor must be determined by calibration This is accomplished by exposing the sensor to a range of accurately known velocities and recording its response Two calibration facilities, namely a gravity tank, which can be used in the range 0 2 to 2ms^{1} and a tow tank, which operates over the velocity range of 0 01 to 0 6ms^{1}, have been developed during the course of this work for the purpose of sensor calibration

3 5 1 Gravity Tank

The simple gravity tank that was developed is shown in Figure 3 15

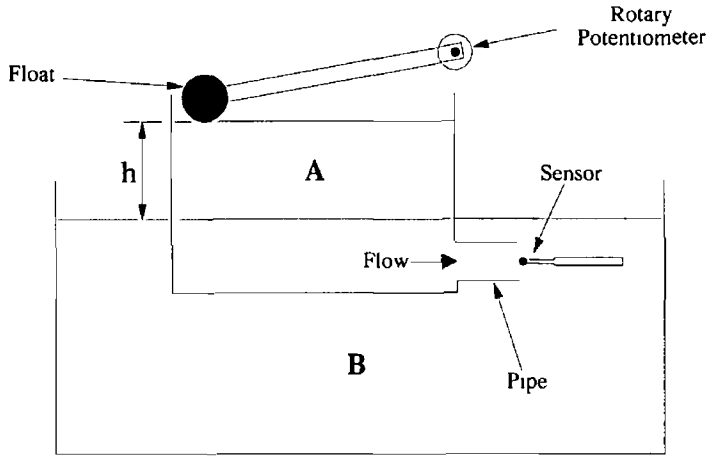

Figure 3 15 Gravity driven calibration system The height h determines the velocity of the water in the pipe and is determined by measuring the voltage from the potentiometer The pipe and sensor are submerged under water to prevent an air bubble from forming around the sensor during calibration

The velocity of the water in the pipe at the base of the tank is dependant on the height of water in the tank so that as it empties the velocity will decrease The sensor is simply placed in the flow at the end of the pipe

It was necessary to submerge the outlet of the pipe in water to prevent a large air bubble from forming around the sensor A number of methods of measuring the velocity of the water in the pipe were used, the first of these being a float based mechanism that measured the height of the water in the tank, which can be related to the velocity of the water in the pipe, U , by

$$U = \sqrt{kgh} \tag{3 39}$$

where h is the height of the water in the tank, g is the acceleration due to gravity and k is a scaling constant, which to a first approximation can be taken to be equal to 2 so that (3 39) becomes

$$U = \sqrt{2gh} \tag{3 40}$$

The float mechanism is also shown in Figure 3 15 and consists of a float that is attached to a low friction potentiometer, the output voltage of which will be a function of the angle of the float Using simple trigonometry this angle can be used to determine the height of the water in the tank

The output voltage of the level sensor potentiometer and the sensor output voltage were recorded simultaneously using two separate channels of the ADC22, which meant that measurements of both quantities were made virtually simultaneously and as such, no further processing was required

The float method of determining the water velocity in the pipe was easy to implement however it was found that accurate results could not be obtained for velocities below ~ 0 2ms ^{1} (see Figure 3 30)

The only other feasible method of measuring the velocity of the water in the pipe was to place a velocity sensor of some description into the pipe beside the sensor being calibrated The only velocity sensor that has small enough dimensions to be used in this situation is a Pitot tube The Pitot tube sensor shown in Figure 3 16 was designed and constructed

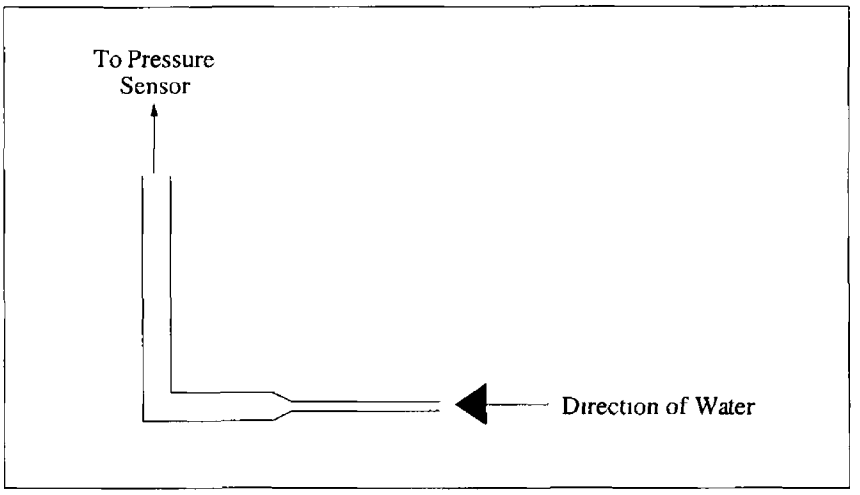

Figure 3 16 Pitot tube velocity sensor for use with the gravity tank calibration facility The tube is placed directly in the flow that is to be measured, as shown

The sensor consists of a Pitot tube, which was constructed by modifying a glass capillary tube, one end of which is placed directly in the flow and other is connected to a pressure sensor It operates on the principle that the pressure in the tube is a function of the velocity of the water It was found to function satisfactorily however it had a lower measurement limit equal to that of the float, which is not adequate and as a result the analysis of its response is being omitted

In working with the gravity tank it became obvious that the absence of a method of accurately measuring low velocities makes any calibration technique that involves water flowing past a stationary sensor unsuitable The only other alternative is to devise a method of moving the sensor through stationary water in the hopes that the

velocity of a moving sensor can be measured to a lower limit than is possible with water.

3.5.2 Tow Tank

The problem of inaccurate calibration of the sensor at low velocities was overcome by developing a tow tank calibration facility in which the sensor is moved at a known velocity through a stationary body of water. Tow tank facilities are widely used to calibrate flow sensors, for example Wu and Bose (1993). Figure 3.17 shows a diagram of the tow tank facility that was developed.

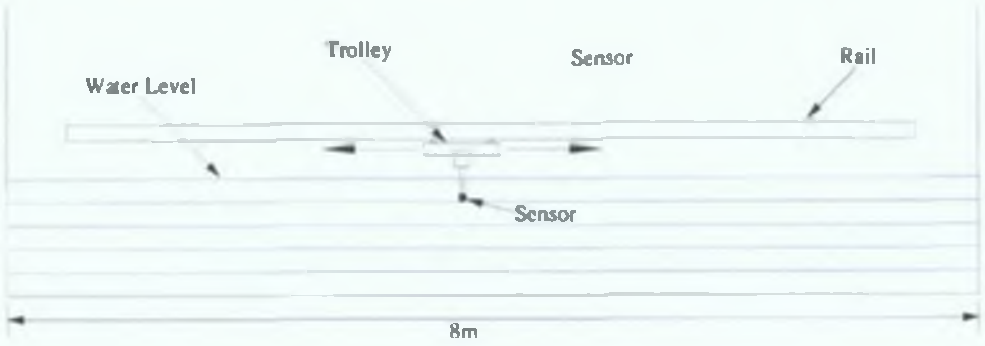

Figure 3.17 Tow Tank Calibration Facility

The facility consists of an 8m long, 0.5m wide and 0.4m deep, water tank, which is also used for water wave and soliton experiments. A rail was installed running along its length above water level. A trolley, on which the sensor is mounted, slides along this rail. Motion of the trolley is controlled using a motor and a system of pulleys as shown in Figure 3.18.

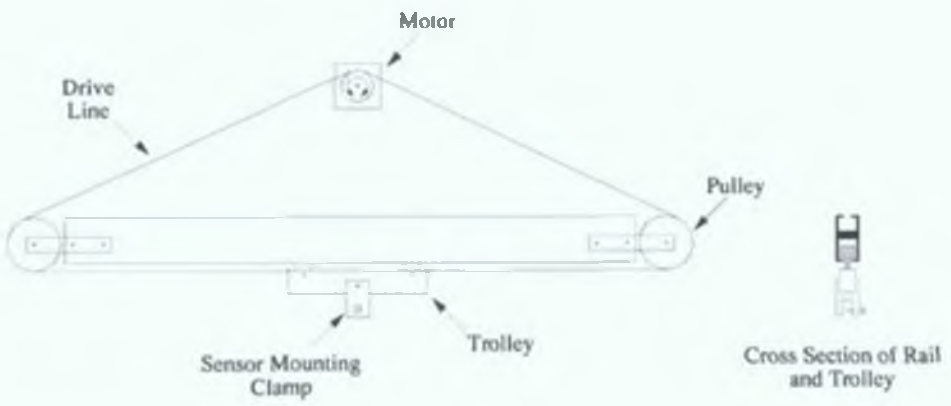

Figure 3.18 Schematic of rail, trolley and drive system. The speed and direction of the motor are variable. Also shown is the sensor mounting clamp that is used to mount the sensors on the trolley. The driveline is made from dyneema, a material that has good water resistance properties and has a high degree of inelasticity.

The operating velocity range of the system is determined by a number of factors including the gearing ratio of the motor gearbox and the size of the pulleys and within this range the velocity is controlled by the supply voltage of the motor. In principle any velocity range should be possible by using the appropriate gearbox and/or pulleys, however in practice the maximum velocity of the trolley is dictated by the torque of the motor and it was found that the maximum velocity that could be attained with the strongest motor that was available was $0.6ms^{-1}$.

3.5.2.1 Velocity Measurement

A number of different methods of measuring the velocity of the trolley and thus the sensor were considered, including at one stage the reflection of acoustic waves from the trolley. The technique that was finally decided upon was to measure the angular velocity of one of the pulleys in the system, which would be directly related to the linear velocity of the trolley.

An optical chopper that passes through a slotted opto-switch is mounted on the pulley wheel and as it rotates the slotted opto-switch gives out a series of voltage pulses that correspond to the passage of blank sections in the optical chopper.

Figure 3.19 Optical chopper and slotted opto-switch assembly. In this picture it is located on Pulley 2 (see Figure 3.23). As the chopper rotates the slotted opto-switch gives out a series of voltage pulses that are ttl compatible, allowing the signal to be connected directly to a PC or other digital device for analysis.

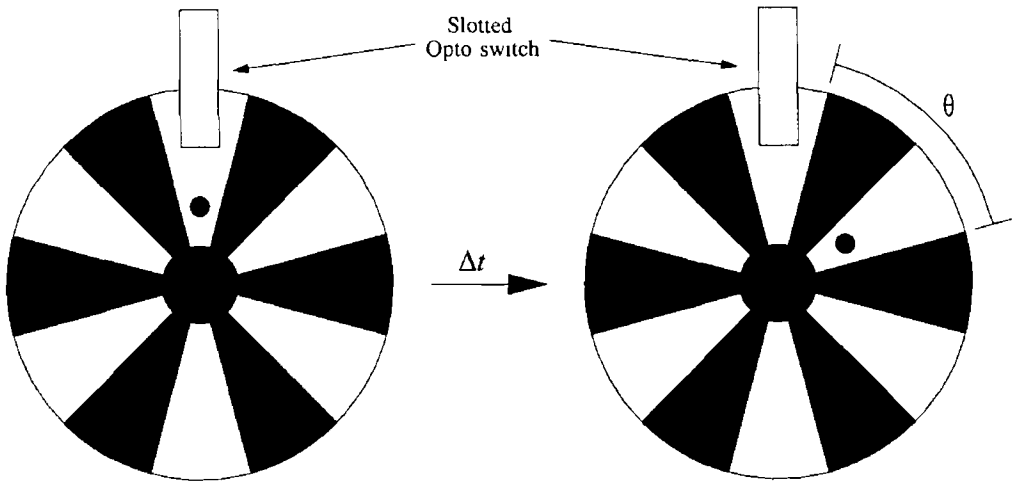

Figure 3 20 Rotation of the chopper that corresponds to one pulse from the slotted opto-switch The time taken or duration of the pulse is Δt and the angle the chopper moves through during the pulse is θ

The time interval, Δt, between the voltage pulses from the slotted opto-switch is the time taken for the chopper to rotate from like segment to like segment Once the distance, D, that the trolley travels during Δt is determined then the velocity, U, of the trolley and the sensor can be calculated using

$$U = \frac{D}{\Delta t} \tag{3 41}$$

The distance, D, that the trolley travels as the pulley rotates through the angle θ (see Figure 3 20) is given by

$$D = r\theta \tag{3 42}$$

where r is the radius of the pulley wheel and θ is measured in radians

The angle θ that corresponds to a pulse from the slotted opto-switch is given by

$$\theta = \frac{2\pi}{n} \tag{3 43}$$

where n is the number of segments in the optical chopper Replacing θ in (3 42) with (3 43) yields

$$D = \frac{2\pi r}{n} \tag{3 44}$$

Combining this with the expression for velocity, (3 41), results in

$$U = \frac{2\pi r}{n\Delta t} \tag{3 45}$$

This expression reveals that the velocity of the sensor can be determined by measuring the duration Δt of the pulses form the slotted opto-switch The resulting

calculated velocity is not an instantaneous measurement but is instead the mean velocity of the sensor over the time interval Δt

Figure 3 21 shows the typical output of the opto-switch as the chopper rotates

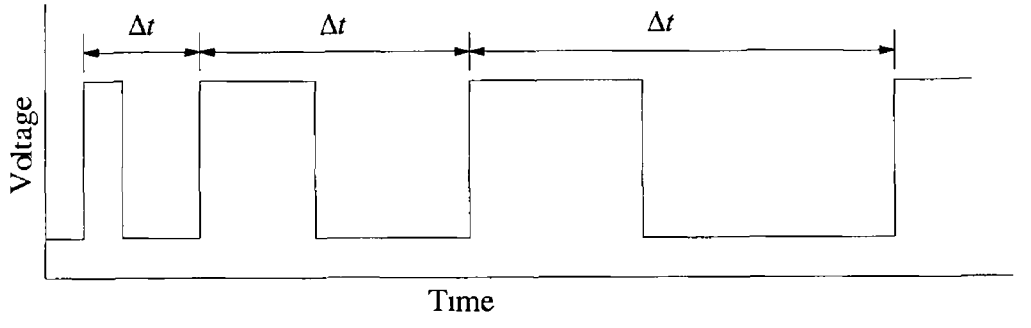

Figure 3 21 Output of slotted opto-switch as chopper rotates The velocity of the chopper is decreasing with time

The digital nature of this output lends itself to analysis using a micro-controller or PC In this case the signal from the opto-switch was connected to a PC using a Bytronics, digital interface card A program, which can be found in Appendix C 2, was written to record the time interval Δt between rising edges of adjacent pulses in the signal and convert these values to sensor velocity By using a continuous polling technique, whereby the input is continuously monitored, an accuracy of $\sim 9\times10^{-6}$s in the measurements of Δt was achieved This corresponds to an accuracy of approximately $1\ 8\times10^{-3}$ms^{-1} in velocity measurements for a velocity of 1ms^{-1} and a pulley radius of 10mm, which constitutes a percentage error of 0 18%, which is well below the magnitude of the velocity variations caused by roughness in the gearbox (see section 4 3 2 2) The program allows the user to specify the properties of the chopper and pulley wheel being used for the measurements, which are required in order to calculate velocity from the Δt data, so that changes may be made to the configuration of the system Each calculated mean velocity is time stamped with the time at the end of the interval Δt over which it was calculated Strictly speaking, the velocity measurement should be assigned to the time at the centre of the interval Δt however the difference only amounts to a few milliseconds and does not lead to any problems Details on the specifics of the program are provided in the form of comments in the code, which can be found in Appendix C 2

A number of factors were found to adversely affect the performance of the tow tank facility and some alterations and improvements of the design were necessary

3.5 2 2 Trolley Oscillation

In order to achieve accurate calibration of the velocity sensor it is desirable to have motion of the trolley along the rail as smooth as possible and to this end the rail and the trolley mounting were kept well lubricated using high quality oils, however the trolley was still found to undergo random mechanical oscillation as it moved along the rail and it was determined that this was caused by the driveline being over-tensioned Oscillation of the trolley is evident in the velocity data shown in Figure 3 22

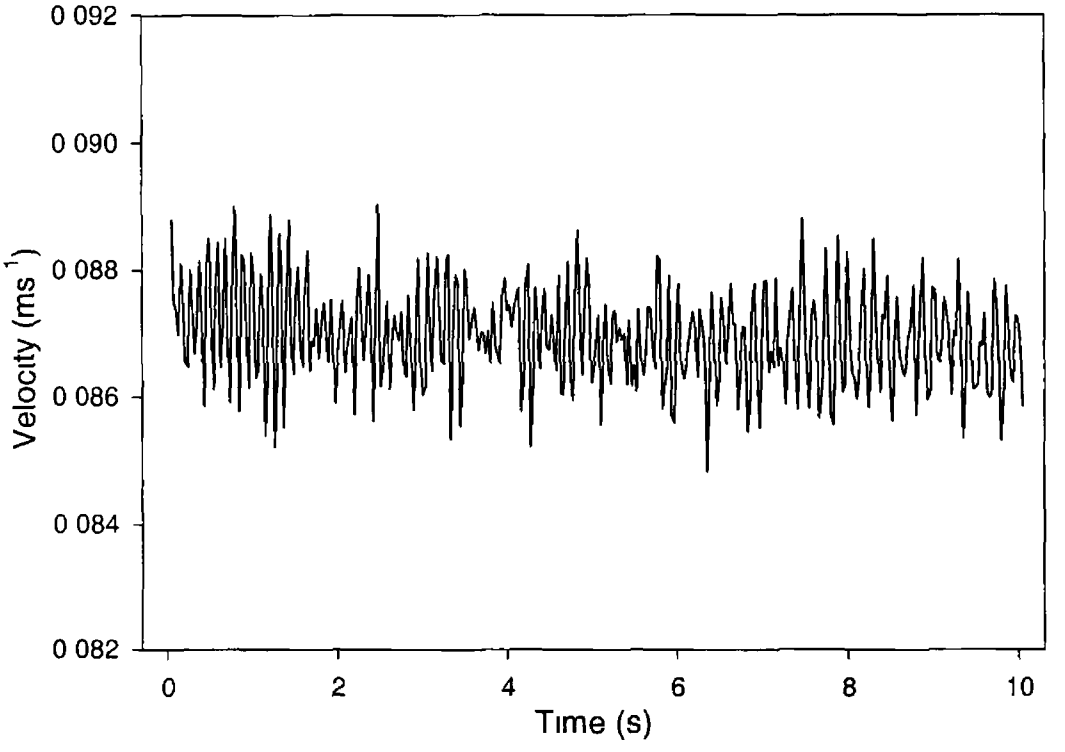

Figure 3 22 Velocity of the trolley as measured with the optical chopper apparatus Oscillation, which is caused by excess tension in the driveline is clearly visible

A tensioner that allowed the tension in the driveline to be accurately adjusted was incorporated into the drive system and is shown in Figure 3 23

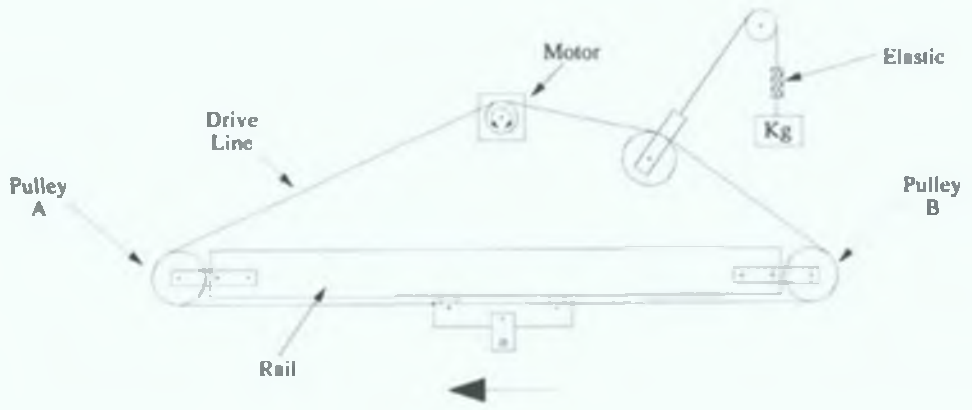

Figure 3.23 Schematic of the trolley drive system, including the tensioner, which has been introduced to prevent oscillation of the trolley.

The tension of the driveline is adjusted by adding weights to the mass hanger allowing it to be precisely controlled. The elastic material is necessary in order to absorb high frequency vibrations that the weight would not be able to respond to due to its inertia. The trolley moves in the direction shown when a sensor is being calibrated so the tensioner was positioned on the "passive" side of the motor so that it would not be affected by any stretching of the driveline caused by non-uniform rail friction, cable drag etc. Figure 3.24 shows graphs of velocity data with and without the tensioner in place and it can be seen that the introduction of the tensioner leads to a significant reduction in the magnitude of the oscillation of the trolley.

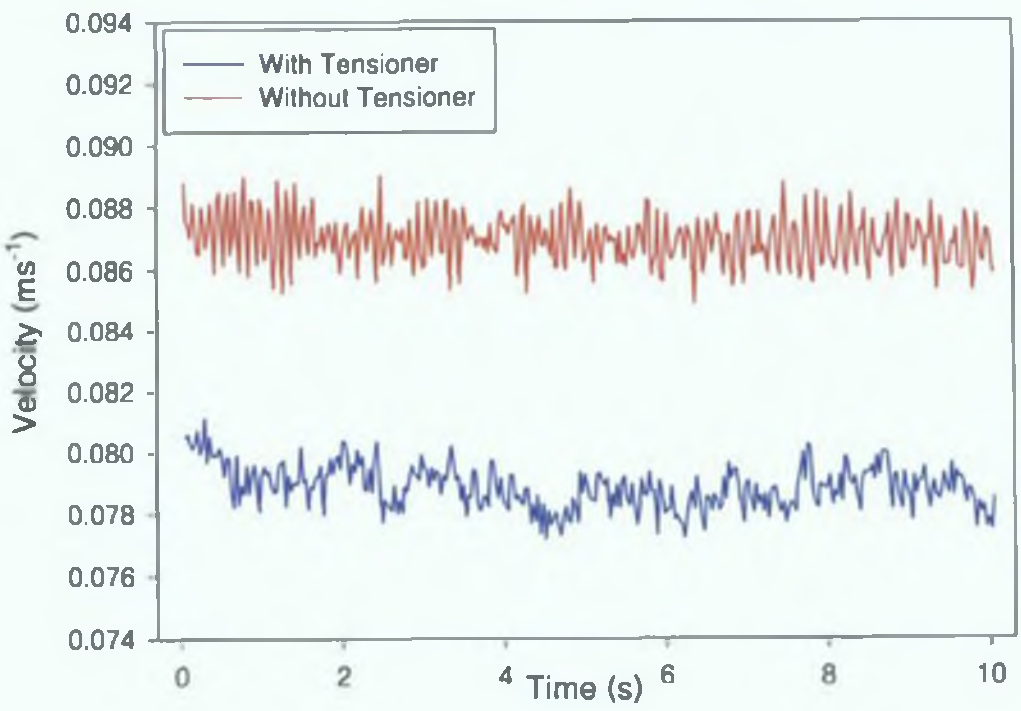

Figure 3.24 Trolley velocity data with and without tensioner for constant motor speed. Introduction of the tensioner leads to a significant reduction in oscillation of the trolley.

3.5.2.3 Chopper Location

Initially the chopper and slotted opto-switch assembly was located on the drive pulley that is attached to the motor however it was found that significant noise was being introduced to the data by roughness in the operation of the motor and the gearbox. This noise signal was not evident in data from the velocity sensor, which would indicate that it is largely absorbed in the driveline. This means that the velocity data from the chopper did not accurately reflect the actual velocity of the sensor. The noise levels in the velocity data analysed for each of the possible chopper locations and it was found that the best performance was obtained when the chopper was located on pulley B. Figure 3.25 shows velocity data that was obtained with the chopper on the motor pulley and pulley B and the reduction in velocity noise or variations is considerable.

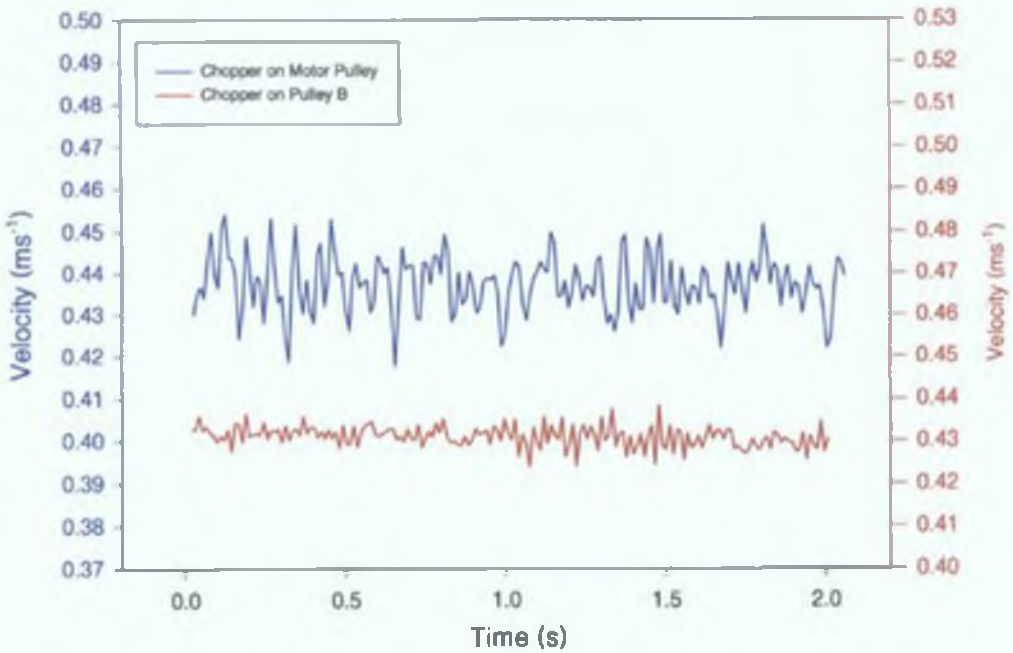

Figure 3.25 Velocity data for identical operating conditions at two chopper locations. A factor of two reduction in the noise in the data is achieved by relocating the chopper from the drive pulley on the motor to Pulley B (see Figure 3.23).

3.5.2.4 Sensor and Cable Mounting

The sensor is mounted on the trolley using a mounting clamp, details of which are shown in Figure 3.18, and the cable is suspended from the rail using nylon sliders, which have a low coefficient of friction. The cable is attached to the sliders in such a way as to ensure that when the trolley and sensor are at the start of the track that the cable is coiled up neatly and doesn't obstruct the sensor in any way. The cable coming into close proximity of the sensor would have a significant effect on its performance

and would render the data set useless. As the trolley moves along the tank the cable uncoils as needed. The picture in Figure 3.26 shows a section of the connecting cable with nylons sliders attached.

Figure 3.26 The sensors connecting cable slides along the rail on low friction nylon sliders. As the trolley moves along the rail the cable coils and uncoils like a spring.

3.5.2.5 Sample Rate

The optical chopper technique uses the time taken to move a certain finite distance to calculate the velocity of the sensor and as a result, the sampling frequency of the velocity data will vary with velocity - as the velocity decreases, so will the effective velocity sampling rate and visa versa. This principle is evident in Figure 3.21.

This does not cause any problems during calibration as, in general, lower sampling rates are adequate for low velocities.

3.5.2.6 Data Synchronisation

The outputs of both the sensor data and velocity data acquisition systems are files containing time stamped sensor and velocity data. In order to use this data for calibration purposes it is necessary that both these sets of data be synchronised – that is, the time stamps of both data sets must be relative to the same starting point.

It is not possible to run both of the data acquisition systems with sufficient accuracy on a single PC so therefore it was necessary to use separate computers for each acquisition system. This meant that the time stamps of both data sets, which are recorded in terms of elapsed time since program start-up, were not synchronised in any way. This problem was overcome by utilising the digital output that is built into the ADC22 Analog to Digital Converter that is used for sensor data acquisition. The

sensor data acquisition program (see appendix C.1) sets the digital output of the ADC22 high when it starts acquiring data. This output is connected to the Bytronic digital interface card that is used to obtain the velocity data and the velocity data acquisition program (see appendix C.2) was altered to start acquiring data when it detected the high signal from the ADC22. This method worked very well and resulted in the data sets being synchronised to within <10μs.

This only resulted in the synchronisation of the first points in each file due to the variable sampling rate of the optical chopper apparatus. Synchronisation of all the points in a given data set requires further data processing, which is discussed in section 4.3.2.1.

3.6 Sensor Design

3.6.1 Glass Bead

The first sensor design used a Thermometrics GM102 glass bead thermistor similar to those used by Katz (1987), LeBarbera and Vogel (1976). Glass bead thermistors are widely used for temperature measurement and so are widely available. Some manufacturers have not recommended their glass bead thermistors for use in applications involving self-heating, however Thermometrics state that the model used is suitable. The thermistor was mounted as part of a probe assembly as shown in Figure 3.27.

Figure 3.27 Glass Bead Thermistor Sensor. The thermistor is mounted in a rigid conical plastic tube. Insulation at the bead/tube interface is achieved using cyanoacrylate-based adhesive. This assembly is then connected to a semi-rigid nylon tubing, through which the connecting cable passes.

The lowest resistance value available, 1kΩ at 25°C, was used in order to minimise the required bridge supply voltage, as discussed in section 3.1.

3 6 1.1 Performance

These sensors were found to function satisfactorily for a number of days or even weeks, however their output would eventually start to drift, with the magnitude of the drift increasing with time Also, some of the sensors were observed to abruptly undergo changes in their velocity response characteristics The glass bead thermistors consist of a bead of thermistor material that is completely encapsulated in glass When viewed under a microscope the thermistor material/glass interface of sensors that had been affected by drift appeared to be different than that of an un-used thermistor, with a possible explanation being that the thermistor material and the glass coating of the sensor that had undergone drift had somehow separated Such a separation would cause a change in the heat transfer properties and thus the velocity response of the thermistor A sensor that drifts is of little use as constant recalibration is necessary In extreme cases it was found that the sensors response would change appreciably in as little as five minutes

Another problem that occurred occasionally with these glass bead thermistors was failure of the thermistor due to cracking of the bead A singular cause of this cracking could never be isolated, however it is suspected that thermal stresses caused by rapid changes in water velocity were a factor

These problems make this particular thermistor type unsuitable for use in water based thermal anemometry applications A review of available glass bead thermistors found that they all had similar design characteristics and as such could be expected to suffer from the same problems as the Thermometrics thermistor that was used

The lack of suitability of glass bead thermistors meant that an alternative had to be found This choice was influenced by the operating range of the glass bead sensor, which is discussed in the next section

3 6 2 Sensor Range

As a result of the intrinsic noise in the output voltage of the velocity sensor, every output voltage measurement will have an uncertainty associated with it, the magnitude of which is determined by the magnitude of the noise Therefore the velocity that is subsequently calculated from each velocity sensor output data point will also have an uncertainty associated with it, with the relationship between the sensor output uncertainty and the uncertainty in the resulting velocity measurement being

determined by the sensitivity of the sensor Figure 3 28 shows a section of the response curve of a typical velocity sensor and illustrates the concept of noise induced measurement uncertainty

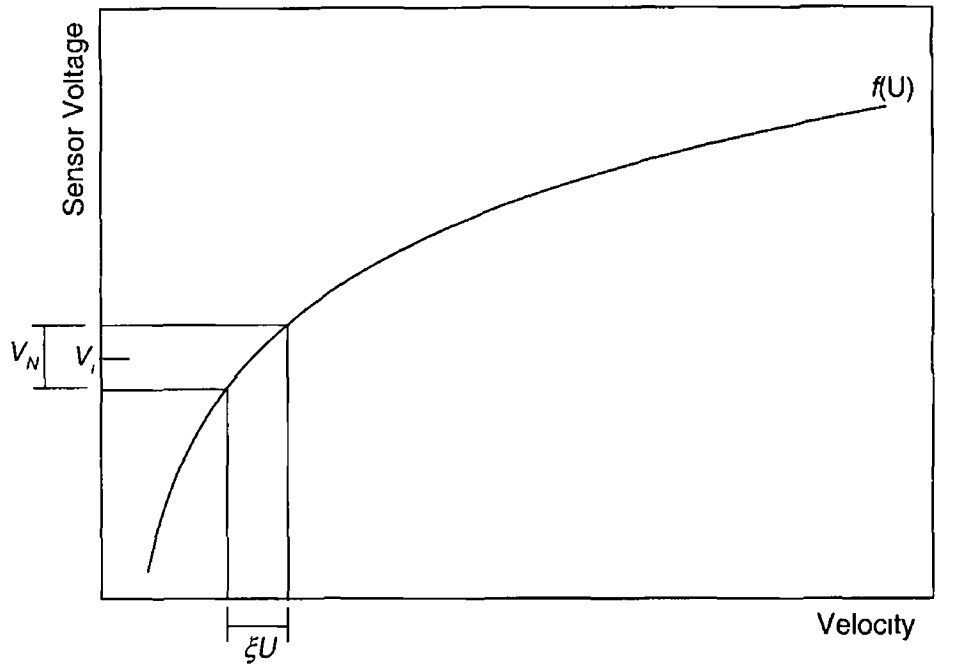

Figure 3 28 *f(U)* is the function that describes the velocity dependence of the output voltage of the sensor, V_N is the peak to peak noise in the output voltage of the sensor and ξU is the velocity measurement uncertainty in the velocity value that results from the sensor voltage V_i

It can be seen that the velocity measurement uncertainty will increase with increasing velocity as a consequence of the decreasing sensitivity of the sensor, until for some velocity it will be greater than what is acceptable The velocity at which this occurs is the maximum velocity that can be measured by the sensor If the velocity response equation of the sensor and the peak to peak noise levels in the sensor output are known then it is possible to calculate the velocity, U_R, at which the uncertainty in the calculated velocity measurement, ξU, will reach a certain specified value

The easiest way to accomplish this is to decide upon the maximum allowed velocity measurement uncertainty, ξU, and to calculate the corresponding sensor output uncertainty, ξV, for a range of velocities The quantity ξV for a particular velocity is the uncertainty in the sensor output that corresponds to the maximum allowed velocity measurement uncertainty and is therefore a measure of the maximum peak to peak noise that can be present in the sensor output This means that the maximum velocity that can be measured to within a given uncertainty is the velocity at which the quantity ξV becomes equal to the peak to peak noise, V_N

The sensor output uncertainty, ξV, that corresponds to a certain velocity measurement uncertainty, ξU, is given by

$$\xi V = f\left(U + \frac{\xi U}{2}\right) - f\left(U - \frac{\xi U}{2}\right) \tag{3 46}$$

where $f(\ )$ is the function that describes the velocity dependence of the sensor voltage The calculation performed by (3 46) is illustrated in Figure 3 29

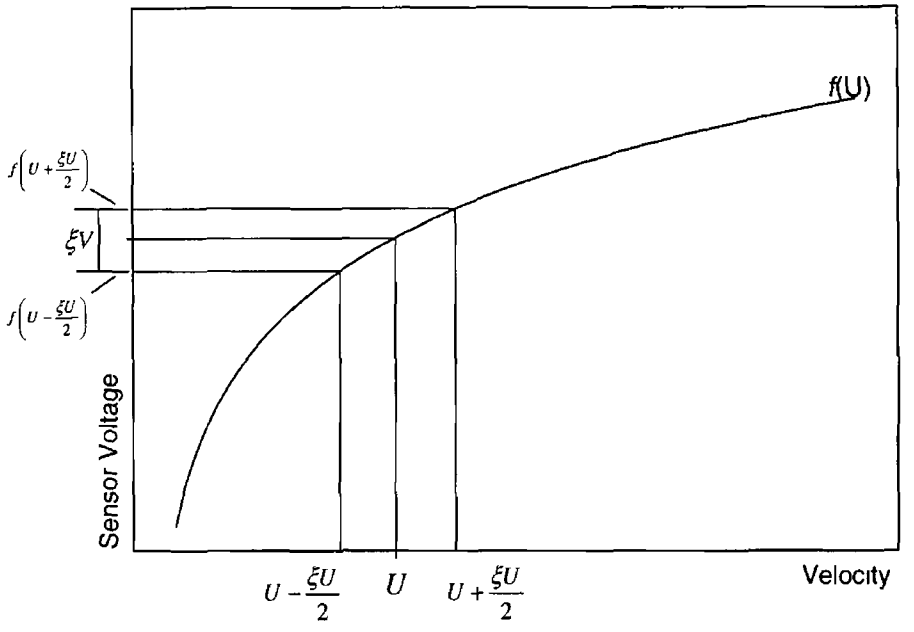

Figure 3 29 Explanation of equation (3 46)

A standard way of representing the uncertainty/possible error in a measurement is to express the error as a fraction or percentage of the measurement itself Using this technique, the uncertainty in the velocity measurement ξU can be expressed as

$$\xi U = \tau U \tag{3 47}$$

where τ is the scaling factor that represents the fractional error in terms of the measurement For example, an uncertainty in a measurement of 10% of the measurement would correspond to a value of τ of 0 1 Combining (3 46) and (3 47) results in

$$\xi V = f\left(U\left(1+\frac{\tau}{2}\right)\right) - f\left(U\left(1-\frac{\tau}{2}\right)\right) \tag{3 48}$$

A graph of this function over the necessary velocity range will give the required voltage uncertainty data and all that remains to be completed in order to determine the maximum velocity, U_R, that can be determined to within a certain fractional error, τ,

is to compare this graph to a graph of the noise level, V_N, as a function of velocity and to determine the velocity at which they intersect

3 6 2 1 Glass Bead Thermistor Sensor Range

The required voltage uncertainty and noise data was determined graphically from calibration data that was obtained using the gravity tank calibration facility (see section 3 5 1)

The velocity and sensor output data sets (see Figure 3 30) contained considerable noise and due to the difficulties involved in analysing graphs that have noise in both axes, the sensor output and water velocity data were plotted separately against time and each graph was analysed separately This was possible since each pair of sensor velocity and sensor output data points were acquired virtually simultaneously by the ADC

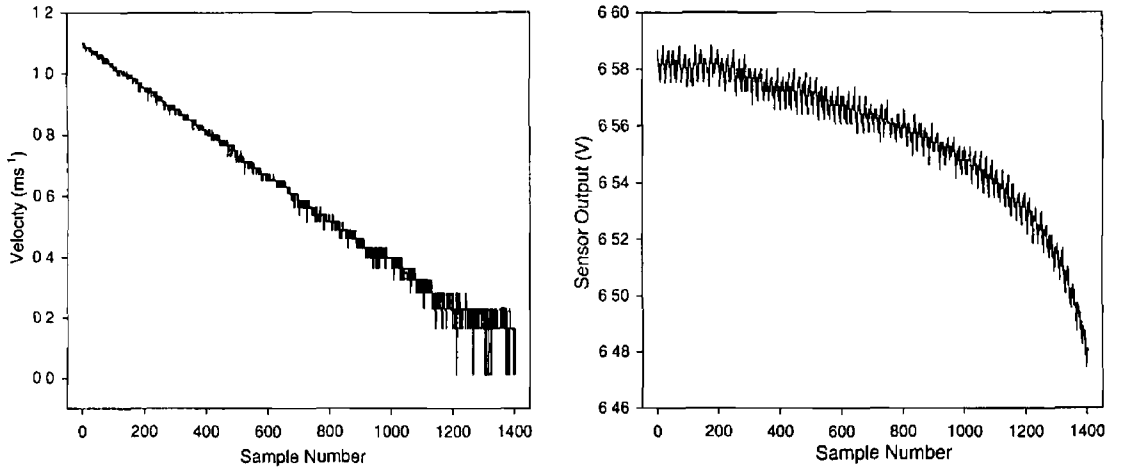

Figure 3 30 Sensor Output and velocity data plotted against sample number, which is equivalent to plotting against time

A measurement uncertainty of 10% of the measurement was chosen and the corresponding voltage uncertainty values that were obtained for a range of velocities are given in Table 3 7

There is an oscillation in the sensor output data in Figure 3 30 that was caused by the control circuit that was being used at the time the data was obtained so it cannot be used to determine noise levels Instead, data that was obtained using the same sensor in identical operating conditions as above with a circuit that did not oscillate was used The data obtained is also in Table 3 7 This oscillation free data could not be used in the rest of the analysis, as there was no velocity data accompanying it and while a comparison of the time data of both data sets provided enough correlation to

obtain noise levels as a function of velocity, this method would not have allowed the response curve to be determined accurately enough to calculate values of ξV .

Velocity (ms^{-1})	ξV (mV)	V_N (mV)
0.085	7.2	1.6
0.193	5.4	2.2
0.308	3.2	2.9
0.481	3.2	3.8
0.716	2.7	3.8
0.955	2.3	4.2

Table 3.7 ξV and V_N for a range of velocities that span the operating range of the sensor.

This data is plotted in Figure 3.31. The intersection of the two graphs gives the maximum velocity U_R that can be measured to within 10% uncertainty with the glass bead sensor at current noise levels.

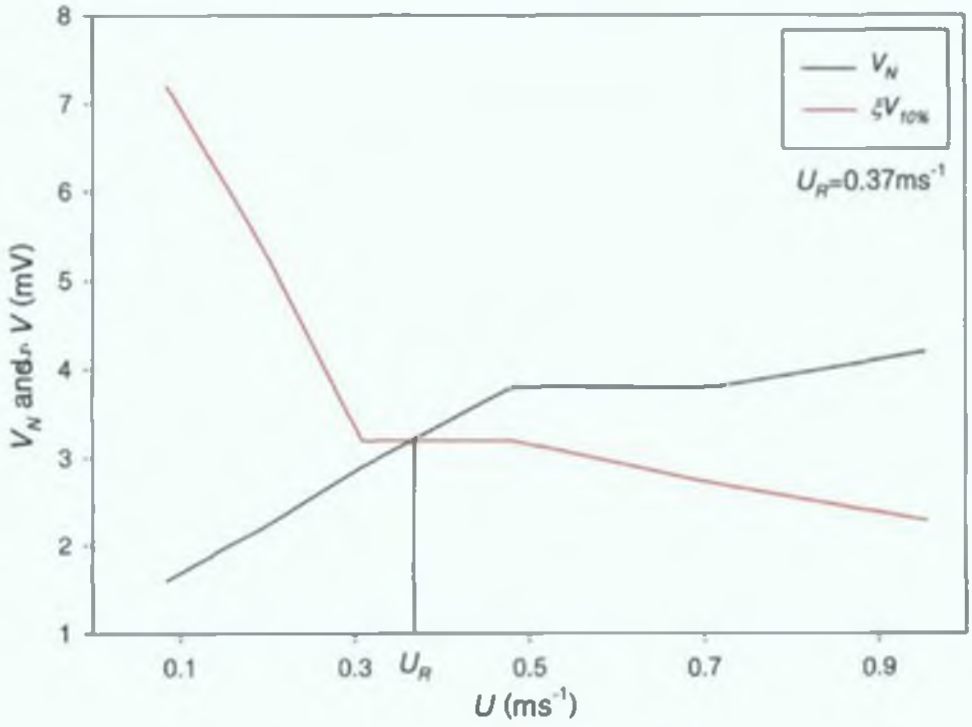

Figure 3.31 Peak-to-peak noise, V_N, in sensor output voltage and voltage uncertainty ξV for glass bead sensor and a measurement uncertainty ξU of 10%.

It should be noted that the data used in this graph was obtained using manual graphical techniques with questionable accuracy, consequently the value of U_R obtained here should only be taken as an approximate value.

The range of the sensor is strongly affected by the intrinsic noise in the sensor output voltage so therefore it follows that if a large range is required then every effort should be made to minimise the noise that is present in the output of the sensor

3 6.3 Sensor Choice

As we found in the last section the glass bead sensors can measure up to a velocity of ~0 4ms ^{1} for a measurement uncertainty of 10%, however it would be desirable to have a sensor that has better range

It follows from Figure 3 28 that an increase in sensitivity would lead to an increase in the range of the sensor The analysis of the effects of coating thickness in section 2 7 4 shows that such an increase in sensitivity could be achieved by decreasing the coating thickness of the sensor Therefore, the desired increase in range can be achieved by reducing the coating thickness of the sensor by a suitable amount

The obvious choice as a replacement to the glass bead sensors would be a sensor that has an epoxy or polymer coating since such materials are generally in full contact with the thermistor material and don't crack as easily as glass These properties could be expected to lead to a reduction or elimination of the problems associated with glass bead thermistors, however it was found that all the epoxy or polymer coated thermistors that were commercially available had coatings that were considerably thicker than that of the glass bead thermistors used initially This means that sensors constructed using these commercially available epoxy or polymer-coated thermistors have a significantly lower range than those using the glass coated thermistor In light of this it was decided to purchase uncoated bead thermistors and to coat them in the lab The aim of this work was to produce a sensor that would have a thinner coating than similar commercially available thermistors, which in turn would, hopefully, have a greater operating range This course of action would also open up the possibility of experimentally determining the effects of coating thickness on sensor performance

Suitable uncoated bead thermistors could not be sourced commercially so it was decided to construct a sensor from surface-mount chip thermistors, which are readily available and have the added advantage of being quite cheap

3.6.4 Surface Mount Chip Thermistors

The sensor was constructed by soldering connecting leads to the ends of the chip thermistor and then soldering this assembly into place between two copper prongs. Pictures of a typical sensor are shown in Figure 3.32.

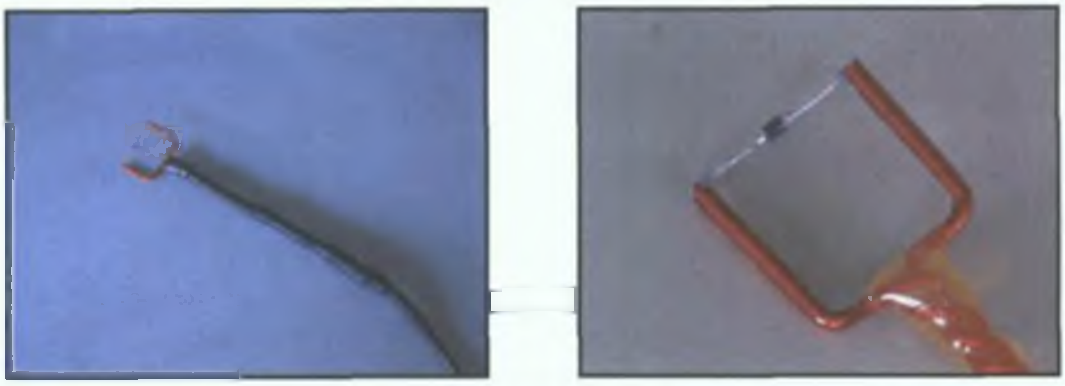

Figure 3.32 Chip Thermistor Sensor probe. The support prongs are made from heavy gauge enamelled copper wire that is twisted together to form the required shape. Adhesive is applied to the sensor support as shown to improve its rigidity and prevent breakage of the connecting wires. It was necessary to insulate the twisted part of the support as breakdown of the enamel occurred in this area of the probe in the event of prolonged immersion. Self-amalgamating tape was used for this purpose and was found to have good performance.

The sensor was then coated with a suitable material. A number of different coatings were used, primarily polymer based, commercially available coatings that contained anti fungal agents.

3.6.4.1 Coating Materials

A large range of coating materials were tested, however from an early stage it was found that coatings containing anti-fungal agents resulted in better stability than those without, so only those which contained anti-fungal agents were seriously considered. Polyurethane, acrylic and silicone based coatings are the most readily available coating materials that contain an anti-fungal agent. A considerable number of sensors were constructed using each of these materials and while they all functioned with a good degree of success, the acrylic based coatings resulted in the most robust sensors and as a result it was chosen as the primary coating material and was used to coat all of the sensors that are referred to from here on in. Attempts were also made to coat the sensors with solgels, however it was found that the coating thickness required made the available sol-gel materials unsuitable. This is discussed further in section 4.6.

3 6.4 2 Coating Techniques

Before beginning to discuss the various coating techniques it needs to be emphasised that it was found to be necessary to thoroughly clean all of the surfaces that were to be coated using alcohol or some other suitable solvent before coating took place

Three coating techniques were used to coat the sensor, those being, aerosol deposition, brush application and dip coating

The aerosol technique involved spraying the coating onto the sensor from an aerosol can This method, while simple had a number of problems and as a result is not the method of choice It is very easy to over apply the coating, resulting in large globules forming on the sensor, which effectively render it un-useable It was also common for inaccessible regions of the sensor to remain uncoated

Brush application was found to work quite well, the only problem being that it was quite difficult to coat the sensor evenly

Dip coating involves immersing the sensor completely in a bath containing the coating material and then removing it slowly, with the thickness of the coating obtained being dependant on the rate at which the sensor is removed from the bath – removing the sensor more slowly results in a thinner coating Dip coating has a number of distinct advantages over the other coating methods in that the thickness of the resulting coating is substantially uniform, it is the easiest of all three methods from a practical point of view and if care is taken to ensure that the withdrawal rate remains reasonably constant then the thickness of the coating resulting from the application of multiple layers can be quantified in terms of the number of coatings that have been applied to the sensor A significant problem that was encountered is that the coating material would not adhere to the connecting leads of the thermistor using dip coating but it was found that if an initial layer of coating was applied to the connecting leads by brush that dip coating could then be used without any problems to coat the actual sensor and for the application of all subsequent layers This joint use of brush application and dip coating proved quite successful and was used in the coating of the majority of the chip thermistor sensors used in this work

Figure 3.33 Manual dip coating of chip thermistor probe. The entire probe is fully immersed in the coating material and is then withdrawn slowly. Note that the sensor is oriented at an angle in relation to the surface of the bath. If this were not the case then the coating material would break away from the sensor abruptly and leave a globule of coating on the sensor, which would dramatically affect its performance.

3.6.4.3 Influence of Thermistor Geometry on Required Coating Thickness

Irrespective of coating method, it was found that a number of layers of coating were necessary to provide electrical insulation. This can be attributed to the fact that the chip thermistor has sharp corners. The thickness of the coating at these corner regions will be much less than on flat regions of the bead, therefore while one coating may be sufficient to insulate flat regions of the thermistors surface, a number of coatings will be necessary to achieve the required coating thickness at the corners. The effects of coating thickness on the sensors performance are analysed in detail in 4.6.

3.6.4.4 Stability and Annealing

The characteristics of chip thermistor sensors were found to change dramatically during their first few hours of operation. Tests have revealed that this is caused by a change in the resistance of the thermistor and it is believed that this change is due to annealing or similar processes taking place in the thermistor. It is likely that the high temperatures that the thermistor is exposed to during soldering could be causing internal changes and that these changes are slowly reversed by the "annealing" process. It has been found that this drift only occurs for the first few hours, after which very stable operation is achieved and therefore to avoid the problems that would be associated with drift of the resistance of the thermistor a procedure was implemented whereby all new sensors were operated continuously for a "burn in"

period of five to six hours before calibration After this period their resistance-temperature characteristics were revaluated and the sensors were then ready for calibration and use

3 6 5 Bubble Formation

As we have mentioned earlier it has been documented by Rasmussen (1967) and Bruun (1995, d) that bubbles form on the surface of hot film sensors used in water if the difference between the operating temperature of the sensor and the ambient temperature of the water exceeds approximately 20°C This was also found to be the case with both the glass bead and chip thermistor sensors developed during the course of this work, however it was found that they could be operated at temperatures of up to 25°C above the ambient water temperature This increase is believed to be due to the fact that the thermistor sensors have a thicker coating than the hot film sensors discussed by Bruun (1995, d) and Rasmussen (1967) and therefore the surface temperature of a thermistor sensor will be slightly lower than that of a hot film sensor with the same core temperature

It was found that the chip thermistor sensors had improved performance over many thermistor-based anemometers that have been previously developed and were therefore used as the final design

Their operating characteristics and performance in general are discussed in detail in Chapter 4

****

Chapter 4 : Results and Analysis

This chapter deals with an analysis of the various response characteristics of the sensor and of the various response specific design features that were not discussed in Chapter 3 We begin with an analysis of the significance of the offset voltage in terms of the frequency response and stability of the system A key requirement of this analysis was a method of quantifying the frequency response of the system and this was fulfilled by using the standard square wave testing technique Square wave testing also forms the basis of the method used to tune the offset voltage so that optimum frequency response characteristics are obtained This is followed by an investigation of the noise in the sensor output, which has implications in terms of the range of the sensor Then we move on to the curve fitting process, which involved finding a general equation that accurately relates both velocity and ambient temperature to the output of the sensor A method of representing the raw calibration data has been developed that allows the benefits associated with time averaging to be realised, while still allowing data obtained over a range of velocities to be properly represented Such data is not represented accurately when standard averaging techniques are used as a result of the non-linear relationship between the sensor output and velocity It has been found that expressing the velocity response of the sensor in terms of a polynomial in the log of the velocity resulted in a function that described the response of the sensor much more accurately than any of the equations that have been used in previous investigations The temperature dependence of the sensor output has been accounted for by introducing a temperature dependency into the coefficients of the velocity response function with the resulting equation being the calibration surface of the sensor We then examine the problems that arise when attempts are made to use a sensor that has been calibrated using the logarithmic polynomial general equation in an actual measurement situation The difficulties involved in inverting the calibration equation are discussed and an efficient solution is presented, which is based on the principle of successive approximation as used in analog to digital converters Successive approximation also proved useful in implementing the method of calculating the range of the sensor that was developed in Chapter 3

An experimental investigation of the influence of coating thickness on the velocity sensitivity and frequency response of the sensor was carried out, which verified the theoretical analysis in Chapter 2 Finally we look at the long-term stability of the

sensor, which was found to be significantly improved on the performance of previous thermistor-based anemometers.

4.1 Frequency Response and Offset Voltage Injection

The Constant Temperature control circuit incorporating offset voltage injection that is discussed in section 3.1.6 was developed in order to improve the frequency response of the system, primarily to allow accurate calibration of the sensor with the tow tank calibration facility. The frequency response of the earlier control circuits was not high enough for the circuit to be able to respond to the intrinsic vibrational noise that results from the trolley moving along the guide rail and any electronic noise present in the system. The effect of this inadequate frequency response is illustrated in Figure 4.1

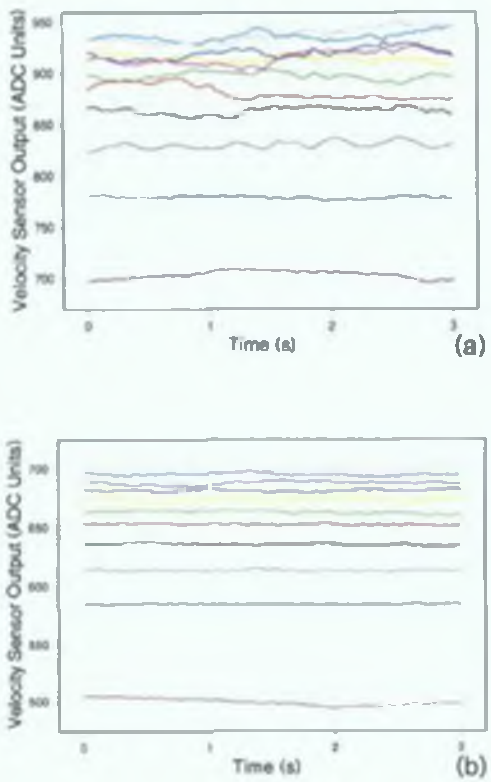

Figure 4.1 Graphs of Sensor Output against time for a range of velocities, obtained using the tow tank calibration facility. The data in (a) was obtained using the basic circuit that does not incorporate offset injection and the data in (b) was obtained using the final circuit that uses offset injection and which has been tuned for optimum frequency response. The rotational speed of the motor remained constant at each velocity.

The data in (a) would tend to indicate that the velocity of the sensor is varying considerably, however this is not the case and the data is clearly of little use for calibration purposes. The data obtained using the offset injection circuit is much

improved and this can be attributed to the frequency response of this circuit being a factor of approximately 80 greater than the basic circuit (see section 4 1 1 2)

The offset voltage not only controls the frequency response of the sensor but also system stability and the noise levels in the sensor output, which as we will see in section 4 2 is directly related to the frequency response of the system

The behaviour of the system for the range of possible offset voltages, which in this case is –13V to 13V is given in Table 4 1

Offset Voltage (V)	Sensor Behaviour
+13 to +10	Sensor exhibits very little response to velocity fluctuations
+8 to -4	Response to velocity fluctuations improves and noise in output increases as offset voltage approaches ~ -4V
-4 to ~ -9	Noise levels increase significantly as voltage decreases through this range
< ~ -9	The exact value varies from sensor to sensor, however below approximately –9V the control circuit starts to oscillate

Table 4 1 The behaviour of the sensor for different offset voltages This data is for a chip thermistor sensor operated at ~45°C

A method of analysing and quantifying the frequency response and stability of the circuit is required Square wave testing is the standard method of analysing the response of proportional control systems and is the basis of the method used to determine the optimum offset voltage in the majority of Constant Temperature anemometers e g Freymuth (1977) and Perry (1982, h)

4 1 1 Square Wave Testing

In the standard square wave testing technique a low amplitude, square wave voltage is applied to the circuit in order to perturb it from its equilibrium point and the response of the system to this perturbation is measured (Bruun 1995, m)

The Constant Temperature control circuit incorporating square wave injection circuitry is shown in Figure 4 2 The square wave signal can be applied to a number of points of the control circuit, however it was decided to inject the signal into one of the arms of the Wheatstone Bridge so that the same technique could be used for all of the control circuits that were used

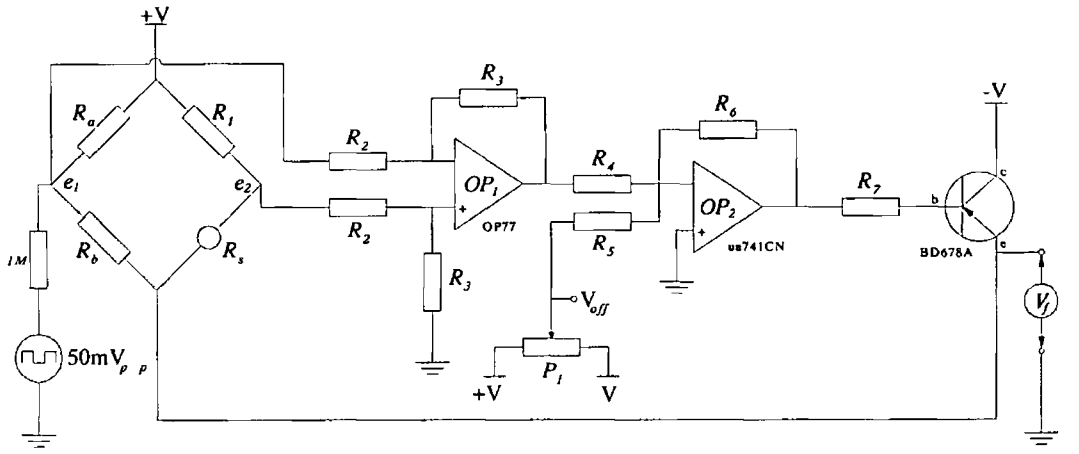

Figure 4 2 Constant Temperature Control Circuit with Offset Injection A square wave signal is added to one of the arms of the bridge for the purposes of square wave testing A signal generator was used as the square wave voltage source The frequency of the square wave is not critical, as long as it is low enough to allow the system to return to equilibrium after each step before the next step occurs

The response of the system to the square wave perturbations, which is commonly referred to as the step response, is determined by monitoring the output of the circuit, which in this case is the feedback voltage V_f The step response of a typical chip thermistor sensor for a range of offset voltages is shown in Figure 4 3

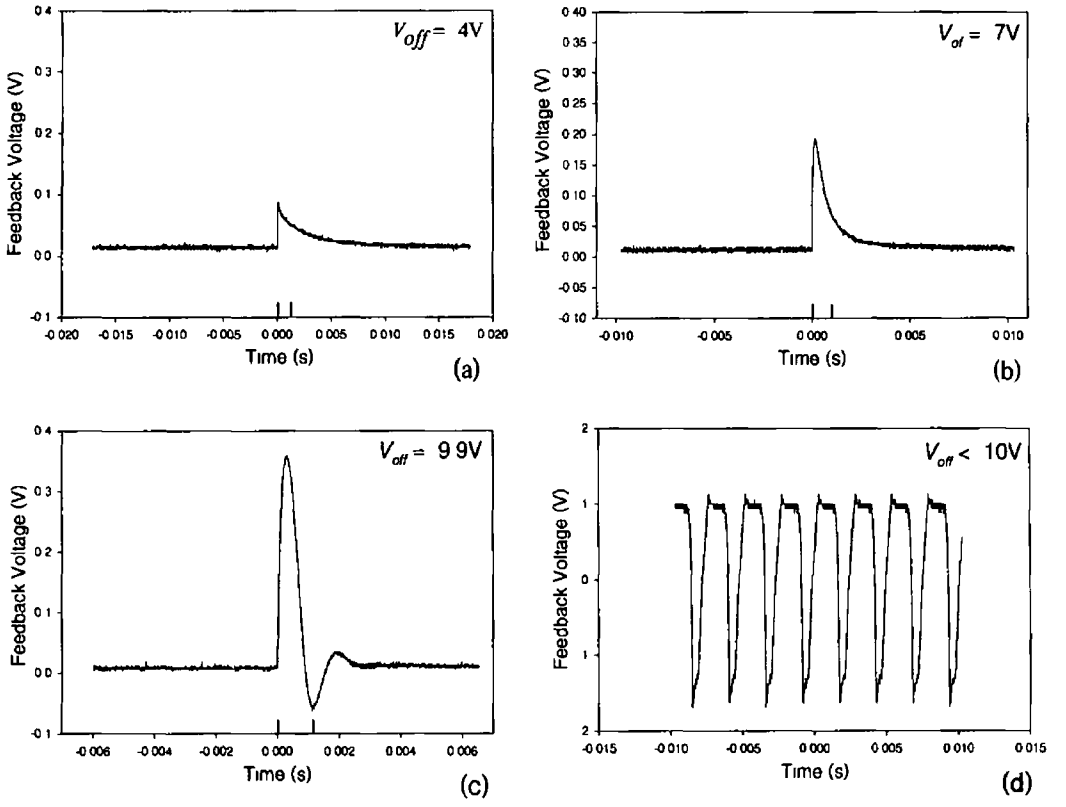

Figure 4 3 (a), (b) and (c) show the response of the circuit to the falling edge of a square wave signal, which is injected as shown in Figure 4 2 for a range of offset voltages The red lines are 1 16ms apart and their purpose is to indicate the time scaling used in each of the graphs (d) shows the output of the circuit in the absence of a square wave signal for an offset voltage above that at which the system becomes unstable The offset voltage that results in optimum damping is different for each sensor, in this case it was –9 9V

It may appear that there is no step change in the output voltage of the sensor after it has settled, however there is in fact a change but it is not of sufficient magnitude to be visible in these graphs

The responses in these graphs can be considered in terms of the response of a damped system The responses in (a) and (b) are indicative of an over-damped system, that of (c) equal to or very close to the response of an optimally damped system and that of (d) an under-damped system, which has become unstable and is undergoing oscillation The desired response characteristic is that of (c), as any deviations of the operating temperature of the sensor from its set point will be corrected for in the shortest possible time

4 1.1 1 Optimum Damping

The step response that indicates optimum damping of a Constant Temperature hot wire system has been determined by Freymuth (1977) and is shown in Figure 4 4 According to Freymuth, optimum response is achieved when the overshoot is approximately 15% of amplitude of the first peak

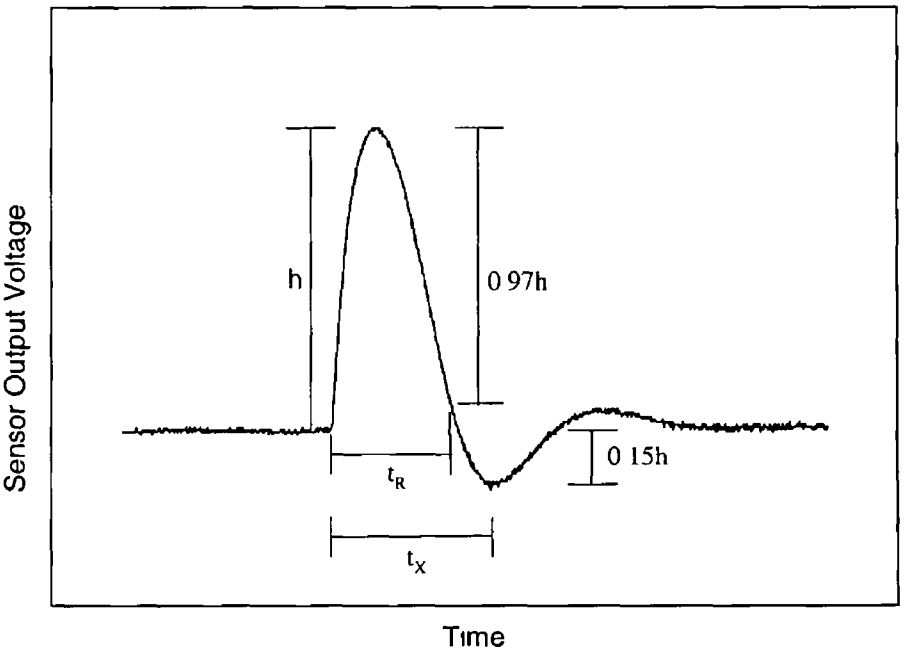

Figure 4 4 The step response for optimum damping of a Constant Temperature anemometer as specified by Freymuth (1977) The corner frequency of the system is given in terms of the transient response time t_R Due to the difficulty involved in accurately measuring t_R the relationship between t_R and t_X which is much easier to measure has been determined, which allows t_X to be used to determine the corner frequency of the system

Freymuth developed this criterion with hot wire sensors in mind however it is the constant temperature aspect of the system that is most important and therefore it can also be expected to apply to the thermistor based sensors being used in this work

The frequency response of a system can be determined from its step response and Freymuth found that the corner frequency of a critically damped system could be given by

$$f_c = \frac{1}{1\ 3t_R} \tag{4 1}$$

where t_R is the transient response time of the system, as indicated in Figure 4 4

The transient response time, t_R, as defined by Freymuth is quite difficult to measure so instead the quantity t_X, as defined in Figure 4 4 was measured Using graphical techniques it was determined that the relationship between t_R and t_X is given by

$$t_R = 0\ 77t_X \tag{4 2}$$

Incorporating this into (4 1) and rounding off to two decimal places results in

$$f_c = \frac{1}{1\ 00t_X} \tag{4 3}$$

The corner frequency is the frequency at which the ratio of the actual sensor output and the expected sensor output is equal to –3dB and is an indication of the maximum frequency that can be measured by the system

The relative transient response time t_X and the corresponding corner frequency of a standard chip thermistor sensor for an open loop gain of 50,000 and an operating temperature of approximately 25°C above ambient are given in Table 4 2

Alternative Transient Response Time t_X (ms)	**Corner Frequency f_c (Hz)**
1 16	862

Table 4 2 Alternative transient response time and corner frequency of a typical chip thermistor sensor

4.1.1.2 Comparison of Frequency Response of Basic and Offset Injection Circuits

It is evident in Figure 4 1 that the frequency response of the earlier basic circuit is much less than that of the more advanced offset injection version It would be of interest to compare the step response characteristics of both circuits The step responses of both circuits operated in identical conditions with the same sensor are shown in Figure 4 5 It can be seen that the form of the frequency response of the

basic circuit in no way resembles that given by Freymuth (Figure 4 4) so its corner frequency cannot be calculated, however an indication of the relative performance of both circuits can be obtained by measuring and comparing the time taken for each system to settle

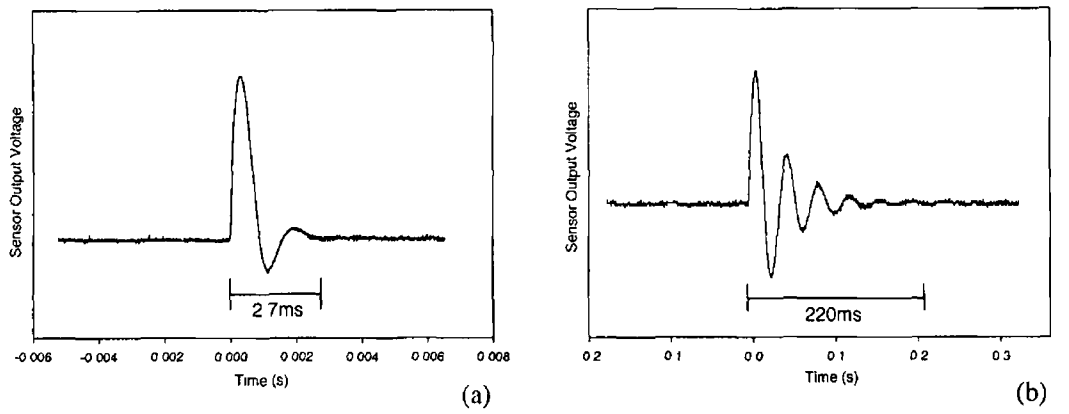

Figure 4 5 (a) is the step response of the system using an optimised offset injection circuit and (b) is the step response using the basic circuit described in section 3 1 3

The offset injection circuit settles a factor of 80 times faster than the earlier basic circuit It can be assumed that the corner frequencies will scale by approximately the same amount, which means that the basic circuit had a corner frequency of the order of 10Hz

4 1 2 Tuning Offset Voltage

The offset voltage that is required for optimum damping is determined by applying a square wave signal to the bridge and adjusting the offset voltage until the step response of the system matches that shown in Figure 4 4 This is the method that is used to tune the offset voltage of almost all Constant Temperature anemometers and was employed during this work without any problems

4 1 2 1 Influence of Offset Voltage on Operating Temperature of Sensor

It has been found that the control circuit does not keep the bridge perfectly balanced and that a slight error voltage always exists between its arms This means that the operating temperature of the sensor is not exactly what it is supposed to be, however this does not lead to any problems, as the slight error will automatically be taken into account by the calibration process

It has also been found that the magnitude of the bridge imbalance is a function of offset voltage Therefore, if the offset is adjusted during operation then the operating temperature of the sensor will change and its response will no longer be described by

its calibration equation. The practical implications of this are that the offset voltage must be set before calibration and must not, under any circumstances be adjusted afterwards, otherwise recalibration would be required.

4.1.3 Effect of Open Loop Gain on Sensor Dynamics

The open loop gain of the control circuit has a significant influence on the dynamic response of the system. The corner frequency of the system for a range of values of open loop gain is shown in Figure 4.6.

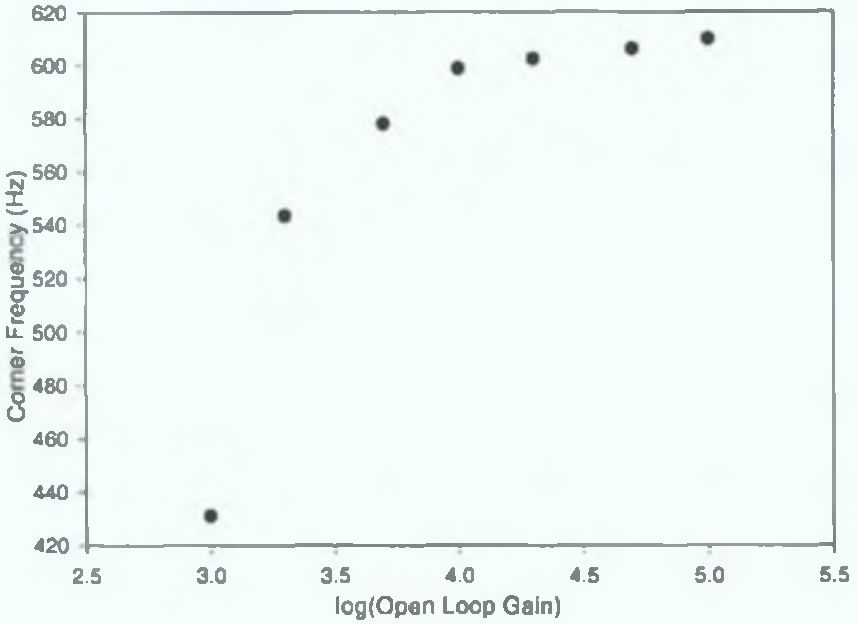

Figure 4.6 Corner Frequency of an optimised system for a range of values of open loop gain. The log of the open loop gain has been plotted in the interests of clarity.

The transient response time and thus the frequency response of the system improves with increasing gain so it is desirable to set the open loop gain as high as possible. As discussed in section 3.1.6.1 the practical limit of the open loop gain of the offset injection control circuit was found to be approximately 50,000. Attempts were made to modify the circuit so that higher gain could be achieved with the aim of increasing the corner frequency of the system, however it was found that this was not possible (see section 3.1.6.1.1).

A different sensor was used to obtain the data in Figure 4.6 than is referred to in Table 4.2. The sensor used to obtain the data in Figure 4.6 has a corner frequency of 606Hz for an open loop gain of 50,000 while the sensor used to obtain the data in Table 4.2 has a corner frequency of 862Hz for the same open loop gain. This considerable difference can be attributed to the fact that the coating thickness of the sensor used for Figure 4.6 is greater than that used in Table 4.2. The effects of the coating thickness

on the frequency response and the behaviour of the sensor in general can be found in section 4 6 1

4 2 Noise

As is the case with all electronic systems there is noise present in the output of the velocity sensor circuit Figure 4 7 is a graph of the output of a typical chip thermistor sensor with optimised frequency response

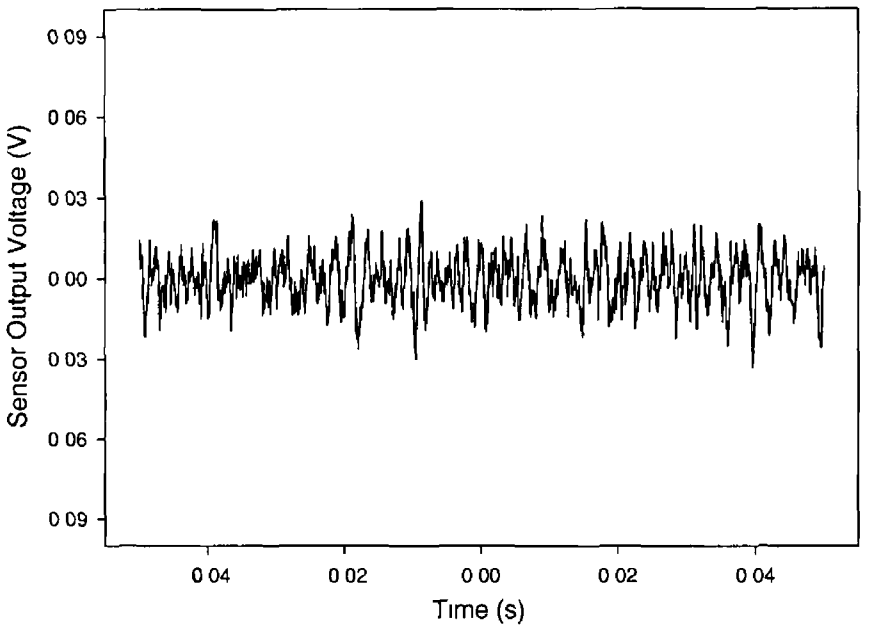

Figure 4 7 Output voltage of an optimised sensor The data has been obtained using an oscilloscope in ac coupled mode and therefore is centred about 0V

Each of the components in the circuit will be a source of standard white and shot noise and there will be additional noise resulting from the semiconductor nature of the sensor It is also likely that the action of the constant temperature control circuit will serve to increase the amplitude of the intrinsic noise in the system even further We have mentioned in section 4 1 that the noise in the sensor output varies with the offset voltage and it has been found that this effect is best quantified in terms of the corner frequency of the system Figure 4 8 shows the noise in the output of a typical sensor for a range of corner frequencies

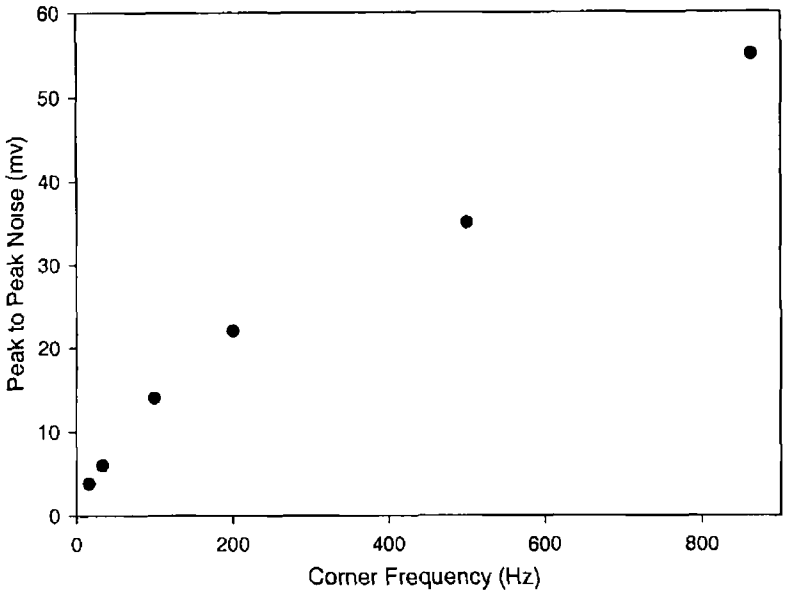

Figure 4 8 Peak to peak noise in the output of the sensor as a function of the corner frequency of the circuit The corner frequency, which in this case is also a measure of bandwidth, was adjusted by changing the cut-off frequency of the low pass filter in the output stage of the circuit (see section 4 2 1)

It can be seen that the noise in the sensor output is strongly dependant on the corner frequency of the system, decreasing from $55mV_{p\,p}$ for optimised corner frequency to $\sim 3mV_{p\,p}$ when the corner frequency of the system has been reduced to 12Hz

The increase in noise levels that accompany an increase in the corner frequency and thus the bandwidth of the system, as shown in Figure 4 8 presents an interesting problem, namely, increasing the corner frequency of the system allows the measurement of higher frequency velocity fluctuations, however, the increased noise will reduce the range of the sensor Therefore the user has the choice of low frequency/slower measurements over a large velocity range, or high frequency/faster measurements over a much-reduced range The range of a typical sensor for a range of corner frequencies is calculated in section 4 5 and the choice that must be made between frequency response and range is clearly illustrated

4 2 1 Setting the Corner Frequency of the Sensor System

The corner frequency of the system can be set at the desired value by suitably adjusting the offset voltage V_{off}, however it was found to be much easier to set the offset voltage at the optimum value as described in section 4 1 2 and to use a low pass filter at the output stage to set the effective corner frequency of the system Bruun (1995, n) also used this technique and states that this method leads to better system

performance than results from using the offset voltage to set the corner frequency A diagram of the low pass filter that is used is given in Figure 4 9

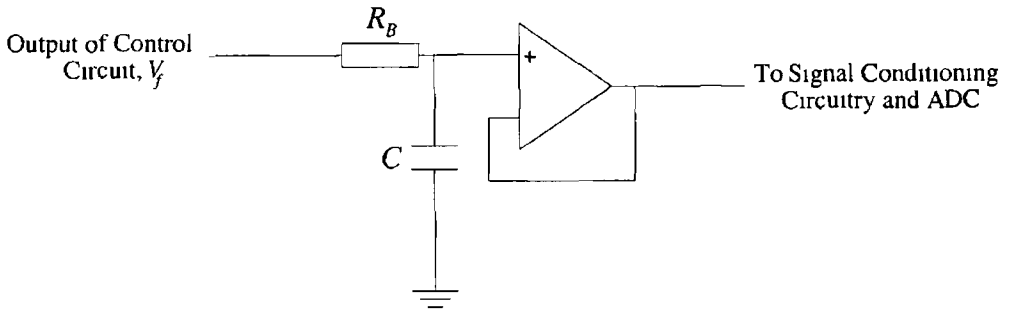

Figure 4 9 Low pass filter for reducing the effective bandwidth of the sensor system and thus reducing noise levels in the sensor output The op-amp which is configured as a voltage follower, is necessary to prevent R_B and the input impedance of the signal conditioning circuitry from forming a potential divider, which would alter the signal

The corner frequency of the filter is given by

$$f_c = \frac{1}{2\pi R_B C} \tag{4 4}$$

It was found by experimentation that a corner frequency of ~35Hz was adequate for tow tank calibration and this is the setting that was used in conjunction with a sampling frequency of 25s ^{1} throughout the calibration work detailed in section 4 3

4 2.2 RF Noise and Circuit Shielding

It was suspected that some of the noise in the output signal was due to radio frequency pickup in the connecting leads of the sensor, which were ~7m long for tests carried out in the tank, however, the use of shielded cable and placing the control circuit in an earthed metal box had no appreciable effect on the noise levels in the output signal so it can be taken that pickup was not an issue

4 3 Calibration and Curve Fitting

In order to use the sensor to measure water velocity it is necessary to develop an equation describing the response of the sensor to velocity and ambient water temperature This can be obtained by fitting the appropriate general equation to simultaneous sensor output, sensor velocity and ambient water temperature data, which can be obtained using the tow tank calibration facility and ambient temperature compensation sensor discussed in the last chapter The fact that the general equation cannot be determined using a theoretical model and therefore must be empirical in

nature (see section 2 7 3 1) means that there are a large number of possibilities and choosing the equation that will give the best results proves to be a significant problem This is discussed in more detail in section 4 3 3

In order to simplify the calibration process the velocity and ambient temperature response of the sensor were determined separately This was accomplished by obtaining sensor output and sensor velocity data at a constant temperature, which allowed the velocity response of the sensor to be determined The temperature response of the sensor was determined at a later stage by determining the velocity response of the sensor at a range of ambient water temperatures

4 3 1 Expressing Sensor Output in Terms of Power Dissipation

The power dissipated by two otherwise identical sensors at the same temperature but with different operating resistances when exposed to the same flow will be the same, whereas the voltage drop across each of the sensors will be different As a result, expressing the sensor output in terms of dissipated power allows data from sensors with different operating resistances but otherwise identical properties to be analysed and compared quite easily This, in conjunction with the method of setting the operating temperature that is discussed in section 3 1 5, overcomes one of the main problems associated with using commercially available thermistors with standard tolerances, which is one of the significant achievements of this work

The power dissipated by a sensor, P_s, can be calculated using

$$P_s = \frac{V_s^2}{R_s} \tag{4 5}$$

where V_s is the voltage drop across the sensor and R_s is its working resistance Combining this expression with equation (3 37), which describes V_s in terms of the ADC output and the parameters of the control circuit, results in

$$P_s = \left(V_p + V_{oU} + \frac{z_U \delta V}{G_{SC}} \right)^2 \frac{R_s}{(R_1 + R_s)^2} \tag{4 6}$$

This equation provides the means of converting the raw sensor output data to the power being dissipated by the sensor at any given time A function has been written to implement this calculation, which can be found in the programs listed in Appendices C 3 and C 4 From here on in the term "sensor output" refers to the power dissipated by the sensor and not the voltage drop across it, V_s, as was the case up to now

4.3.2 Calibration Data

Calibration data was obtained by moving the sensor along the tow tank at as constant a velocity as possible and recording the resulting sensor output, sensor velocity and ambient temperature data for a number of seconds. This process was repeated for a number of velocities that span the velocity range of interest and resulted in a set of sensor output, sensor velocity and ambient temperature data files, recorded as a function of time, for each run. A typical set of raw calibration data is shown in Figure 4.10. The sensor output is expressed in terms of dissipated power. The temperature of the tank remained constant at 14.7°C while this data was being acquired and as a result the ambient temperature data obtained has been omitted from Figure 4.10 for the sake of clarity.

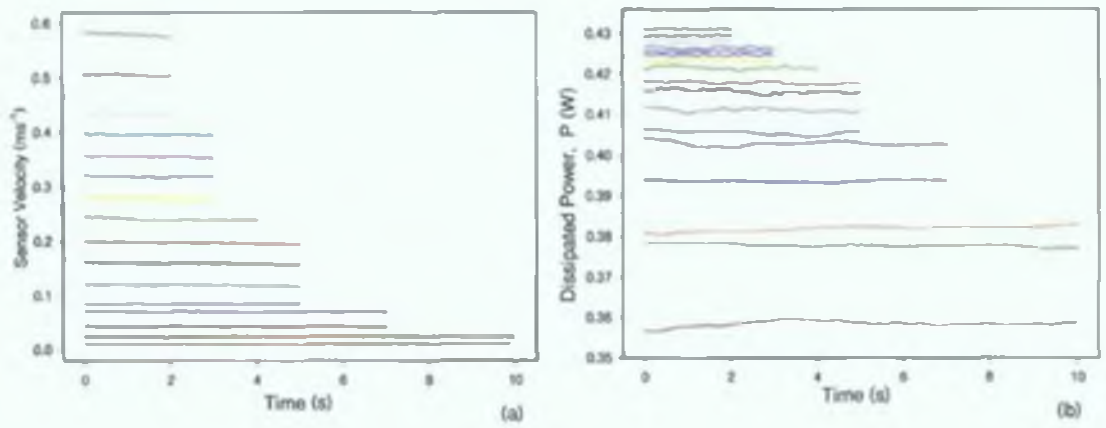

Figure 4.10 Raw sensor velocity and corresponding dissipated power for a range of approximately constant velocities, recorded and plotted here as a function of time. The duration of the measurement period decreases with increasing velocity due to the limited length of the tank. The effects of lateral oscillation can be seen in the red and black lines in (b) and the effect of low frequency movement of the water in the tank is evident in the data that lies in the range 0.40 to 0.41ms^{-1}.

A distinct advantage of obtaining the calibration data in this manner is that since the data is recorded over a number of seconds, time averaging techniques can be used to significantly reduce the effects of noise in the outputs of the sensor and the velocity measurement system. As well as the intrinsic noise in the outputs of the velocity measurement system and the sensor, lateral oscillation of the trolley and sensor assembly was a significant problem at early stages and was reduced significantly by adding appropriate weights to the trolley, however it still occurs to a small extent at certain velocities. It is also suspected that residual movement of the water in the tank also makes a significant contribution to the noise at low velocities. The effects of both lateral oscillation and movement of the water in the tank are evident in Figure 4.10.

The simplest and most obvious method of processing raw calibration data, such as that shown in Figure 4 10, is to simply average each of the corresponding sets of data - "lines" of the same colour in the graphs in Figure 4 10, to obtain pairs of sensor output and sensor velocity data All of the resulting points can be used to obtain a graph of sensor output as a function of velocity The graph of the data that results from averaging the data in Figure 4 10 is shown below in Figure 4 11

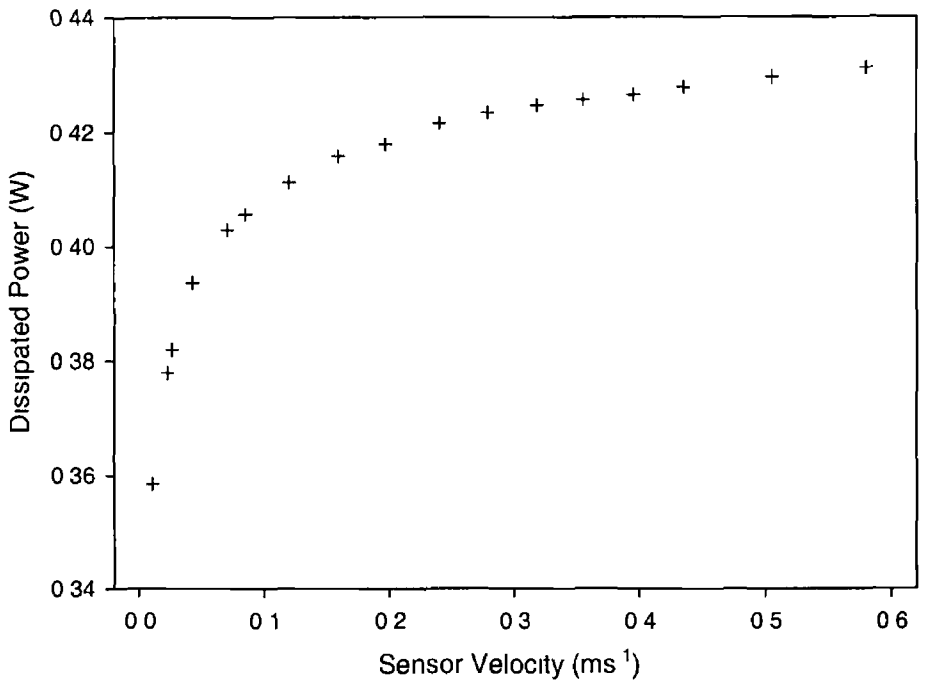

Figure 4 11 Dissipated power as a function of sensor velocity using time averaged data

The graph in Figure 4 11 can be fitted with the appropriate general equation in order to determine the response equation of the sensor While averaging is simple to implement there are a number of problems associated with using it in a situation such as this where the relationship between the quantities that are being averaged is so non-linear These problems result in the need for an entirely different approach to processing the raw data that involves synchronising the sensor output and velocity data points

4 3.2 1 Synchronised and Interpolated Data

While averaging is simple to implement and appears to work quite well there is one intrinsic problem with using it with this system Despite efforts to keep it as constant as possible the velocity of the trolley can vary as it traverses the tank, due to non uniform coefficients of friction, connecting cable drag etc Therefore a single corresponding set of sensor output and sensor velocity data may contain data for a

range of sensor velocities As a result of the highly non-linear inter dependence of the dissipated power and the velocity of the sensor, if a set of dissipated power data that contains data that was obtained over a range of sensor velocities is averaged then the resulting figure will not correspond to the average of the corresponding set of sensor velocity data In other words, the resulting data point will be moved off the calibration/response curve of the sensor by the inherently linear nature of averaging A solution to this problem is to plot all of the sensor output and sensor velocity data, instead of averaging each individual set to obtain a single data point The data will still be "averaged" by the action of the curve fitting process so that all of the benefits of obtaining data for a period of time will still be realised and any individual sets of data that cover a range of sensor velocities will be properly represented

The first data points of the sensor output and sensor velocity data files are synchronised (see section 3 5 2 6), however, as a result of the non-uniform, velocity dependent, sampling rate of the velocity measurement system, subsequent points are not Therefore, corresponding data points in each file cannot simply be paired off and some form of interpolation must be used to obtain the required pairs of data points The diagrams in Figure 4 12 are representative of typical sensor output and sensor velocity data files and illustrate the fact that the measurements are not made simultaneously

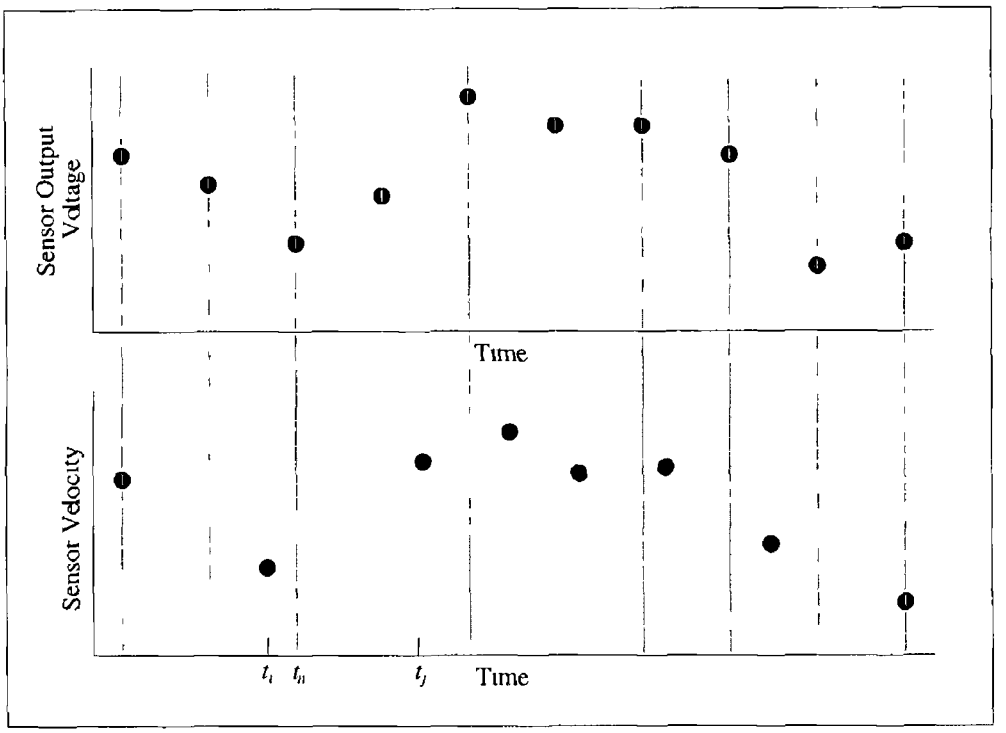

Figure 4 12 Representative diagrams of a typical set of sensor output and sensor velocity data as a function of time Gridlines have been included to emphasise the point that the measurements take place at different times

It is desirable to have the processed data evenly spaced on the time axis so the sensor output data has been left unchanged and the sensor velocity that corresponds to each sensor output data point has been calculated This has been achieved using linear interpolation whereby the sensor velocity, U_n, at time t_n is given by

$$U_n = U_i + \frac{(U_j - U_i)}{(t_j - t_i)}(t_n - t_i) \tag{4 7}$$

where U_i and U_j are the velocities of the sensor at times t_i and t_j respectively (see Figure 4 12) A function has been written to implement this equation and has been combined with functions that calculate the dissipated power of the sensor and the ambient temperature of the water from the raw ADC data, to obtain a program that carries out all of the data processing that is necessary in order obtain synchronised calibration data This program can be found in Appendix C 3 and contains detailed notes on its operation A problem arose during the implementation of this program arising from its inherently iterative nature and the fact that for low velocities there are more sensor output data points than sensor velocity data points while for high velocities there are considerably more sensor velocity than sensor output data points

A solution was obtained and is described in detail in the program code in Appendix C 3

The output of the data processing program is a file that contains synchronised sensor output and sensor velocity data that was obtained during a single traverse of the tank A synchronised data file is produced for each of the sets of raw calibration data and finally, all of the synchronised data files are combined to form one file, which contains all of the data that has been obtained, in a form to which a curve fit can easily be applied In principle it should be possible to synchronise all of the data in a complete set of calibration data at once however file-handling constraints prevented such a procedure from being implemented A typical graph of the sensor output and velocity components of the synchronised file that resulted from processing the Sensor 1 data shown in Figure 4 10 is shown in Figure 4 13

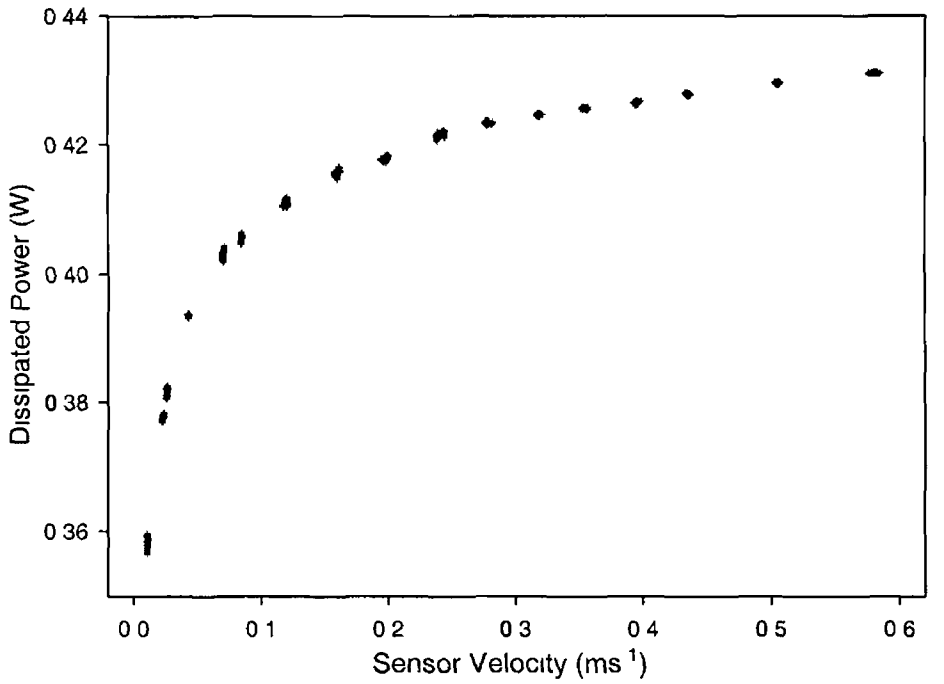

Figure 4 13 Dissipated Power as a function of sensor velocity using synchronised time series data In addition to presenting all of the data correctly this method allows the user to gain an appreciation for the noise that is present in the calibration data and to assess the noise as a function of velocity

4 3 2 2 Smoothing of Velocity Data

There is considerable variation in the sensor velocity data that is not reflected in the sensor output data It has been determined that this variation is caused by roughness in the motor and its gearbox and that it is absorbed to a large degree by the trolley driveline and is negated further by the inertia of the trolley and never actually affects the sensor, however since the optical chopper assembly is located on a pulley that is

approximately mid way between the motor and the trolley, it will experience variations of a considerably larger magnitude than that which the trolley undergoes Therefore it is acceptable to smooth the velocity data so that it more accurately reflects the actual velocity of the sensor, which will lead to an improvement in the quality and accuracy of the curve fit obtained from the data A number of methods of smoothing the data were tested, including multiple point moving averages and low pass filters and it was found by graphically comparing the smoothed data to the sensor output data that using an FFT smoothing filter gave the best performance An FFT smoothing filter works by removing the Fourier components of the data that are above a certain frequency The cut-off frequency is specified in terms of the number of points that are to be considered at any one time by the smoothing function with the number of points being termed the "smoothing coefficient" It was necessary to use a different smoothing coefficient for each set of velocity data since the sampling rate of each was different All of the calibration data that required smoothing was obtained at approximately the same velocities and these velocities, the corresponding motor supply voltages and the smoothing coefficients that were found necessary are listed in Table 4 3

Sensor Velocity (ms ^{1})	Motor Voltage (V)	Smoothing Coefficient
0 01	1	2
0 02	1 25	3
0 30	1 5	4
0 45	2	5
0 60	2 5	6
0 80	3	7
0 12	4	8
0 16	5	9
0 20	6	10
0 24	7	11
0 28	8	12
0 32	9	13
0 36	10	14
0 40	11	15
0 44	12	16
0 52	14	17
0 60	16	18

Table 4 3 Approximate velocities used to obtain calibration data and the smoothing coefficients that were found to be necessary to remove adequate amounts of variation from the sensor velocity data

The built-in FFT smoothing algorithm of Microcal Origin 6 0 was used during the course of this work Graphs of raw velocity data and the resulting smoothed data are shown in Figure 4 14 The smoothing that was implemented effectively set the cut-off frequency of the velocity measurement system to ~2Hz By inspection of graphs of time series sensor output and sensor velocity data it was found that this was the maximum rate at which the velocity measurement system could respond to changes in the velocity of the sensor This limit is due in a large part to the elasticity of the driveline

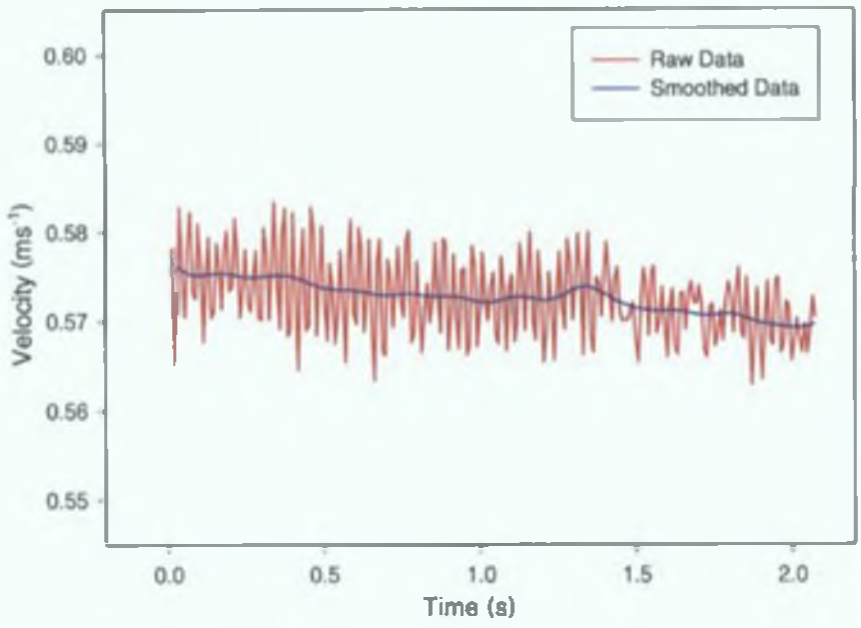

Figure 4.14 Raw and smoothed sensor velocity data

4.3.3 Velocity Response of the Sensor

As we have mentioned in the last section the velocity and temperature response of the sensor has been determined separately. In order to be able to analyse the velocity response of the sensor independently of the ambient temperature of the water the temperature of the water in the tank must remain uniform and constant for the time it takes to obtain a set of calibration data. This was accomplished by removing any heat sources in the vicinity of the tank and mixing the water thoroughly before the starting to acquire data.

The velocity response of the sensor can be determined by fitting a general expression to the data contained in the synchronised file discussed in the previous section.

For hot wire and hot film anemometers the general form of their velocity response can be determined by carrying out a theoretical analysis of their heat transfer characteristics, however, as discussed in section 2.7.3.1, this approach does not work for thermistor based anemometers. Therefore the general form of the response equation has to be guessed. As a starting point the various response equations that are reported in the literature are analysed in terms of quality of fit. The various response equations that have been used by investigators over the years are listed in Table 2.1. In order to be able to fit these equations to the data it was necessary to rewrite them in terms of dissipated power. The altered expressions are given in Table 4.4.

Investigator	Response Equation
Rasmussen (1962)	$P_s = A + B(1 - e^{-CU})$
Le Barbera and Vogel (1976), MacIntyre (1986)	$P_s = A + B(\ln U)^2$
Okamoto (1994)	$P_s = \frac{A}{\ln U - B}$
Grahn (1962), Katz (1987)	$P_s = A + B \ln U$
Riedl and Machen (1972), Yang (1988)	$P_s = A + BU^{0.5}$

Table 4 4 The various calibration relations that have been applied to thermistor sensors and the investigators who used them It was necessary to alter the equation of Le Barbera and Vogel (1976) in order to be able to use it with dissipated power data Riedl and Machen (1972) and Yang (1988) have used King Law

A number of fitting programs and packages, all of which were based on the principle of least squares fitting, were used and evaluated during the calibration process and the "fit" function in Gnuplot was found to be the easiest to use and also provided a large degree of control over the fit parameters, an area in which other packages were found lacking

The equations in Table 4 4 have been fitted to the Sensor 1 data referred to in the last section and graphs of the resulting functions superimposed on the calibration data can be found in Figure 4 15 The coefficients of the best-fit functions are listed in Table 4 5

Response Equation	A	B	C	n
$P_s = A + B(1 - e^{-CU})$	0 35004	0 0736368	18 4729	-
$P_s = A + B(\ln U)^2$	0 428148	- 0 00345666	-	-
$P_s = \frac{A}{\ln U - B}$	-8 87858	19 6849	-	-
$P_s = A + B \ln U$	0 447128	0 0182791	-	-
$P_s = A + BU^{0.5}$	0 363857	0 109698	-	-
$P_s = A + BU^n$	-7 29945	7 74667	-	0 00237341

Table 4 5 Calibration coefficients of the best-fit functions shown in Figure 4 15

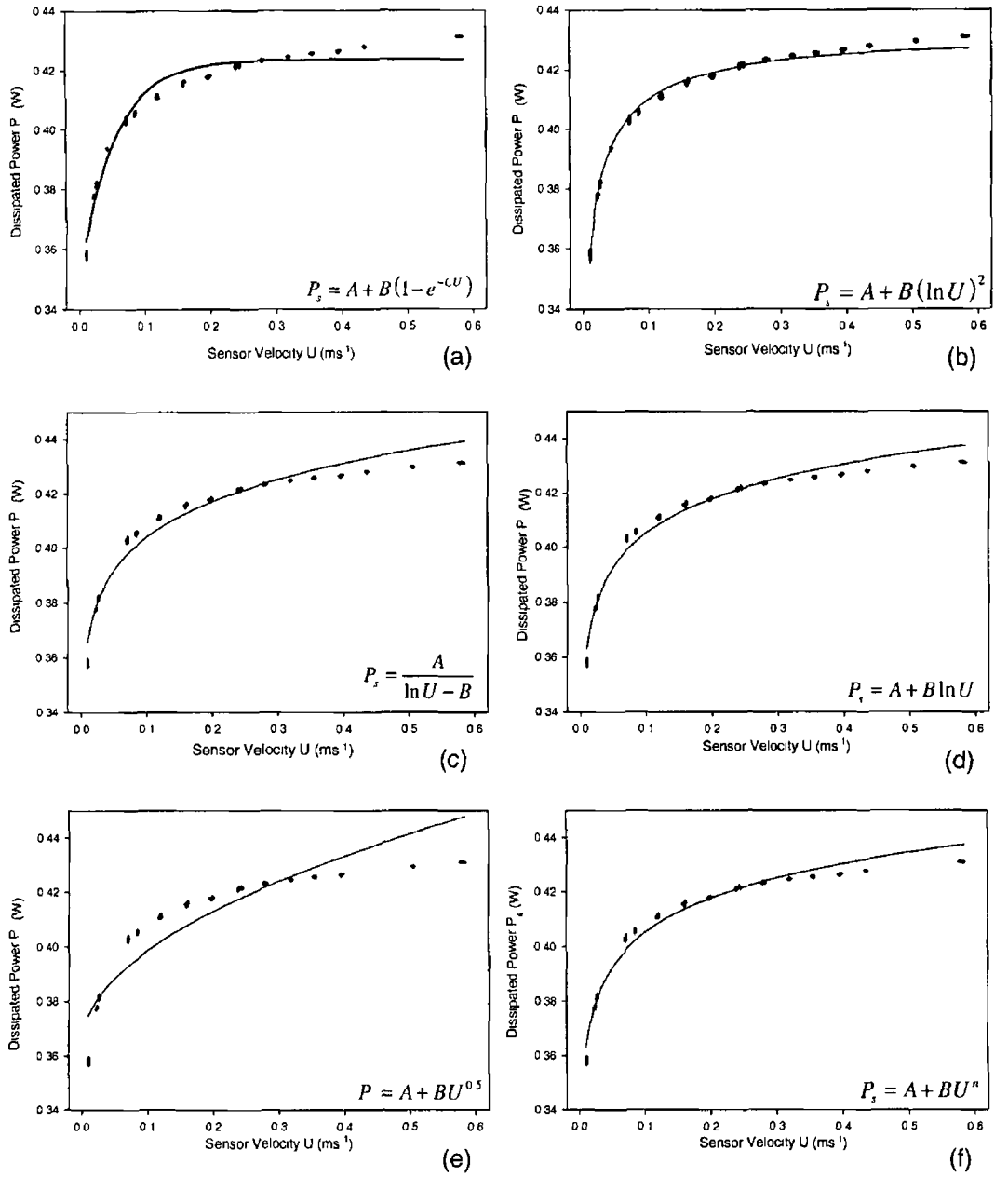

Figure 4 15 Graphs of the best fit functions that results from fitting various general response equations to calibration data obtained using Sensor 1

None of the functions shown above describe the data very well with the equation used by Riedl and Machen (1972) and Yang (1988), which is Kings Law, and is shown in Figure 4 15(e), being the worst fit of all This clearly demonstrates the fact that thermistor based sensors cannot be described by conventional theoretical models The modified version of Kings Law, which was introduced by Bruun (1995, b) has been fitted to the data and can be seen in Figure 4 15(f) There is significant improvement over Kings Law however the quality of the fit obtained is still quite poor

While visual inspection and analysis of curve fits can be very useful it is somewhat subjective and a method of mathematically quantifying or measuring the quality or "goodness" of a curve fit is necessary There are a number of quantities that can be calculated in order to assess the quality of a curve fit, the most readily available being the Sum of Squared Residuals (SSR) of the function The SSR is the sum of the difference or residual between each data point and the corresponding point of the fit function and is given by

$$SSR = \sum_{i=1}^{N} \left(y_i - f(x_i) \right)^2 \qquad (4\ 8)$$

where $f(\ )$ is the current fit function and N is the number of sets of data points being fitted

The smaller the SSR, the more accurately the function describes the data The following table gives the SSR values of each of the curve fit functions that are shown in Figure 4 15

Response Equation	SSR
$P_1 = A + B(1 - e^{-CU})$	0 0261633
$P_2 = A + B(\ln U)^2$	0 0045248
$P_3 = \dfrac{A}{\ln U - B}$	0 0396742
$P_4 = A + B \ln U$	0 0227968
$P_5 = A + BU^{0.5}$	0 1600300
$P_6 = A + BU^n$	0 0231832

Table 4 6 SSR values of the curve fit functions shown in Figure 4 15

The SSR values that have been obtained confirm what was found by the graphical analysis of Figure 4 15 in that the function originating from that of LeBarbera and Vogel (1976) has the smallest SSR and is therefore the best fit, while that of Kings Law is the largest and is therefore the worst fit It should be noted that the SSR will depend on the number of points in the data file, assuming random distribution, so therefore the SSR cannot be used to compare the quality of fit of a function to two sets of data of different sizes There are alternative statistical quantities that could have been used, such as the correlation coefficient, however they are quite

complicated to implement and since the same set of data was used throughout this analysis the SSR based analysis proved satisfactory

4 3.3.1 Improved General Response Equations

As discussed previously the quality of fit obtained with all of the general equations that have been tested so far are quite poor Therefore it is necessary to find a general equation that will better describe the velocity response of the sensor

Wu and Bose (1993) have used the general equation

$$V_s^2 = A + BU^n + CU^{2n} \tag{4 9}$$

to describe the response of a hot film sensor being used in a velocity range similar to that being used here The justification given for the use of this expression, which is basically an extended form of Kings Law, was that the relationship between the Nusselt number, Nu, of the sensor and the Reynolds number, Re, of the fluid is better described by a polynomial in Re rather than by the empirical relationships that are the basis of Kings Law It seems reasonable that the same might apply to a thermistor-based sensor so this equation was fitted to the data to determine if it is an improvement It first had to be expressed in terms of dissipated power, P_s, which was accomplished by dividing through (4 9) by R_s to get

$$P_s = A + BU^n + CU^{2n} \tag{4 10}$$

The coefficients and SSR of the best-fit function are given in Table 4 7

A	B	C	n	SSR
-16 6068	9 20774	3 92314	0 00107467	0 0229714

Table 4 7 Coefficients and SSR that resulted from fitting (4 10) to the calibration data

The SSR of this equation is only marginally (~0 0002) less than that of the modified Kings Law of Bruun (1995, b) and is therefore of little benefit Attempts were made to improve on this equation by using the more general expression

$$P_s = A + BU^n + CU^m \tag{4 11}$$

however problems were encountered while trying to fit expressions of this form to the data The fitting program was returning functions that were obviously not the best fit and it was found that different functions were returned if different starting values of the coefficients were used According to the user manuals of Gnuplot, Sigmaplot and

Origin this problem can occur under certain circumstances and that there is no known solution The problem is caused by the internal expression that the program is trying to minimise having many local minima Fitting programs cannot determine if the minimum that has been reached is the global minimum or not, so when they reach a minimum they stop, which leads to the possibility of multiple results being returned by a fitting program for certain equations and sets of data For the majority of general equations and data sets this problem does not occur and the program will converge on the global minimum, however it must be borne in mind that curve fitting is not foolproof! Theoretically, it should be possible to find the global maximum by manually iterating through different starting values for the coefficients until a satisfactory SSR is obtained This would be a very time consuming process and would also present the user with the problem of identifying when the minimum SSR has been attained – an impossible task! Therefore while some particular polynomial in U may describe the data very well it would be very difficult and time consuming to find this polynomial and as a result they are not suitable for use in the current circumstances

4 3 3 1 1 Logarithmic Polynomial

The equation that resulted from that of Le Barbera and Vogel (1976) has given the best quality fit of all of those tested to date The expression, which is

$$P_3 = A + B(\ln U)^2 \tag{4 12}$$

can be considered to be a partial polynomial in $\ln U$ This introduces the possibility that a more complex polynomial in $\ln U$ may result in a better fit

The general function

$$P_4 = A + B\ln U + C(\ln U)^2 + D(\ln U)^3 \tag{4 13}$$

which is a third order polynomial in $\ln U$, was fitted to the data and a high quality fit was obtained The problems associated with fitting polynomials in U were not encountered for polynomials in $\ln U$, in fact the fitting program calculated the best fit function on average eight to ten times faster than for any other equations, which proved to be an advantage when dealing with large data sets Figure 4 16 shows graphs of the data and the best-fit function obtained with (4 13) The coefficients and SSR of the curve fit function are listed in Table 4 8

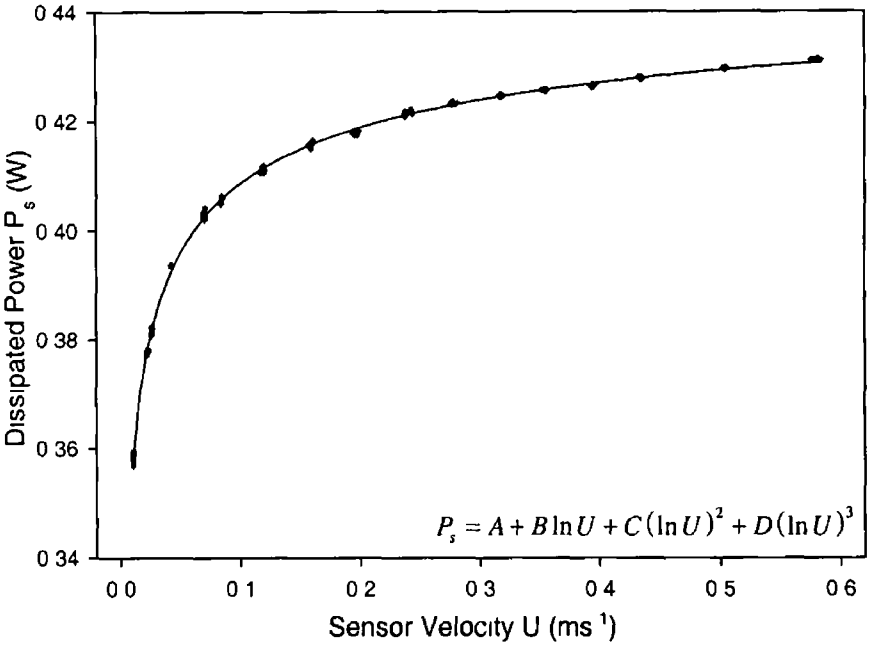

Figure 4 16 Curve fit function obtained with third order polynomial in ln$U$

A	B	C	D	SSR
0 434906	0 00687478	-0 00182121	0 0000815792	0 00085721

Table 4 8 Curve fit function coefficients and SSR for third order polynomial in ln$U$

It is apparent from visual comparison that the quality of the fit of (4 13) to the data is far superior to any of the other functions tested Its SSR value is a factor of six times smaller than that of the next best function, which is quite a significant improvement In reality, none of the previous functions could have been used with the expectation that meaningful velocity data would have been obtained, however the quality of the fit obtained with this equation means that describing the response of the sensor with a general function for the purposes of data processing is now viable If a function of suitable quality could not be found then another method such as look up tables etc would have had to be employed Such alternative methods would be significantly more difficult to implement and use so therefore finding an expression that accurately describes the velocity response of the sensor is a significant milestone in the development of a useable sensor

4.3.3 1 2 Alternate Logarithmic Functions

The data has been curve fitted with fourth and fifth order polynomials, however there was very little improvement in the fit when compared with that of the third order equation and it was decided that the magnitude of the improvement did not justify the added complexity of using higher order equations

Steinhart and Hart found that the temperature dependence of a thermistor could be described by the expression

$$\frac{1}{T} = A + B\ln R + C(\ln R)^2 + D(\ln R)^3 \qquad (4\ 14)$$

which is of the same form as (4 13) They also found that it could be replaced by the simpler expression

$$\frac{1}{T} = A + B(\ln R) + C(\ln R)^3 \qquad (4\ 15)$$

with negligible effects on accuracy It would be interesting to see if the same will apply to (4 13) The expression

$$P_s = A + B\ln U + C(\ln U)^3 \qquad (4\ 16)$$

was fitted to the data and the coefficients and SSR listed in Table 4 9 were obtained

A	B	C	SSR
0 433713	0 0112097	0 000305896	0 00109558

Table 4 9 Coefficients and SSR of three-term, third order logarithmic polynomial curve fit function

The fit functions of the three and four term equations, (4 13) and (4 16) are graphically almost identical with the SSR of the three term function is $2\,4\times10^{-4}$ greater than that of the four term function Therefore, the four-term equation would yield more accurate results and should be used where possible, however the difference between the quality of the fit obtained by both functions is quite small and the more computationally efficient three term equation could be used with little degradation in the quality of velocity data obtained in circumstances with limited computational resources, for example, the implementation of the raw data to velocity conversion using a micro-controller etc

4.3.4 Temperature Response

We found in section 2.6 that as a result of the relatively small temperature difference that must exist between the velocity sensor and the surrounding water that the output of the sensor will be sensitive to even small changes in the ambient temperature of the water. This is clearly evident in Figure 4.17, which shows the calibration functions that describe data obtained at a number of different ambient temperatures. Temperature calibration of the thermistor anemometer has been carried out in terms of ambient temperature so that any deviation in its actual operating temperature from its theoretical value resulting from the intrinsic characteristics of the control circuit, as discussed in section 4.1.2.1, will automatically be taken into account by the calibration process. It should be noted that a key requirement of this very useful technique is that the operating parameters of the control circuit, for example offset voltage are not altered after calibration has taken place.

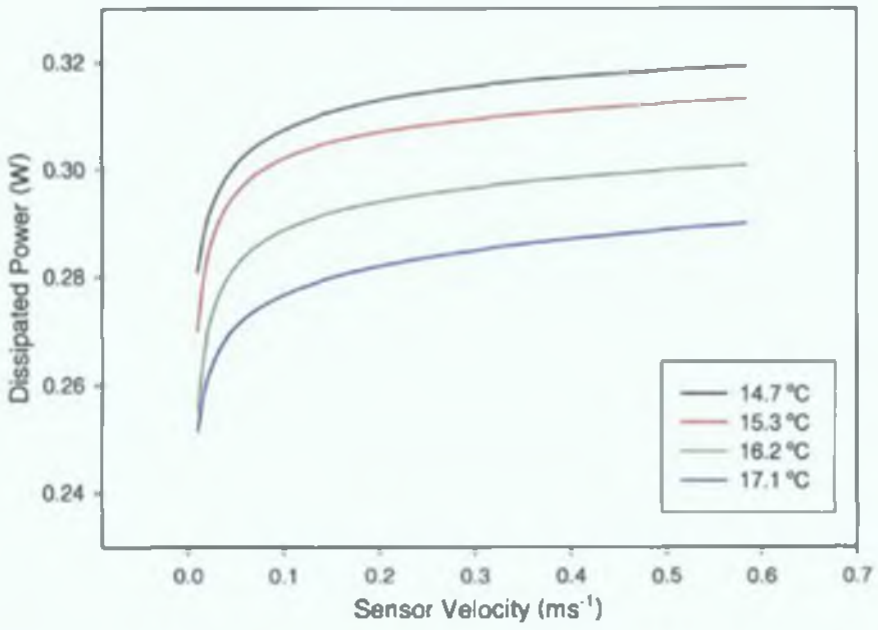

Figure 4.17 Four term calibration functions of Sensor 2 data taken at a number of different ambient water temperatures. The operating temperature of the velocity sensor remained constant for all of the data. As the temperature of the water increases the power dissipated by the sensor decreases.

The data in this graph shows how significant a problem changes in ambient temperature are for anemometers that used in water. A temperature change of just 3°C has resulted in a change in the output of the velocity sensor of approximately 75% of its range at 15°C. An accurate method of detecting and accounting for changes in ambient temperature is therefore essential. The ambient temperature measurement

system that has been developed, which is discussed in detail in 3 2, has a measurement resolution of ~0 0011°C This corresponds to a change in the dissipated power of ~0 003% of the output range of the sensor, which is well below the amplitude of the intrinsic noise in the velocity sensor circuit output

The most straightforward method of taking account of both the temperature and velocity dependence of the thermistor anemometer sensor, whereby the general form of the sensors calibration expression will be obtained is to introduce the temperature dependence as a correction to the known velocity response characteristics of the sensor It turns out that this is quite simple to achieve Table 4 10 lists the coefficients of the best-fit functions in Figure 4 17 Examination reveals that the A and B coefficients of the functions are approximately linearly related to temperature This can be seen in Figure 4 18 where A and B of the four functions are graphed as a function of temperature

Ambient Water Temperature (°C)	A	B	C	D
14 7	0 321691	0 00387645	-0 000936411	0 000032496
15 3	0 316707	0 00684630	0 00114204	0 000405580
16 2	0 304437	0 00710628	0 00104388	0 000397239
17 1	0 294570	0 00894075	0 00108797	0 000257337

Table 4 10 Coefficients of curve fit functions shown in Figure 4 17 The functions are identified in terms of the ambient temperature of the water at which the data they describe was obtained

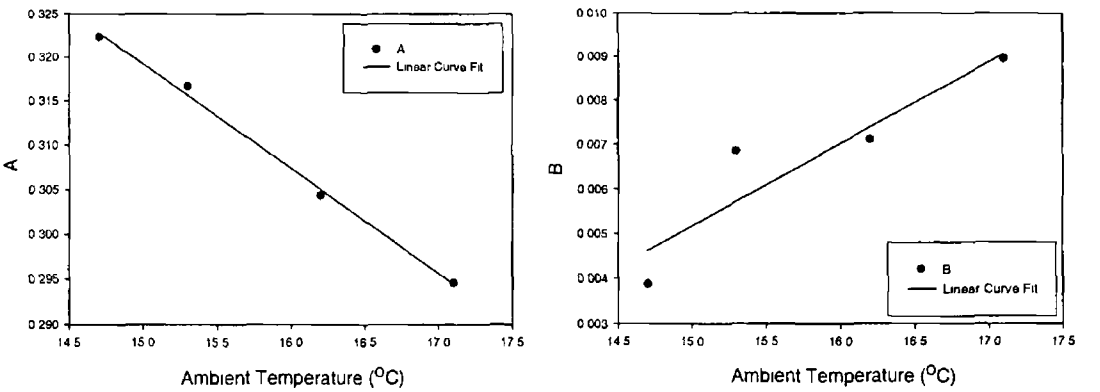

Figure 4 18 Graphs of the A and B coefficients of the curve fit functions shown in Figure 4 17 as a function of ambient water temperature

The linear relationship between A, B and ambient water temperature, T_a, can be described by

$$\begin{aligned} A &= m_A T_a + c_A \\ B &= m_B T_a + c_B \end{aligned} \qquad (4\ 17)$$

where m_A, m_B, c_A and c_B are arbitrary constants that can be determined by curve fitting the relevant data

While the coefficients A and B clearly have a linear dependence on temperature there doesn't seem to be a discernible relationship between C, D and temperature This is believed to be caused by the effects of noise and the fact that a number of different combinations of C and D can result in very similar functions As a result of this it is not possible to determine the functional form of the ambient temperature dependence of C and D by inspection

If it is assumed that the dependence of C and D on ambient temperature is also linear, which as we will see later is a valid assumption, then the four-term velocity calibration curve given by (4 13) becomes

$$P_{\backslash} = m_A T_a + c_A + (m_B T_a + c_B)\ln U + (m_C T_a + c_C)(\ln U)^2 + (m_D T_a + c_D)(\ln U)^3 \qquad (4\ 18)$$

where the coefficients m_A m_D, c_A c_D can be determined by fitting the equation to simultaneous sensor output, sensor velocity and ambient water temperature data

Equation (4 18) is the equation of the surface that describes the response of the thermistor anemometer to velocity and ambient water temperature Sensor output, sensor velocity and ambient temperature data has been obtained using Sensor 1 for a range of ambient water temperatures and has been combined into a single synchronised file that was subsequently fitted with (4 18) The resulting calibration surface and the data that it describes can be seen in Figure 4 19 and the coefficients of the calibration surface and its SSR are listed in Table 4 11

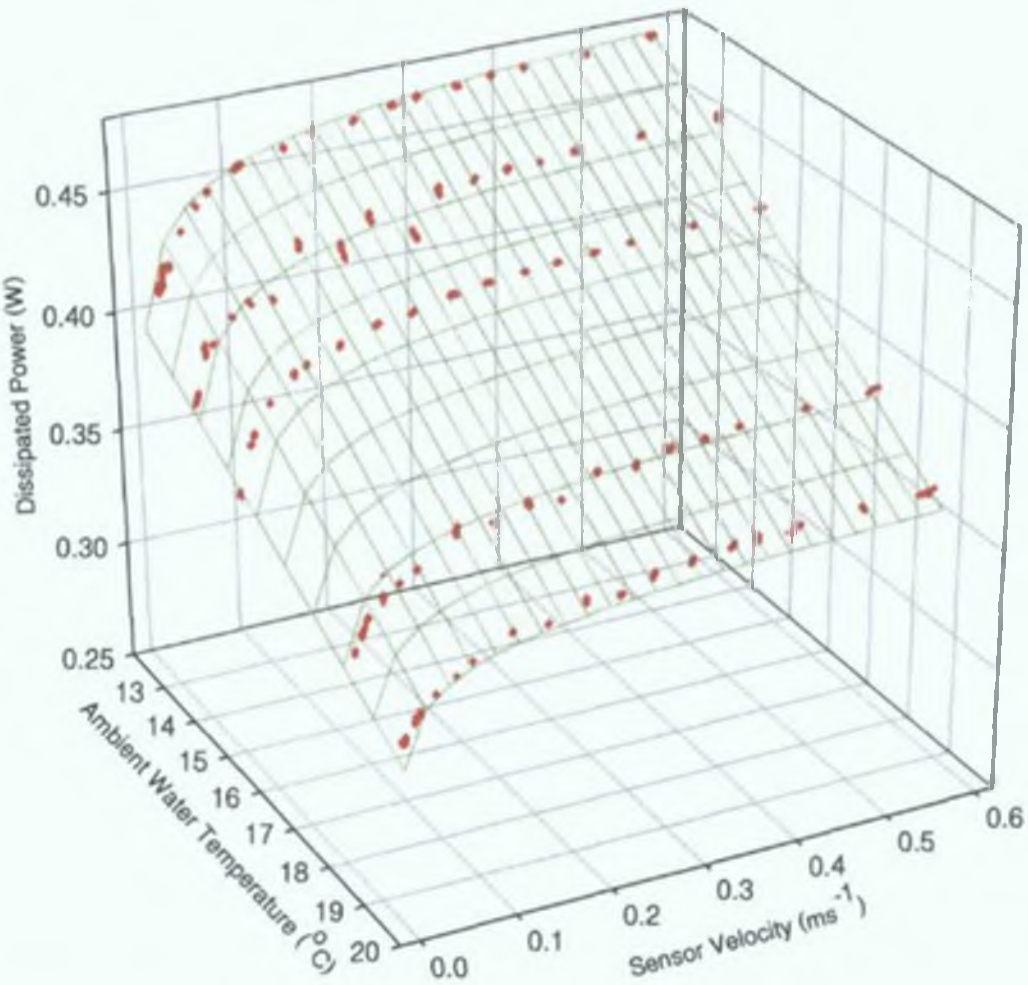

Figure 4.19 Calibration Surface for Sensor 1 for the velocity range 0.01 to 0.6ms^{-1} and the ambient temperature range of 12°C to 20°C. No attempt was made to keep the temperature of the tank constant while this data was being obtained with the resulting temperature distribution being clearly visible in the data. The temperature range that has been chosen corresponds to the range of temperatures that are likely to be experienced in Irish coastal waters during the summer months.

m_A	0.669787
c_A	-0.157083
m_B	0.0186999
c_B	-0.000811231
m_C	-0.00367243
c_C	-0.0000921059
m_D	0.000556217
c_D	-0.0000311095
SSR	0.0071928

Table 4.11 Coefficients and SSR of best fit of the general velocity and ambient temperature equation response equation to sensor output, sensor velocity and ambient temperature data obtained over a range of velocities and ambient temperatures.

It is quite difficult to determine the quality of a surface fit visually, however comparing its SSR with that of the 2-D velocity response curve fit discussed in the last section will give an indication of its quality Since a different number of data points were used to obtain each curve fit the SSR values of the fits will have to be adjusted or normalised before they can be meaningfully compared When the relative number of data points that were used to obtain each fit is considered the surface fit SSR becomes 0 0014, which compares quite favourably with the SSR of the four-term velocity response curve fit, which is 0 0008 This confirms that for the temperature range in question that the assumption that the temperature dependence of the C and D coefficients of the four-term velocity response equation is a valid one and that equation (4 18) accurately describes the response of the sensor in the velocity and ambient temperature ranges in question

The calibration surface in Figure 4 19 clearly demonstrates the effect that the temperature difference between the sensor and the water has on the sensitivity of the circuit The sensor is noticeably more sensitive to velocity at lower ambient temperatures, which corresponds to a larger temperature difference Therefore the operating temperature of the sensor should be set at the maximum possible value that will not lead to bubble formation (see sections 2 5 1 and 3 6 5)

4 4 Measuring Water Velocity with Calibrated Thermistor Anemometer Probe

A complete, calibrated velocity measurement probe consists of a velocity sensing thermistor sensor, the response of which to velocity and ambient temperature is fully known, and a temperature sensing thermistor sensor that measures the temperature of the water The temperature sensor is mounted as close to the velocity sensor as possible without causing any mutual interference The output of the complete sensor system is a data file that contains raw ADC data that can be processed to obtain time referenced dissipated power and ambient temperature values Then, all that remains to do is to calculate the velocity of the water using the calibration equation of the velocity sensor This however, is not as trivial as it may seem! In order to calculate velocity form dissipated power and ambient temperature data the calibration equation, (4 18), must be solved for velocity Since it is a polynomial this can only be achieved by determining its roots

4 4 1 Calculating the Roots of the Calibration Equation

The roots of polynomials up to the fourth order can be determined using analytical techniques so therefore applying the relevant technique should result in an expression that will give the velocity of the water in terms of the measured dissipated power and ambient temperature values

The calibration equation is a third order or cubic polynomial Abramowitz (1964) states that the three roots of a cubic polynomial of the form

$$z^3 + a_2 z^2 + a_1 z + a_0 = 0 \tag{4 19}$$

are given by

$$\boxed{\begin{aligned} z_1 &= -\tfrac{1}{3} a_2 + (S+T) \\ z_2 &= -\tfrac{1}{3} a_2 - \tfrac{1}{2}(S+T) + \tfrac{1}{2} i\sqrt{3}(S-T) \\ z_3 &= -\tfrac{1}{3} a_2 - \tfrac{1}{2}(S+T) - \tfrac{1}{2} i\sqrt{3}(S-T) \end{aligned}} \tag{4 20}$$

where

$$S = \sqrt[3]{R + \sqrt{D}}$$

$$T = \sqrt[3]{R - \sqrt{D}}$$

$$D = Q^3 + R^2$$

$$Q = \frac{3a_1 - a_2^2}{9}$$

$$R = \frac{9a_1 a_2 - 27a_0 - 2a_2^3}{54}$$

In order to be able to calculate the roots of the calibration equation, which is

$$P_s = m_A T_a + c_A + (m_B T_a + c_B)\ln U + (m_C T_a + c_C)(\ln U)^2 + (m_D T_a + c_D)(\ln U)^3$$

using the formulae given in (4 20), the calibration equation must be rewritten in the general form of (4 19) This can be achieved by letting

$$a_2 = \frac{m_C T_a + c_C}{m_D T_a + c_D}$$

$$a_1 = \frac{m_B T_a + c_B}{m_D T_a + c_D}$$

$$a_0 = \frac{m_A T_a + c_A - P_s}{m_D T_a + c_D}$$

We now have all of the necessary equations and relations to calculate the three roots of the calibration equation. A program has been written to perform the necessary calculations and determine the three roots of the calibration equation and can be found in Appendix C.5. It was found that the calculations involved were considerably more complex than they appear on the surface. This was due to the fact that a number has three cube roots, two of which are always complex, which means that there are three equally valid possibilities for the values of S and T in the equations in (4.20) for a single pair of P_s and T_a data, each of which will result in a different set of roots of the calibration equation. It was possible, using rules regarding the possible combinations of cubic polynomial roots that can exist, to determine when the correct values of S and T were being used, however no reference could be found to any method of mathematically determining the correct choice. Resulting from a trial and error analysis, it was found that the correct choice of the three possibilities of S and T that exist could be related to the numerical properties of $R+\sqrt{D}$ and $R-\sqrt{D}$. The details of the relationship, which is quite complex, are not discussed here for reasons that will soon become apparent! They have been implemented in the program that calculates the roots of the calibration equation and are commented reasonably well in the code, which can be found in Appendix C.5, if details are required.

4.4.1.1 Downfall of Root finding Method

The calibration equation has three roots and only one of them will be the correct value of $\ln U$ for a given pair of dissipated and velocity data, or from another point of view, only one of the equations in (4.20) will return the correct value for a particular pair of data points. In an ideal world, the same equation would return the correct value of $\ln U$ for all values of P_s and T_a, which would mean that a single equation could be

used to convert dissipated power and temperature data to velocity However this is not the case, so all three roots must be evaluated and the correct one chosen by inspection It was found that for certain values of P_s and T_a, that all three roots were very close together, which ruled out the possibility of implementing a rule based algorithm for choosing the correct value The possibility of the existence of a relationship between the values of P_s and T_a and the equation that would gave the correct answer was investigated extensively, however no such relationship could be found Therefore finding the roots of, or by implication, any form of algebraic manipulation of the calibration equation cannot be used to convert P_s and T_a values to velocity

4 4 2 Alternative Calibration Equations

The most obvious solution to this problem is to obtain a calibration equation that expresses velocity as a function of ambient temperature and dissipated power This would eliminate the need for algebraic manipulation of any kind, as the calibration equation would already be in the required form Bruun (1995, o), Swaminathan (1986) have applied this principle to hot wire anemometers and expressed the velocity in terms of a polynomial in the sensor voltage, V_s Attempts were made to fit a polynomial of the form

$$U = A + BP_s + CP_s^2 + DP_s^3 \tag{4 21}$$

to the data used previously, however the problem of convergence of the fitting program on incorrect functions was encountered, as before It is believed that the response of the sensor is not suitable for description by polynomials in either P_s or U A polynomial in $\sqrt{P_s}$ was also tested so that the equation would be equivalent to that of Bruun (1995, o) and Swaminathan (1986), however there was no improvement in performance Other equations, such as polynomials in $\ln P_s$ were tested, but while they converged rapidly to the best-fit function, the quality of the fit was quite poor Therefore, while the method worked well when applied to hot wire anemometers it is not suitable for use with thermistor-based anemometers and that the only viable calibration equation is equation (4 18)

4.4.3 Successive Approximation Technique

A technique based on the principle of successive approximation, as used in ADC's (see Horowitz and Hill 1998), has been developed for the calculation of velocity from

P_s and T_a data using the calibration equation of the sensor It gives problem free, efficient operation at a fraction of the computational cost of the root finding method A program has been written to convert raw ADC data to dissipated power and ambient temperature and to calculate velocity from this data using the successive approximation technique, the code for which can be found in Appendix C 4 The successive approximation algorithm has been written with a four-term calibration equation in mind and reads in the coefficients of the equation from a file specified by the user The required tolerance was set to 1×10^{-10} W, which is well below the precision to which the dissipated power is measured It has been found that the algorithm will converge to the specified tolerance in a maximum of 45 iterations for any velocity in the range 0 01 to 0 6ms ^{1}

The successive approximation technique has proven extremely useful and if it were not used then a less accurate calibration equation that could be inverted would have been necessary We saw earlier that the fits obtained with other calibration equations were quite poor and if one of them had to be used out of necessity of an equation that could be inverted then the quality of any velocity measurements obtained with the sensor would have been significantly reduced The computational efficiency of the technique makes it suitable for implementation on a micro controller etc, which would make real-time measurements a possibility No reference could be found to the use of a successive approximation technique for thermal anemometry, meaning that its inclusion in this work is of significant importance

4 5 Sensor Range

A procedure was developed in section 3 6 2 for calculating the range of a sensor from its response equation, output voltage noise levels and the allowed uncertainty in the resulting velocity measurements The basic principle of this method is that the maximum velocity, U_R, that can be measured to within a certain fractional accuracy is determined by equating the peak to peak noise voltage in the sensor output, V_N, and the quantity ξV_R, which is given by (3 48) and is

$$\xi V_R = f\left(U_R\left(1+\frac{\tau}{2}\right)\right) - f\left(U_R\left(1-\frac{\tau}{2}\right)\right) \tag{4 22}$$

where $f(U)$ is a function describing the velocity dependence of the voltage drop across the sensor, V_s, and τ is the allowed fractional uncertainty in the velocity

measurement Evaluation of ξV_R using (4 22) requires that the velocity response of the sensor be expressed in terms of the sensor voltage, however the sensors have been calibrated in terms of dissipated power This problem can be overcome by either modifying (4 22) so that the sensor calibration equation, which describes the response of the sensor in terms of dissipated power, can be used or by converting the peak-to-peak noise voltage levels into equivalent dissipated power noise levels From a mathematical point of view, the most straightforward approach is to modify (4 22) The standard calibration equation, which is of the form, $P_s = f_p(U,T_a)$, where f_p is the function that describes the velocity and temperature dependence of the dissipated power, can be expressed in terms of sensor voltage by to get

$$V_s = \sqrt{f_p(U,T_a)R_s} \tag{4 23}$$

Incorporating this into (4 22) result in

$$\xi V_R = \sqrt{f_p\left(U_R\left(1+\frac{\tau}{2}\right),T_a\right)R_s} - \sqrt{f_p\left(U_R\left(1-\frac{\tau}{2}\right),T_a\right)R_s} \tag{4 24}$$

Therefore the relationship between the sensor output voltage noise, V_N, the velocity response of the sensor, $f_p(U,T_a)$, the maximum allowed fractional error in velocity measurements, τ , and the maximum velocity that can be measured by the sensor, U_R, is given by

$$V_N = \sqrt{f_p\left(U_R\left(1+\frac{\tau}{2}\right),T_a\right)R_s} - \sqrt{f_p\left(U_R\left(1-\frac{\tau}{2}\right),T_a\right)R_s} \tag{4 25}$$

As discussed in section 4 4 1 1 it is not possible to solve $f_p(U,T_a)$ in terms of U, therefore, (4 25) cannot be algebraically manipulated to obtain an expression in terms of U_R, however it can be calculated using the successive approximation technique described in section 4 4 3 A program has been written to implement (4 25) and when applied to the velocity response of Sensor 1 at 15°C and the noise data given in Figure 4 8 for fractional uncertainties of 0 1 and 0 05, the maximum velocity values in Table 4 12 were obtained

Corner Frequency (Hz)	Maximum Velocity for τ =0 1 (ms^{1})	Maximum Velocity for τ =0 05 (ms^{1})
16	>0 6	>0 6
33	>0 6	>0 6
100	0 59	0 139
200	0 27	0 026
500	0 06	<0 01
860	0 02	<0 01

Table 4 12 Maximum velocity that can be measured to within a certain fractional error, τ, for a range of sensor system corner frequencies

The data in the above table clearly demonstrates the choice that must be made between frequency response and operating range

4 6 Influence of Coating Thickness on Sensor Characteristics

The theoretical analysis of the effect of coating thickness on the heat transfer characteristics of a coated anemometer indicated that the thickness of the coating has a dramatic effect on the sensitivity and thus the operating range of the anemometer Experimental evidence has been found that confirms that this is indeed the case Figure 4 20 shows the calibration curves of a number of sensors with different coating thicknesses at an ambient water temperature of 19 5°C The operating temperature of each of the sensors was 45°C The coating thickness has been quantified in terms of the number of times the sensor was dip coated The use of dip coating means that it can be assumed that the overall coating thickness increases by a uniform amount with each individual coating

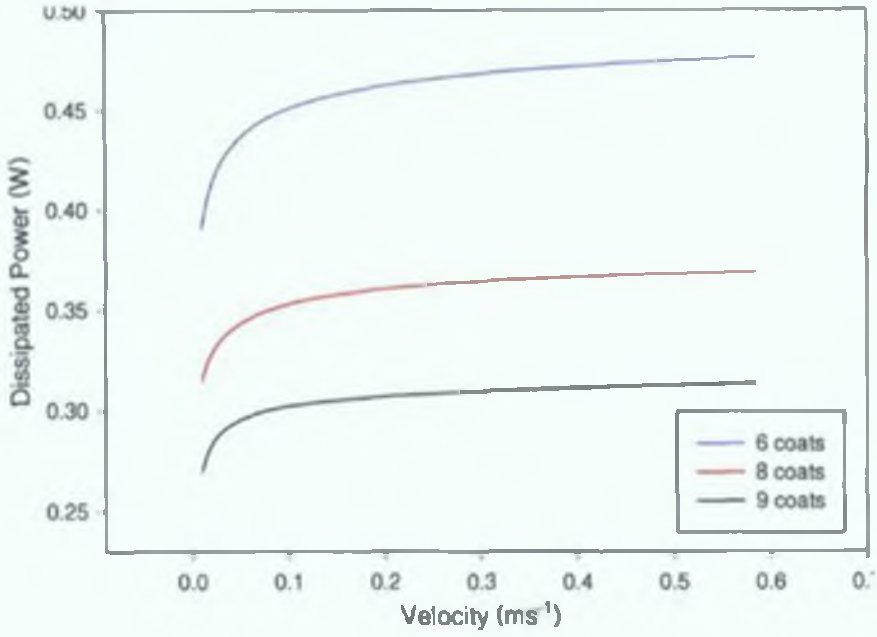

Figure 4.20 Calibration curves for a number of sensors with different coating thicknesses.

While it is not very pronounced, it can be seen that there is a decrease in the sensitivity of the sensor as the coating thickness is increased.

Attempts were made to make sensors with thinner coatings, however the coating would not remain intact for long enough to obtain calibration data. The cause of the failure has been attributed to the reduced thickness of the coating at the corners of the thermistor due to surface tension effects and the fact that any stresses in the coating due to a mismatch of the thermal expansion coefficients of the thermistor and the coating material will be concentrated at these points. It is likely that a thinner coating could be used with a cylindrical thermistor, however no such thermistors could be sourced commercially. The use of such thermistors would also introduce the possibility of using different coating materials, for example solgels, which could not be used with the chip thermistor because of the coating thickness required.

While calibration data could not be obtained for a sensor with thinner coatings than those described by Figure 4.20, it was possible to determine the range of output voltages that corresponded to the velocity range of the tow tank. Comparing this range to the range of one of the robust sensors whose sensitivity is known, will give an indication of the improvement in sensitivity that would result from the reduced coating thickness. The output voltage range of Sensor 1, which was dip coated six times and the output voltage range of a sensor which was dip coated three times are given in Table 4.13.

Coating Thickness	Output Voltage Range (V)
6 coats	2 1
3 coats	7

Table 4 13 Sensor output voltage range that corresponds to the velocity range of the tow tank for sensors with different coating thicknesses

The data in Table 4 13 indicates that the sensitivity of the reduced coating thickness sensor was a factor of three times greater than that of Sensor 1 This clearly demonstrates the effect of coating thickness on sensor performance and highlights the importance of development of thermistors that can be used with a thinner coating

4 6.1 Frequency Response

We mentioned in section 4 1 3 that the coating thickness of a sensor has a significant effect on the frequency response characteristics of the sensor Table 4 14 gives the response time, t_X, and the corresponding corner frequency of the sensors whose velocity response is shown in Figure 4 20

Coating Thickness	Response Time (ms)	Corner Frequency (Hz)
6 coats	1 16	862
8 coats	1 58	632
9 coats	1 8	555

Table 4 14 Square wave response time and corner frequency of a number of sensors with different coating thicknesses

The corner frequency of the sensor increases as the coating thickness of the sensor decreases, which gives yet another reason for keeping the sensor coating as thin as possible The reason for the increase in corner frequency with decreasing coating thickness is that the thermal capacity and thus inertia of the coating will decrease as it gets thinner, which results in a decrease of the overall response time of the sensor

4 7 Effects of Coating Failure on Sensor Performance

When the coating of a sensor fails two things happen Firstly, the response characteristics of the sensor are altered as a result of the physical change to the coating that occurs and secondly, the control circuit becomes electrically connected to the body of water in which the sensor is operating The altered response characteristics mean that the calibration of the sensor that has been carried out is no

longer valid and that recalibration is necessary Figure 4 21 shows a set of calibration data that has been obtained using a leaking sensor

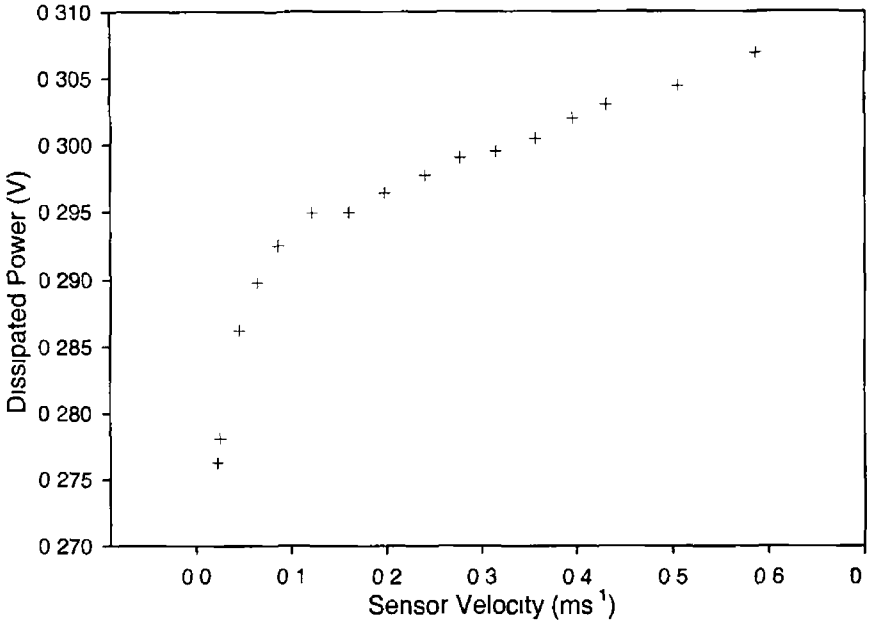

Figure 4 21 Calibration data that was obtained using a sensor that was later found to be leaking The data was obtained using the averaging method

It can be seen that the changes in characteristics that occur are random in nature This means that once a sensor begins to leak it will no longer give reliable measurements The electrical connection between the control circuit and the water results in a dramatic increase in the sensor output noise The noise in the output of an optimised sensor has been observed to increase from 60mV to ~500mV, which makes it impossible to make measurements with the sensor

4.7 1 Detecting Coating Failure

Complete coating failure is generally quite simple to diagnose due to the characteristic increase in sensor output noise and significant drift in its response Experience has revealed that coating failure does not occur instantaneously, so a number of useful techniques for detecting the onset of coating failure have been developed The simplest of these is to disconnect the sensor form the control circuit and test for a conduction path between its connecting wires and the water in which the sensor is placed using the 200MΩ scale of a digital multimeter It has been found that when the coating is in the initial stages of failure that any variations in the output voltage of the circuit also appear with reduced amplitude in the water in the vicinity of the sensor, so therefore the integrity of the coating can be examined by comparing the voltage that

appears between an electrode placed in the vicinity of the sensor and ground and the output voltage of the sensor If there is any correlation then the coating is about to fail This method has proven to be very accurate and could detect the onset of failure when none of the other signs were present

The majority of problems involving coating failure were encountered while trying to make sensors with thin coatings and while comparing the performance of various coating materials Sensors with six and above coatings with an acrylic-based material were found to be remarkably robust, with the main cause of failure/destruction being accidents in the lab As a general rule it was found that if coating failure did not occur during the first 2-3 hours of operation then it would not occur at all This time scale falls within the "burn in" time of the sensors, which means that if the coating of the sensor is intact after this period then the user can be confident in possessing a good quality sensor

4.8 Stability and Contamination Induced Drift

Drift due to contamination of the sensor is a major problem with hot film sensors and to a lesser degree with thermistor-based sensors that are used in water For hot film sensors in unfiltered tap water stability could only be achieved for a number of hours (Wu and Bose 1993) and for epoxy coated thermistor sensors drift started to occur after a number of weeks (MacIntyre 1986)

During the course of this work a single chip thermistor sensor with an acrylic based coating was used to obtain measurements in the tow tank, which was filled with unfiltered tap water, for a period in excess of three months without any drift in the response characteristics of the sensor This represents a significant improvement and it is believed to be due, at least in part, to the anti-fungal agents contained in the coating and the possibility that the acrylic based coatings that were used are more flexible than the epoxy used by MacIntyre (1986)

4.9 Directional Sensitivity

The chip thermistor sensor has been found to exhibit a degree of directional sensitivity, which is a result of its non-uniform geometry Tests have found that the change in output that corresponds to a 90° change in orientation is of the order of 15%

4 10 Calibration by Inference

It is not possible to infer or extrapolate the response of an uncalibrated sensor from that of another which has been calibrated since no two sensors are identical It is not possible to ensure that the exact same coating thickness has been applied to each sensor and there is also the possibility that the operating temperatures of different sensors may be slightly different due to resistance measurement errors or the offset voltage dependence of the operating temperature As a result of this each sensor must be calibrated individually

4 11 Multi Sensor Arrays

A multi sensor array could be constructed simply by mounting individual calibrated sensors, which will each have there own modular control and signal conditioning circuit, on a suitable support structure The replacement of a damaged/broken sensor would simply involve removing the malfunctioning sensor and control circuit module and replacing it with a new calibrated sensor unit complete with control circuit

Chapter 5 : Conclusions

A complete thermistor anemometer measurement system for use in water has been designed and implemented This includes the velocity sensor element, Constant Temperature control circuit, ambient temperature sensor and circuitry, data acquisition facilities and software and a complete calibration facility that allows the sensor to be calibrated over the velocity range of 0 01 to 0 6ms^{1} In addition significant contributions have been made to the area of thermistor anemometry

The primary aims were that the sensor would have good spatial and temporal resolution, be suitable for use as part of a multi-sensor array and be inexpensive The chip thermistor sensors that were developed have a cross-section of ~3mm, a corner frequency of ~800Hz when tuned for optimum response and are constructed from standard commercially available SMT chip thermistors which are mass-produced and are therefore very cheap This means that the sensor will be able to detect velocity changes with a spatial resolution of 3 to 4mm and a timescale of ~1 2ms, which would be more than adequate when the type of structures that are likely to be generated by breaking waves are considered

The use of a sensor with an acrylic coating has resulted in a number of advantages over the standard glass bead or epoxy coated thermistors that have been used previously for thermistor anemometers Thinner coating thicknesses can be achieved than are found on commercially available thermistors and therefore the resulting sensors have increased sensitivity and range Also, the sensors were found to be much less susceptible to contamination induced drift and coating failure than sensors based on standard thermistors This decrease in drift and reduction of occurrence of coating failure has led to sensors that give stable performance for up to three months This compares to a few weeks for previous thermistor anemometers The increased stability has now made thermistor anemometers viable for mid to long-term measurements

The only suitable uncoated thermistors that were available were rectangular chip thermistor sensors with sharp corners, which resulted in there being a minimum coating thickness that could be used It is believed that thinner coatings could be used with uncoated bead thermistors or chip thermistors with a circular cross-section, and if this were the case then their availability would lead to the production of a sensor with improved sensitivity and range

The introduction of the concept of "burn-in" time has proven to be quite useful when commissioning new sensors It provides a means of stabilising the drift in the resistance of the sensor and thus in its response to velocity It also allows the identification of sensors with poor quality coatings before they have been used to take measurements This avoids valuable time being wasted by using faulty sensors to obtain data that will essentially be useless

Changing the configuration of the control circuit from that which is normally used has had a number of important implications Firstly, the reduction in the voltage drop across the sensor coating decreased the possibility of coating failure occurring This is considered to be a possible reason for the improved long-term stability of the sensor Secondly, the altered configuration has led to the current drams on the power supplies being evenly distributed between the positive and negative supplies, which will increase the amount of time that the sensor can be used in the field before the batteries need to be recharged

The relatively simple technique that has been developed to set the operating temperature of the sensor has overcome one of the major problems facing the use of thermistors in a multi-sensor array, that is, the large variation in resistances that exists between otherwise identical thermistors, with most commercial suppliers quoting a resistance tolerance of 20%

Possibly the most significant achievement in this work in terms of the advancement of thermistor anemometry is the development of a general equation that describes the response of the sensor much more accurately than any of the equations that have been used previously and which also accounts for the dependence of the sensor output on ambient temperature The use of this improved general equation has been made possible by the application of the successive approximation technique to the conversion of raw data into velocity values It is very likely that the lack of a suitable method of achieving this has prevented other investigators from using the general equation that has been used here with such good results The successive approximation technique has proved to be very efficient and it is possible that it could be implemented on a suitable micro-controller to obtain what would be very close to a real time measurement system

This work has overcome many of the problems associated with the operation of a thermal anemometer in water, such as bubble formation, contamination etc and in

doing so has demonstrated that thermistor anemometers are a viable instrument for velocity measurements in an uncontrolled environment

****

References

Abramowitz, M and Stegun, I A (1964), *Handbook of Mathematical Functions* National Bureau of Standards, Section 3 8 2, p17

Adrian, R J (1983) *Laser Velocimetry* In Fluid Mechanics Measurements 2nd Ed , pp175-300 Ed R J Goldstein Taylor and Francis

Bruun, H H (1995) *Hot-Wire Anemometry Principles and Signal Conditioning* Oxford University Press, Oxford

Bruun (1995, a) Section 2 2 1, p32

Bruun (1995, a) Section 2 2 1, p32

Bruun (1995, b) Section 2 1 2 3, p29

Bruun (1995, c) Section 4 5, p99

Bruun (1995, d) Section 4 10 2, p114

Bruun (1995, e) Section 2 3 2, pp 38-39

Bruun (1995, f) Chapter 7, pp 208-233

Bruun (1995, g) Figure 7 3(b), p216

Bruun (1995, h) Section 2 2 2 1, p36

Bruun (1995, i) Section 2 2 2, pp 34-35

Bruun (1995, j) Section 4 10 2, pp 115-116

Bruun (1995, k) Section 4 10 2, p113

Bruun (1995, m) Section 2 3 3 1, pp 51-52

Bruun (1995, n) Section 2 3 1 1, p37

Bruun (1995, o) Section 4 4 5, pp 98-99

Catellani, A , Stacchietti, R , Taroni, A , (1982/83) *Performance and Temperature Stability of an Air Mass Flowmeter Based on a Self-Heated Thermistor*, Sensors and Actuators, **3**, pp 23-30

Comte-Bellot, G , Sarma, G R , Faure, T M (1999) *Performance Studies of the Constant Voltage Anemometer in a Mach 2 3 Boundary Layer,* ICIASF Record, Int Cong on Inst in Aero Sim Facil , Toulouse, June 14-17, 1999 IEEE USA, pp 40 1-40 9

Fannay, A H , Dougherty, B P (1987) *Measurement of Buoyancy-Induced Flow Using a Thermistor Flowmeter*, Trans ASME J of Solar Energy Eng , **109**, No 1, pp 34-39

Fingerson, L M and Freymuth, P (1983) *Thermal Anemometers* In Fluid Mechanics Measurements 2nd Ed , pp 115-174 Ed R J Goldstein Taylor and Francis

Freymuth, P (1977) *Frequency Response and Electronic Testing for Constant-Temperature Hot-Wire Anemometers*, J Phys E Sci Inst , **10**, No 7, pp 705-710

Fujita, H , Ohhashi, T , Asakura, M , Yamada, M , Watanabe, K (1995) *A Thermistor Flowmeter for Low-Flow-Rate Measurements*, IEEE Trans Instr and Meas , **44**, No 3, pp 779-782

Grahn, A R , Paul, M H , Wessel, H U (1968) *Design and Evaluation of a New Linear Thermistor Velocity Probe*, J of Appl Physiol , **24**, No 2, pp 236-246

Holman, J P (1992) *Heat Transfer, 7th Ed in S I Units* McGraw Hill International (UK)

Holman (1992, a) Section 1 3, p11

Holman (1992, b) Appendix A, pp 654-663

Horowitz, P and Hill, W (1998) *The Art of Electronics 2nd Ed* Cambridge University Press

Johnson, D R (1987) *A Surface Current Meter*, Cont Shelf Res , **7**, Iss 8, pp 975-986

Katz, I M , Shaughnessy, E J (1987) *Digital Temperature Compensation of a Thermistor Flowmeter*, J Phys E Sci Instr , **20**, pp 561-564

Katz, I M , Shaughnessy, E J (1988) *An Electronically Switched Flowmeter and Temperature Sensor Employing a Single Thermistor Probe*, J Phys E Sci Instr , **21**, pp 108-112

Kegerise, M A , Spina, E F (2000) *A comparative Study of Constant-Voltage and Constant-Temperature Hot-Wire Anemometers*, Exps in Fluids, **29**, pp 154-164

Kim, C H , Randall, R E , Boo, S Y , Krafft, M J (1992) *Kinematics of 2-D Transient Water Waves Using Laser Doppler Anemometry*, J of Waterway, Port, Coastal and Ocean Eng , **118**, No 2 pp 147-165

King, L V (1914) *On the Convection of Heat from Small Cylinders in a Stream of Fluid Determination of the Convection Constants of Small Platinum Wires with Applications to Hot-Wire Anemometry* Phil Trans Roy Soc , **A214**, pp 373-432

Kramers, H (1946) *Heat Transfer from Spheres to Flowing Media* Physica, **12**, pp61-80

Lane, A , Knight, P J , Player, R J (1999) *Current Measurement Technology for Near-Shore Waters*, Coastal Eng **37**, pp 343-368

Lawless, B (1976) *An Investigation of the Surface of the Sea Using Inverted Sea Bed Mounted Echo Sounders* Unpublished Email bl@physics dcu ie

LeBarbera, M and Vogel, S (1976) *An Inexpensive Thermistor Flowmeter for Aquatic Biology*, Limnol Oceanogr , **21**, pp 750-756

Lueck, R G , Osborn, T R (1980) *The Characteristics of Internally Heated Thermistors*, Deep-Sea Research, **27**, Part 3-4A, pp 273-292

MacIntyre, S (1986) *A Flow Measuring System for use in Small Lakes*, Limnol Oceanogr , **31**, No 4, pp 900-906

Okamoto, K , Ohhashi, T , Asakura, M , Watanabe, K (1994) *A Digital Anemometer*, IEEE Trans Instr and Meas , **43**, No 2, pp 116-120

Osborn, T , Vagle, S , Farmer, D , Cure, M , Thorpe, S , Hall, A (1993) *Bubble Plumes and Turbulence*, In Natural Physical Sources of Underwater Sound Sea

Surface Sound (2) Ed B R Kerman Kluwer Academic Publishers, Dordrecht, Boston, London

Ossofsky, E (1948) *Constant Temperature Operation of the Hot-Wire Anemometer at High Frequency*, Rev Sci Inst , **19**, pp 881-889

Perry, A E (1982) *Hot-Wire Anemometry* Clarendon Press, Oxford

Perry (1982, a) Section 2 2, pp 11-12

Perry (1982, b) Figure 3 2 1, p34

Perry (1982, c) Section 3 2, pp 33-38

Perry (1982, d) Figure 5 2 1, p60

Perry (1982, e) Chapter 5, pp 59-80

Perry (1982, f) Section 5 2, p59

Perry (1982, g) Section 5 6, pp 68-70

Perry (1982, h), Section 5 5, pp 66-67

Raffel, M , Willert, E C , Kompenhans, J (1998) *Particle Image Velocimetry A Practical Guide* Springer, London, Berlin

Rasmussen, C G (1962) *Application of Thermistors to Measurements in Moving Fluids*, Rev Sci Inst **33**, No 1, pp 38-42

Rasmussen, C G (1967) *The Air Bubble Problem in Water Flow Hot-Film Anemometry*, DISA Information, No 5 pp 21-26

Riedl, R J and Machen, R (1972) *Hdrodynamic Patterns in Iotic Interstitial Sands and Their Bioclimatological Implications*, Marine Biology, **13**, pp 179-209

Samways, A L , Ali, J , Al-Deen, M F N , Bruun, H H (1994) *Calibration of and Measurement with Cylindrical Hot-Film Probes in Water Flows*, Meas Sci Tech , **5**, No 12, pp 1551-1559

Sarma, G R (1998a) *Transfer Function Analysis of the Constant Voltage Anemometer*, Rev Sci Inst , **69**, No 6, pp 2385-2391

Sarma, G R , Comte-Bellot, G , Faure, T M (1998b) *Software Corrected Hot Wire Thermal Lag for the Constant Voltage Anemometer Featuring a Constant Bandwidth at the Selected Compensation Setting,* Rev Sci Inst , **69**, No 9, pp 3223-3231

Sarma, G R , Lankes, R W (1999) *Automated Constant Voltage Anemometer with in Situ Measurements of Overheat and Time Constant of the Hot Wire*, Rev Sci Inst , **70**, No 5, pp 2384-2386

Sarma, G R , Comte-Bellot, G (2002) *Automated Constant Voltage Anemometer for Measurements with Fluid Temperature Drifts*, Rev Sci Inst, **73**, No 3, pp 1313-1317

Sherif, S A and Pletcher, R H (1986) *Temperature Correction for the Output Response of a Constant-Temperature Hot-Film Anemometer in Nonisothermal Flows with Strong Property-Temperature Dependence*, Proc 8th Intern Heat Transfer Conf San Francisco, pp 549-554

Smits, A J , *Introduction to Hot Wire Anemometry in Supersonic Flows*, ASME Fluid Eng Division, **97**, Heuristics of Thermal Anemometry, pp 35-40

Steinhart, J S and Hart, S R (1968) *Calibration Curves for Thermistors*, Deep Sea Research, **15**, Iss 4, pp 497-503

Steurer, J (1998) *Adaptive Controlled Thermal Sensor for Measuring Gas Flow*, Sensors and Actuators, **A65**, pp 116-122

Swaminathan, M K , Rankin, G W , Sridhar, K (1986) *A Note on the Response Equations for Hot-Wire Anemometry,* ASME, J Fluids Eng , **108**, pp 115-118

Thorpe, S A , Hall, A J , Packwood, A R , Stubbs, A R (1985) *The Use of a Towed Side-Scan Sonar to Investigate Processes Near the Sea Surface*, Cont Shelf Res , **4**, No 5, pp 597-607

Thorpe, S A (1995) *Dynamical Processes of Transfer at the Sea Surface*, Prog Oceanog , **35**, pp 315-352

Toba, Y and Kawamura, H (1996) *Wind-Wave Coupled Downward-Bursting Boundary Layer (DBBL) Beneath the Sea Surface*, J of Oceanography, **52**, pp 409-419

Truzzi, G E , Sarma, G R (2002) *Constant Voltage Anemometer Operated Hot Wire at Subsonic Speeds over Wide Overheats in Unsteady Flows*, Rev Sci Inst , **73**, No 12, pp 4363-4368

Veloso-Gomes, F , Taveira-Pinto, F , Proenca, M F (2001) *Spatial Regular Wave Velocity Field Measurements Near Submerged Breakwaters*, Proc Int Symp Ocean Wave Meas and Anal , **2**, pp 1136-1149

Weller, R A and Davis, R E (1980) *A Vector Measuring Current Meter*, Deep Sea Res **27**, Iss 7, pp 565-566

Whitaker, S (1972) *Forced Convection Heat Transfer Correlations for Flow in Pipes, Past Flat Plates, Single Cylinders, Single Spheres, and for Flow in Packed Beds and Tube Bundles*, J AIChE, **18**, No 2, pp 361-371

Williams, A J (1993) *Free Drifting Measurement of Mid-Water Mixing by an Acoustic Current Meter array in NATRE*, Proc Conf Oceans 93, pp 131-136

Wu, S and Bose, N (1993), *Calibration of a Wedge-Shaped Vee Hot-Film probe in a Towing Tank*, Meas Sci Tech **4**, pp 101-108

Yang, C , Kummel, M , Soeberg, H (1988), *A Self-Heated Thermistor Flowmeter for Small Liquid Flow in Microchannels*, Sensors and Actuators, **15**, No 1, pp 51-62

Appendix A Derivation of Equation (2.21) and Data in Table 2.2

Derivation of Equation (2 21)

The purpose of equation (2 21) is to show that the sensitivity of the anemometer to changes in ambient temperature, T_a, will increase as the temperature difference between the sensor and the surrounding water decreases

We begin with equation (2 20), which is

$$V_s^2 = h(U)(T_s - T_a) \tag{A 1}$$

Introducing the quantity SO, which is the sensor output and adding a change in ambient temperature ΔT_a to the ambient temperature results in

$$SO + \Delta SO = h(U)(T_s - T_a + \Delta T_a) \tag{A 2}$$

This can be rearranged to get

$$SO + \Delta SO = h(U)(T_s - T_a) + h(U)\Delta T_a \tag{A 3}$$

Combining (A 1) and (A 3) leads to

$$\Delta SO = h(U)\Delta T_a \tag{A 4}$$

(A 1) and (A 4) can be used to obtain an expression for the ratio $\Delta SO/SO$

$$\frac{\Delta SO}{SO} = \frac{\Delta T_a}{(T_s - T_a)} \tag{A 5}$$

and finally

$$\Delta SO = SO\frac{\Delta T_a}{(T_s - T_a)} \tag{A 6}$$

Calculating Data in Table 2.2

This section details the calculation of the constants A and B in Table 2 2

For spheres Kramers (1946) found that the heat transfer could be given by

$$Nu = 2 + 1\,3(Pr)^{0\,15} + 0\,66(Pr)^{0\,31}\,Re^{0\,5} \tag{A 7}$$

The Nu and Re numbers are given in section 2 4 1 and are

$$Nu = \frac{hd}{k} \quad \text{Nusselt Number}$$

$$\mathrm{Re} = \frac{\rho U d}{\mu} \quad \text{Reynolds Number}$$

and substituting these into (A 7) and solving for h results in

$$h = \frac{k}{d}\left(2+1\ 3Pr^{0\ 15} + 0\ 66Pr^{0\ 31}\left(\frac{\rho Ud}{\mu} \right)^{0\ 5} \right) \qquad \text{(A 8)}$$

Assume a 3mm diameter metal sphere coated with glass, therefore $d = 3\times10^{-3}\text{m}$, the thermal conductivity, k, of water at the film temperature of 30°C is ~0 65Wm ^{1}k ^{1} (Holman 1992, b), the density, ρ, of water is 1000Kgm ^{3}, and the viscosity, μ, of water at 20°C is 9 8×10^{-4}kgm ^{1}s^{-1} (Holman 1992, b) For metal spheres in water at 19°C Kramers found that the Pr number is 7 3

Substituting these values into (A 8) results in

$$h(U) = 813\ 75 + 14647U^{0\ 5} \qquad \text{(A 9)}$$

In the derivation of (2 30) the surface area of the sensor was included in $h(U)$ so therefore (A 9) must be multiplied through by the surface area of the sensor, which is $2\ 83\times10^{-5}\text{m}$ This results in

$$h(U)\ S = 0\ 023 + 0\ 414U^{0\ 5} \qquad \text{(A 10)}$$

so therefore

$$A = 0\ 023$$
$$B = 0\ 414$$

Appendix B Guide to Using the Sensor

This is a guide to the steps that are necessary to set up and calibrate both temperature and velocity sensors and on how to set them up at the start of each measurement session

Velocity Sensor

1) "Burn in" the sensor for 5 to 6 hours by operating it at a temperature greater than that which it will be used at so that its resistance temperature characteristics will have stabilised before calibration
2) Test for leaks, preferably using the oscilloscope method
3) Determine the R-T characteristics of the sensor or else evaluate its resistance at the required operating temperature - whichever is relevant for the application at hand
4) Calculate and set R_t using the equation $R_t = \frac{R_s}{2}$
5) Immerse the sensor in water and connect up the square wave testing circuitry and set the offset voltage for optimum system performance
6) Set the required corner frequency by varying the resistance of the resistor in the low pass filter

The sensor is now ready to be calibrated after which none of the quantities, which have been set in 1) to 5) above, should be adjusted

7) Calibrate the sensor by exposing it to a range of velocities and ambient water temperatures and determine the coefficients of its calibration equation by fitting the general equation to the calibration data Store the resulting calibration coefficients in a file, as they are required by the successive approximation algorithm that converts the raw sensor data

Temperature Sensor

1) Determine the resistance-temperature characteristics of the temperature sensor and store the resulting Steinhart Hart equation coefficients in a file for use by the conversion software
2) Choose R_X such that the output of the temperature sensor circuit is equal to zero volts at the centre of the predicted temperature operating range

Making Measurements

1) Place the velocity and temperature sensor assembly into water that is at the lowest temperature that the sensor will be operated at and set the signal conditioning offset voltages of both sensors such that the voltage going into the ADC is equal to zero volts

It was found that using this procedure with a signal conditioning scaling factor, G_{SC}, of one, allowed measurements in the velocity range 0 01 to 0 6ms^{-1} to be carried out without any adjustment of the circuit in a 3°C ambient temperature band, however if the temperature changes more than this then the signal conditioning offsets would have to be changed It should be noted that the signal conditioning voltages have no effect on the response of the sensors, however they must be recorded for use by the data processing software

Note that step 1) has to be completed before and possibly during calibration of the sensor and it has been found to be good practice to verify the settings and adjust them if necessary before the commencement of each new series of measurements if there is any possibility that a change in ambient temperature of greater than 3°C occurred since the last measurement session

Appendix C Code Listings

Appendix C 1 Sensor Data Acquisition Program

Program Name tolka cpp

This program, which is a modified version of the driver provided with the ADC, reads in data from the specified channels of the ADC for the specified amount of time and stores it in the specified output file

```
/*************************************************************
 *
 * Product        PICO ADC-22
 *
 * Module         adc22drv C
 *
 * Author         Alan Tong
 *                Pico Technology Limited
 *                Broadway House
 *                149-151 St Neots Road
 *                Hardwick
 *                Cambridge CB3 7QJ UK
 *                Tel  +44-954 211716
 *                Fax  +44-954 211880
 *
 * Copyright 1994 Pico Technology Limited
 *
 * Description
 * This module provides routines to drive the
 * PICO ADC-22 analog to digital
 * converter
 *
 *   History
 *   13Jan94 ADT Created
 *   10Apr94 MKG Add timeout for no ADC connected
 *   10Jul94 MKG Tidy up for production release
 *
 * Revision Info
 *          "file %n date %f revision %v"
 *      "file ADC22DRV C date 10-Jul-94,11 21 44 revision 1"
 *
 * Modified by John Moore on various
 * occasions between 2001 and 2003
 *
 *************************************************************/

#define TRUE 1
#define FALSE 0

#include <stdio h>
#include <dos h>
#include <conio h>
#include <process h>
#include <timer h>
#define ADC22_INVALID_READING 0xFFFF

#define DATA_BITS     10
#define ADDRESS_BITS  4
```

```
#define OFF     0x00
#define POWER   0x38
#define CLK     0x04
#define CS      0x00
#define CS_OFF  0x81
#define ADDR    0x02
#define DOUT    0x40

#define EOC_A   0x80
#define EOC_B   0x20
#define DATA_A  0x08
#define DATA_B  0x10

#define ASHIFT 1

static unsigned int adc22_output_address,
static unsigned int adc22_input_address,
static unsigned char adc22_do_value,
static unsigned int last_channel,
/* Address of BIOS printer port table
 *  segment 0040 offset 8
 */
static unsigned int far * printer_ports
            = (unsigned int far *) 0x00400008L,

/*************************************************************
 * adc22_driver_open
 *
 *   This routine turns on the power to the ADC-22
 *   and initialises the clock
 *
 * accepts
 *    1 - use LPT1
 *    2 - use LPT2
 *    3 - use LPT3
 *    4 - use LPT4
 *
 * sets
 *    adc22_input_address
 *    adc22_output_address
 *    adc22_do_value
 *
 * returns
 *    TRUE - port opened successfully
 *    FALSE - port not opened
 *************************************************************/

int adc22_driver_open (int port)
  {
  int ok,

  /* Check that port is valid
   */
  if ((port >= 1) && (port <= 4))
    {
    /* Check that printer port exists (address is non-zero)
     */

      adc22_output_address = printer_ports [port-1],
    if (adc22_output_address > 0)
      {
```

```
      adc22_input_address = adc22_output_address + 1,
      adc22_do_value = 0,
      outportb (adc22_output_address,
                              adc22_do_value + POWER + CS_OFF),

      ok = TRUE,
      }
    else
      ok = FALSE,
    }
  else
    ok = FALSE,

  return ok,
  }

/*************************************************************
 *
 * adc22_get_value
 *
 *   This routine starts a conversion from channel
 *   "next_channel" and reads in the previous conversion
 *
 *   The routine first waits for EOC to go low, indicating
 *   that the previous conversion has been completed
 *
 *   *CS is then asserted,
 *
 *   The previous conversion is clocked into the PC by
 *   DATA_BITS high-to-low transitions on CLK
 *   The address is clocked out to the ADC-22
 *   simultaneously on the first 4 of these transitions,
 *   as a 4-bit pattern, most significant bit first
 *
 *   accepts
 *  next_channel -
 *  0  21  - channel for next conversion (Converters A, B)
 *  22     - zero reference     (512)    (Converter 'A')
 *  23     - midrange reference (0)      (Converter 'A')
 *  24     - maximum reference  (1023)   (Converter 'A')
 *
 *  25     - zero reference     (512)    (Converter 'B')
 *  26     - midrange reference (0)      (Converter 'B')
 *  27     - maximum reference  (1023)   (Converter 'B')
 *
 *   returns
 *     0  1023 - result of conversion
 *
 *************************************************************/

int adc22_get_value (int next_channel)
  {
  unsigned char         i,
  unsigned int          value,
  unsigned char         data_ab,
  unsigned char         address,
  unsigned int          timeout,

  /* This table contains the address for each channel
   *  the address bits are in reverse order
   */
```

```
static unsigned char reverse_bits [28] =
{
0x02,   0x0C,   0x04,   0x08,   0x00,   0x09,   0x05,
0x01,   0x0E,   0x06,   0x0A,   0x02,   0x0C,   0x0A,
0x06,   0x0E,   0x01,   0x05,   0x09,   0x00,   0x08,
0x04,   0x0D,   0x03,   0x0B,   0x0D,   0x03,   0x0B
},

static unsigned char input_bit [28] =
{
DATA_A, DATA_A, DATA_A, DATA_A, DATA_A, DATA_B, DATA_B,
DATA_B, DATA_B, DATA_B, DATA_B, DATA_B, DATA_B, DATA_A,
DATA_A, DATA_A, DATA_A, DATA_A, DATA_A, DATA_B, DATA_B,
DATA_B, DATA_A, DATA_A, DATA_A, DATA_B, DATA_B, DATA_B,
},

value = 0,

/* We are reading the result of the previous conversion
 * if the last channel refered to converter B,
 * we must get the result from that unit,
 * even if we are clocking the next address
 * into  converter A
 */

data_ab = input_bit [last_channel],

/*Store which ADC the current conversion refers to
 */
last_channel = next_channel,

/* Use address table to invert order of address bits
 * MSB must be clocked out first
 */
address = reverse_bits [next_channel] << ASHIFT,

/* Wait for both ADC-22's to finish converting
 */
timeout = 0,
while (((inportb (adc22_input_address) & EOC_A) == 1)
&&     (timeout++ < 1000)),

while (((inportb (adc22_input_address) & EOC_B) == 0)
&&     (timeout++ < 1000)),

if (timeout >= 1000)
  return (ADC22_INVALID_READING),

/* Assert *CS
 */
outportb (adc22_output_address,
                        adc22_do_value + POWER + CS),

/* For the first bits,
 *  clock in data and out address
 */
for ( i = 0 , i < ADDRESS_BITS , i++ )
  {
  /* CLK low
   */
  outportb (adc22_output_address,
```

```
                        adc22_do_value + (address & ADDR)
                        + POWER + CS),

  /* CLK high
   */
  outportb (adc22_output_address,
                        adc22_do_value + (address & ADDR)
                        + POWER + CS + CLK),

  address >>= 1,

  value <<= 1,
  if ((inportb (adc22_input_address) & data_ab) != 0)
    {
    value++,
    }
  }

/* For the remaining bits,
 *  clock in data (no address)
 */
for (, i < DATA_BITS , i++ )
  {
  /* CLK low
   */
  outportb (adc22_output_address,
                        adc22_do_value + POWER + CS),

  /* CLK high
   */
  outportb (adc22_output_address,
                        adc22_do_value + POWER + CS + CLK),

  value <<= 1,
  if ((inportb (adc22_input_address) & data_ab) != 0)
    {
    value++,
    }
  }

/* Negate *CS
 */
outportb (adc22_output_address,
                adc22_do_value + POWER + CS_OFF),

return (value),
}
```

```
/*************************************************
 *
 * adc11_digital_output
 *
 * This routine controls the ADC-11
 * digital output (pin 1)
 *
 * By default, it is turned off by the
 * open function  JM(3 12 02)
 *
 * accepts
 *   do_state = TRUE - turn on the digital output
 *              FALSE - turn off the digital output
 * sets
 *    adc11_do_value
 *
 * returns
 *   nothing
 *
 *************************************************/

void adc22_digital_output (int do_value)
  {

  if (do_value)
    adc22_do_value = DOUT,
  else
    adc22_do_value = 0,

  outportb (adc22_output_address,
                 adc22_do_value + POWER + CS_OFF),

  }
/*************************************************
 *
 * main program
 *
 * IF you wish to use link this module into
 * another program change to #undef MAIN
 *
 * To compile this module as a complete program,
 *leave as #define MAIN
 *
 *************************************************/
#define MAIN

#ifdef MAIN

void main(void)
  {
  int i,
  int value,
  int ok,
  int do_value,
  long int samples,
  int ch,
  long int n,
  char name[20],
  float time=0,sample_time,
  FILE *out,
  Timer t,
```

```
 printf ("ADC-22 C driver V1 0\n"),
 printf ("Copyright 1994 Pico Technology Limited\n"),
 printf ("This version of the driver switches on the
               digital output when acquiring data\n"),


 /* Open the driver
  */
                            /*The arguement is the */
 ok = adc22_driver_open (1),/*printer port that the*/
 if (ok)                    /*ADC-22 is connected to*/
   printf ("ADC-22 opened successfully\n"),

 else
   {
   printf ("Unable to open ADC-22\n"),
   exit (99),
   }

  printf ("\n Enter sample time in seconds  "),
  scanf ("%f",&sample_time),

  printf ("\n Enter no  of channnels  "),
  scanf ("%d",&ch),

  printf ("\n Enter filename  "),
  scanf ("%s",name),

t reset(),

out = fopen(name,"w"),

adc22_digital_output(1),

t start(),
n=1,

while(time<sample_time)
   {
    adc22_get_value (0),
    t stop(),
    time=t time(),
    t start(),
    fprintf (out,"%61d %f ", n,time),

      for ( i = 0 , i<ch , i++ )
     {
     value = adc22_get_value (i+1),
     fprintf (out,"%4d ", value),
     }

      fprintf(out,"\n"),
    delay(40),/*Change this value to change */
    n++,      /*the sampling rate of the ADC*/
                    /*40=25samples/s on 33Mhz PC  */
   }
   adc22_digital_output(0),
fclose(out)
}
#endif
```

Appendix C.2 Velocity Data Acquisition Program
Program Name: chopper.cpp

This program measures the time interval between rising edges of consecutive pulses from the slotted opto-switch and calculates the mean velocity of the trolley and the sensor over that time interval

```
//Last Revised  11 02 2003 15 20
#include <stdio h>
#include <conio h>
#include <stdlib h>
#include <timer h>
int main()
{
Timer t,
int x,status,i=0,j=0,k,z,p,
float dt=0,a= 145,v,t1,t2,b,//a=diameter
char name[25]="d \\temp dat",namev[25],

FILE *in, *out, *outv,

clrscr(),                /************************/
window(10,10,70,15),     /*Set up display window */
textcolor(YELLOW),       /************************/
textbackground(BLUE),

cprintf("Connect the chopper to port B              \r\nand the
         digital output of the ADC to port C\r\nThe diameter used
         to calculate the velocity is % 3fm\n",a),

printf("\n Enter filename for velocity data  "),
scanf("%s",&namev),
out=fopen(name,"w"),

                     /*********************************************/
outportb(647,0x8B), /* 10001011 A=out, B,C=in                     */
outportb(644,0xAA), /* Use this to test card  writes 10101010 to */
                     /*port A                                     */
t reset(),           /*********************************************/

while(inportb(646)!=0xFF)   //646 = Digital Output of ADC
 {
  p++,p--,
 }
t start(),
while(inportb(646)==0xFF)
 {

  loop1
   if (inportb(645)!=0xFF) goto loop1 ,
   t stop(),
   dt=t time(),
   t start(),
   j++,
   fprintf(out,"%d %f\n",j,dt),

  loop2
   if (inportb(645)==0xFF) goto loop2,,
 }
fclose(out),
```

```
in=fopen(name,"r"),
outv=fopen(namev,"w"),
fscanf(in,"%i %f",&z,&t1),    //This captures the
                              //first time in the file so it
                              //cant be used to calculate velocity
 fscanf(in,"%i %f",&z,&t1),   //This is necessary since the first
                              //reading is not necessarily at
 for(k=0,k<j-2,k++)           //the rising edge
  {
    fscanf(in,"%i %f",&z,&t2),
    dt=t2-t1,
    t1=t2,
    i++,
    v=a/(30*dt),              //a = diameter

    fprintf(outv,"%i %f %f\n",i,t2,v)
    if (kbhit()!=0) exit(status),
  }

fclose(in),
fclose(outv),
return 0,
}
```

Appendix C.3 Calibration Data Processing Program

Program name convert c

This program carries out all of the necessary data processing to obtain calibration data that can be curve fitted The user simply has to "cat" all of the output files for a particular set of calibration data together to obtain a data file that can be curve fitted

```
/*****************************************************************  */
/*This is program uses interpolation to match the velocity data to   */
/*the other data                                                     */
/*It also converts the ADC outputs to power and temperature          */
/*The input and output files are passed to the program as command */
/* line arguments                                                    */
/*The format is as follows,                                         */
/*exec 'sensor data' 'velocity data' output file' 'parameter file'*/
/*The parameters necessary to calculate the power and temp output */
/*are read in from the parameter file                               */
/*The velocity data is assumed to be in a 2 column file             */
/*of the form  "timestamp velocity" and the format of the sensor  */
/*data is assumed to be                                             */
/*"'Identifier' 'timestamp' 'sensor data' 'temp data'"              */
/*The format of the output file is                                  */
/*Identifier   Time   Interpolated Velocity                         */
/*Sensor Output   Tempurature Data                                  */
/*****************************************************************/

#include <stdio h>
#include <stdlib h>
#include <math h>
double vin, vint, voff, vofft, n, rs, r1, ra, rx, g,
            sth1, sth2, sth3,
float convert2temp(double z),
float convert2power(double z),
int main(int argc, char *argv[])
{
int i,j,k,m,volt,status,j0,temp,
float vel=0,adc_t,chopper_t=0,vel0=0,chopper_t0=0,vel_interp=0,c,
double h,

FILE *chopper, *adc, *out ,*par,

 printf("\nThe format of the output file is  ID   TIME  VELOCITY
            SENSOR  TEMP\n"),

if((adc=fopen(argv[1],"r"))==NULL)
 {
  printf("\nThe ADC filename you entered is incorrect\n"),
  exit(status),
 }

if((chopper=fopen(argv[2],"r"))==NULL)
 {
  printf("\nThe CHOPPER filename you entered is incorrect\n"),
  exit(status),
 }

if((par=fopen(argv[4] "r"))==NULL)
 {
```

```
   printf("\nThe parameter filename you entered is incorrect\n"),
   exit(status),
 }

/*Read in variables from file and check that*/
/*they are all there If not, exit           */

if ((fscanf(par,"vin=%lf \nvoff=%lf \nvint=%lf \nvofft=%lf
                 \nn=%lf \nrs=%lf
                 \nr1=%lf \nra=%lf \nrx=%lf \ng=%lf \nsth1=%lf
                 \nsth2=%lf \nsth3=%lf",
               &vin,&voff,&vint,&vofft,&n,&rs,&r1,&ra,&rx,
               &g,&sth1,&sth2,&sth3))!=13)

{
    printf("\nAn error has occured while reading in the
            parameter file\n"),
    exit(status),
  }

/* Count rows in sensor file*/
while(fscanf(adc,"%d %f %d %d\n",&i,&adc_t,&volt,&temp)!=EOF),

 k=i,
printf("The no  of rows in the file is  %d\n",k),

rewind(adc),

if((out=fopen(argv[3],"w"))==NULL)
  {
   printf("\nThe output file cannot be opened\n"),
   exit(status),
 }

fscanf(chopper,"%f\t%f",&chopper_t0,&vel),/*Set velocity for */
                                          /*t=0 equal to first*/
                                         /*velocity entry in file*/
chopper_t0=0,

rewind(chopper),  /*Puts the scanf pointer back to the*/
                  /*start of the file                */

/*****Interpolation loop****************/
/*To understand what this loop is doing */
/*draw the two files as number lines    */
/*The program needs to be able to deal  */
/*with velocity(chopper) files that     */
/*are longer and shorter than the       */
/*sensor data files                     */
/***************************************/
for(m=0,m<k,m++)
  {
    fscanf(adc,"%d %f %d %d",&i,&adc_t,&volt,&temp),

    if (chopper_t<adc_t)

      {

      chopper_t0=chopper_t,
      vel0=vel,
      while(fscanf(chopper,"%f\t%f",&chopper_t,&vel)!=EOF)
```

```
      {
        if (chopper_t>adc_t) break,
        chopper_t0=chopper_t,
        vel0=vel,
      }
    }
   vel_interp = vel0 + (adc_t - chopper_t0)*
                ((vel-vel0)/(chopper_t - chopper_t0)),

      /* y-y1=m(x-x1)*/

   h=convert2temp(temp),
   c=convert2power(volt),
   fprintf(out,"%d %f %f %f %f\n",i,adc_t,vel_interp,c,h),

  }

fclose(adc),
fclose(chopper),
fclose(out),
fclose(par),
return 0,
}
            /**********************/
            /*Conversion Functions*/
            /**********************/
float convert2temp(double z)
  {
    double vout, vref, b, a, t, rt,
    vout=z*n,
    vref = vint*rx/(ra+rx),
    rt = (ra*(-vofft - vout - g*vref))/(g*(vref - vint)
           + vofft + vout),
    b=log(rt),
    a=sth1 + sth2*b + sth3*(pow(b,3)),
    t=1 0/a,
    return t,
  }


float convert2power(double z)
  {
    double p,
    p=pow((vin+voff+n*z),2)*(rs/pow((r1+rs),2)),
    return p, }
```

Appendix C.4 Program for Converting Raw Sensor Data into Velocity

Program name: process.c

The program converts the raw data to dissipated power and temperature and calculates the corresponding velocity data from the calibration equation of the sensor using successive approximation. It reads in the necessary parameters and the coefficients of the calibration equation form user specified files. Some interactive help has been included in the program and can be viewed by typing "executable_name –help".

```
#include <stdio.h>
#include <math.h>
#include <string.h>
double vin, vint, voff, vofft, n, rs, r1, ra, rx, g, sth1, sth2,
       sth3, a, at, b, bt, c, ct, d, dt, tol = 1e-10;


double convert2temp(double z);
double convert2power(double z);
double approx(double px, double tx);


int main(int argc, char *argv[])
{

int i,status,volt,temp;
double p, t, u;
float raw_t;
FILE *raw, *par, *coeff, *out;

/****************Help Routine****************/
if(argc == 1)
 {
  printf("\nUsage: %s 'raw data filename' 'output filename'
      'sensor parameter filename'",argv[0]);

  printf("                'calibration coefficient filename'\n\n");
  printf("Type '%s -?' or '%s -help' for more info.\n\n",argv[0]
         ,argv[0]);
  exit(status);
 }

if (argc = 2 && ((strcmp(argv[1],"-?")==0) ||
                 (strcmp(argv[1],"-help")==0)))
 {
  printf("\nUsage: %s 'raw data filename' 'output filename'
                 'sensor parameter filename'",argv[0]);

  printf("                'calibration coefficient filename'\n\n");

  printf("\nThis program reads in a sensor data file of the
      format:\n\n\tID\tTIME\tSENSOR DATA\tTEMP DATA\n\n");

  printf("and converts the sensor data to dissipated power,
           the temp data to\ntemperature and uses");

  printf(" these values to determine the fluid velocity by
```

```
   \nsuccessive approximation \nTolerance (p - pg) = % 10lf\n",tol),

  printf("The Time, Velocity and Temperature are written to
                  the output file\nwith the format \n\n\t"),

  printf("TIME\tVELOCITY\tTEMPERATURE\n"),

  printf("\nThe sensor parameter file contains the parameters
      required to convert\nthe raw data to power and temp\n"),

  printf("It must have the format \n"),

  printf("\tvin=\n\tvoff=\n\tvint=\n\tvofft=\n\tn=\n\
      trs=\n\tr1=\n\tra=\n\trx=\n\tg=\n\tsth1=\n\tsth2=\n\tsth3=\n"),

  printf("\nThe calibration coefficient file contains the
      coefficients of the \ncalibration surface and must have "),

  printf("the format\n\ta  =  number\n\tat =  number\n\tb
      =  number\n\tbt =  number\n\tc  =  number\n\tct =  number"),

  printf("\n\td  =  number\n\tdt =  number\n"),
  exit(status),
 }

  else if (argc == 2)
   {
    printf("Invalid operand '%s'\n",argv[1]),
    exit(status),
   }
                        /*End of help Routine*/

                         /*Open input files*/

if((raw = fopen(argv[1],"r"))==NULL)
 {
  printf("\nCould not open the sensor data file\n"),
  exit(status),
 }

if((par = fopen(argv[3],"r"))==NULL)
 {
  printf("\nCould not open sensor parameter file\n"),
  exit(status),
 }

if((coeff = fopen(argv[4],"r"))==NULL)
 {
   printf("\nCould not open calibration coefficient file\n"),
   exit(status),
 }


/*Reads in global variables from file and checks that*/
/*they are all there If not, exit*/


if ((fscanf(par "vin=%lf \nvoff=%lf \nvint=%lf \nvofft=%lf
                 \nn=%lf \nrs=%lf
                 \nr1=%lf \nra=%lf \nrx=%lf \ng=%lf \nsth1=%lf
                 \nsth2=%lf \nsth3=%lf",
```

```
                &vin,&voff,&vint,&vofft,&n,&rs,&r1,&ra,&rx,
                &g,&sth1,&sth2,&sth3))!=13)
  {
    printf("\nAn error has occured while reading in the parameter
            file\n"),
    exit(status),
  }

if ((fscanf(coeff,"a = %lf \nat = %lf \nb = %lf \nbt = %lf
            \nc = %lf
            \nct = %lf \nd = %lf \ndt = %lf",&a,&at,&b,&bt,&c
            ,&ct,&d,&dt)) !=8)
  {
    printf("\nAn error has occured while reading in the
            coefficient file\n"),
    exit(status),
  }

/*Open output file*/

if((out = fopen(argv[2],"w"))==NULL)
  {
   printf("\nCould not open output data file\n"),
   exit(status),
  }

/*Scan raw data and covert it to power and temp and */
/*determine the velocity*/

while(fscanf(raw,"%d %f %d %d\n",&i,&raw_t,&volt,&temp)!=EOF)
  {
   p = convert2power(volt),
   t = convert2temp(temp),
   u = approx(p,t),
   fprintf(out,"%f %lf %lf\n",raw_t, u, t),
  }

fclose(raw),
fclose(par),
fclose(coeff),
fclose(out),
return 0,
}

/** Function that converts raw temperature data to temperature */

double convert2temp(double z)
  {
    double vout, vref, b, a, t, rt,
    vout=z*n,
    vref = vint*rx/(ra+rx),
    rt = (ra*(-vofft - vout - g*vref))/(g*(vref - vint)
            + vofft + vout),
    b=log(rt),
    a=sth1 + sth2*b + sth3*(pow(b,3)),
    t=1 0/a,
    return t,
  }

/* Function that converts raw sensor data to dissipated power*/
```

```
double convert2power(double z)
  {
    double p,
    p=pow((vin+voff+n*z),2)*(rs/pow((r1+rs),2)),
    return p,
  }

/* Successive Approximation Function that calculates velocity from*/
/* ambient water temperature and dissipated power data  This      */
/* function currently supports the 4 term calibration equation    */

double approx(double px, double tx)

  {
    double pg,ug,interval,range = 1 ,

    ug = range/2,

    pg = a+at*tx + (b + bt*tx)*log(ug) + (c + ct*tx)*pow(log(ug),2)
      + (d +dt*tx)*pow(log(ug),3),

    interval = range/2,

    while (fabs(px - pg)>tol)
      {

            if (pg<px)
            ug += interval/2,

            if (pg>px)

            ug -= interval/2,

            pg = a+at*tx + (b + bt*tx)*log(ug)
                 + (c + ct*tx)*pow(log(ug),2)
                   + (d +dt*tx)*pow(log(ug),3),

            interval = interval/2,

      }

     return ug,
   }
```

Appendix C 5 Program for Calculating Roots of Calibration Equation

Program Name cuberoot c

```
#include<stdio h>
#include<stdlib h>
#include<math h>
#include<complex h>
int main(int argc, char *argv[])
{
double A,B,C,D,P,T,a,at,b,bt,c,ct,dc,dt,
long double q,r,d,a0,a1,a2,
long double complex cmplx,z1,z2,z3,s,t,sqrtd,sx,tx,
FILE *coeff,

/*Open coefficient file and read in the */
/*coefficients of the calibration equation*/

/*The program currently reads in the ambient temperature and */
/*dissipated power values from the command line  */

coeff = fopen(argv[1],"r"),
fscanf(coeff,"a = %lf \nat = %lf \nb = %lf \nbt = %lf \nc = %lf
            \nct = %lf \nd = %lf \ndt = %lf",&a,&at,&b,&bt,&c
            ,&ct,&dc,&dt),

P = strtod(argv[2],(char**)NULL),
T = strtod(argv[3],(char**)NULL),

A = a + at*T,

B = b + bt*T,

C = c + ct*T,

D = dc + dt*T,

printf("\nA = %lf  B = %lf  C = %lf  D = %lf\n",A,B,C,D),

a2 = C/D,

a1 = B/D,

a0 = (A - P)/D,

printf("a0 = %llf  a1 = %llf  a2 = %llf\n",a0,a1,a2),

q = (3*a1 - powl(a2,2 0))/9,

r = (9*a2*a1 - 27 0*a0 - 2 0*powl(a2 3 0))/54,

d = powl(q,3) + powl(r,2),

sqrtd = csqrtl(d),


/*If r+sqrtd is complex or real and negative then     */


if ( (cimagl(r+sqrtd)'=0) || (creall(r+sqrtd)<=0))
```

```
      s = (cpowl((r + sqrtd),1/3 0)),
       /*first cube root of r+sqrtd*/

      else
            /*only option left is real and positive*/

            {
              s = (-1/2 0 - I*sqrtl(3)/2)*(cpowl((r + sqrtd),1/3 0)),
              /*cube root times 2nd primitive of unity*/
            }

if ((cimagl(r-sqrtd)!=0)) /* If r-sqrtd is complex then   */

      t = cpowl((r - sqrtd),1/3 0), /*first cube root of r-sqrtd*/

       /*If r-sqrtd is real and negative */
       else if ( (creall(r-sqrtd)<0) && (cimagl(r - sqrtd)==0) )

            {
             t = conjl(cpowl((r - sqrtd),1/3 0)),
             /*third cube root of r-sqrtd*/
            }

      else  /*only option left now is real and positive*/

            {
             t = (-1/2 0 + I*sqrtl(3)/2)*(cpowl((r - sqrtd),1/3 0)),
             /*cube root times 1st primitive of unity*/
            }

/*Calculate the roots of the equation*/

z1 = -(a2/3) + (s + t),

z2 = -a2/3 - (s + t)/2 + I*sqrt(3)*(s - t)/2,

z3 = -a2/3 - (s + t)/2 - I*sqrt(3)*(s - t)/2,

printf("\nz1 = %lf %lfi\n",creal(z1),cimag(z1)),
printf(  "z2 = %lf %lfi\n",creal(z2),cimag(z2)),
printf(  "z3 = %lf %lfi\n",creal(z3),cimag(z3)),

fclose(coeff),
return 0,
}
```

Appendix D Notation

A	General equation coefficient
B	General equation coefficient
c_P	Specific heat of fluid at constant pressure
C	General equation coefficient
d	Diameter
D	Distance travelled by trolley as chopper rotates through one segment and a general equation coefficient
e_1, e_2	Voltages at the corners of the Wheatstone Bridge in the velocity sensor control circuit
f_t	Velocity sensor system corner frequency
G_{OL}	Open loop gain of velocity sensor control circuit
G_{SC}	Signal conditioning scaling gain
G_T	Temperature sensor circuit amplifier gain
G_1	Gain of difference amplifier in advanced control circuit
G_2	Gain of inverting adder in advanced control circuit
H	Heat transfer rate from a heated object in a flow
k	Coefficient of thermal conductivity
n	Exponent term in general equations
Nu	Nusselt number
Pr	Prandtl number
P_s	Power dissipated by velocity sensor
Q	Theoretical heat transfer rate from coated spherical thermistor, as used by Lueck (1980)
r	Radius of spherical coated thermistor
R_a, R_b	Resistors that form the passive side of the bridge in the velocity sensor control circuit
Re	Reynolds number
R_G	AD620 gain resistor (temperature sensor amplifier)
R_L	Series resistor in Temperature sensor circuit
R_s	Operating resistance of velocity sensor
R_x	Resistor in temperature circuit bridge
R_1	Resistor in series with sensor in velocity sensor control circuit

SO	Sensor output in section 2 6
SSR	Sum of Squared Residuals
T_a	Ambient fluid temperature
t_R	Transient response time
T_s	Operating temperature of velocity sensor
t_X	Alternative transient response time
U	Velocity
U_R	Maximum velocity that can be measured for a given fractional uncertainty
V_f	Control circuit feedback voltage
V_n	Negative supply voltage
V_o	Signal conditioning offset voltage
V_{off}	Velocity sensor control circuit offset voltage
V_{oU}	Velocity sensor signal conditioning offset voltage
V_{oT}	Temperature sensor signal conditioning offset voltage
V_p	Positive supply voltage
V_{ref}	Temperature sensor circuit reference voltage
V_s	Voltage drop across velocity sensing thermistor
V_{supply}	Temperature sensor bridge supply voltage
V_T	Voltage drop across temperature sensing thermistor
V_U	Velocity sensor ADC input voltage
V_{TC}	Temperature sensor ADC input voltage
z_U	ADC output for velocity sensor
z_T	ADC output for temperature sensor
α	Temperature coefficient of resistance
β	Material constant of thermistors
δT	Temperature measurement uncertainty
δV	ADC resolution and conversion factor
Δ	Coating thickness
Δt	Time taken for chopper to rotate through one segment

μ	Molecular viscosity
ρ	Density
τ	Fractional uncertainty in velocity measurements obtained with the velocity sensor
ξU	Velocity measurement uncertainty
ξV	Sensor voltage uncertainty that corresponds to a certain velocity measurement uncertainty